uOttawa

L'Université canadienne
Canada's university

FACULTÉ DES ÉTUDES SUPÉRIEURES ET POSTOCTORALES

uOttawa

L'Université canadienne
Canada's university

FACULTY OF GRADUATE AND POSDOCTORAL STUDIES

Yves D. Landry

AUTEUR DE LA THÈSE / AUTHOR OF THESIS

M.Sc. (Biochemistry)

GRADE / DEGREE

Department of Biochemistry, Microbiology and Immunology

FACULTÉ, ÉCOLE, DÉPARTEMENT / FACULTY, SCHOOL, DEPARTMENT

ABCA1 Expression Disrupts Lipid Raft Plasma Membrane Microdomains through its ATPase-Related Functions

TITRE DE LA THÈSE / TITLE OF THESIS

Xiaohui Zha

DIRECTEUR (DIRECTRICE) DE LA THÈSE / THESIS SUPERVISOR

CO-DIRECTEUR (CO-DIRECTRICE) DE LA THÈSE / THESIS CO-SUPERVISOR

EXAMINATEURS (EXAMINATRICES) DE LA THÈSE / THESIS EXAMINERS

Johné Liu

Ross Milne

Gary W. Slater

Le Doyen de la Faculté des études supérieures et postdoctorales / Dean of the Faculty of Graduate and Postdoctoral Studies

ABCA1 Expression Disrupts Lipid Raft Plasma Membrane Microdomains through its ATPase-Related Functions

Yves D. Landry

Thesis submitted to the Faculty of Graduate and Postdoctoral Studies in partial fulfillment of the requirements for the degree of Master of Science

Supervisor: Dr. Xiaohui Zha

Department of Biochemistry, Microbiology and Immunology
Faculty of Medicine, University of Ottawa

Library and
Archives Canada

Published Heritage
Branch

395 Wellington Street
Ottawa ON K1A 0N4
Canada

Bibliothèque et
Archives Canada

Direction du
Patrimoine de l'édition

395, rue Wellington
Ottawa ON K1A 0N4
Canada

Your file Votre référence
ISBN: 978-0-494-49229-1
Our file Notre référence
ISBN: 978-0-494-49229-1

Abstract

The ATP-binding cassette transporter A1 (ABCA1) is known to mediate cholesterol efflux to lipid-poor apolipoprotein A-I. In addition, ABCA1 has been shown to influence functions of the plasma membrane, such as endocytosis and phagocytosis. Here, we report that ABCA1 expression results in a significant redistribution of plasma membrane cholesterol and sphingomyelin from lipid rafts to non-raft regions. Caveolin, a lipid raft/caveolae protein marker, also redistributes from punctate, caveolae-like structures to the general area of the plasma membrane upon expression of ABCA1. Furthermore, we observed a significant reduction of Akt activation in ABCA1-expressing cells, consistent with lipid raft disruption. Cholesterol content in the plasma membrane was, however, not altered. Moreover, we provide evidence that the non-functional A937V-ABCA1 mutant, with a point mutation in the nucleotide binding domain, fails to redistribute cholesterol, sphingomyelin, or caveolin. A937V also fails to influence Akt activation. Finally, we show that apolipoprotein A-I preferentially associates with non-raft membranes in ABCA1-expressing cells. Our results thus demonstrate that ABCA1 causes a change in overall lipid packing of the plasma membrane, likely through its ATPase-related functions. Such reorganization by ABCA1 effectively expands the non-raft membrane fractions and, consequently, pre-conditions cells for cholesterol efflux.

Acknowledgements

During the past few years, I have had the opportunity to work with some extraordinary people that have helped me to develop as a scientist, as well as an individual. First and foremost, a great deal of thanks and respect go out to my supervisor, Dr. Xiaohui Zha. Her curiosity and enthusiasm have been contagious since day one, and I am grateful to have had the chance to be a member of her laboratory. Another important influence has been Dr. Maxime Denis. His long hours of instruction and assistance have not gone unnoticed. His patience and expertise were crucial in obtaining my first publication, an accomplishment of which I am truly proud. I would also like to thank my thesis advisory committee members, Dr. Rhian Touyz and Dr. Alexander Sorisky, for their assistance and insight throughout my graduate studies. In addition, Dr. Sorisky has been an important mentor that has always found time in his busy schedule to provide advice and insight. Finally, I would like to thank all of my fellow lab members, past and present, not only for providing an intuitive research environment, but for making the past few years a lot of fun. I wish them all the best of luck in their future endeavors.

This work is dedicated to my family, whose love and encouragement have always driven me to challenge myself and to appreciate the important things in life.

Table of Contents

List of Figures

Abbreviations

A937V	Alanine937Valine
ABCA1	ATP binding cassette transporter A1
ABCA2	ATP binding cassette transporter A2
ABCG1	ATP binding cassette transporter G1
ABCG4	ATP binding cassette transporter G4
ABCG5	ATP binding cassette transporter G5
ABCG8	ATP binding cassette transporter G8
ACAT	Acyl-coenzyme A:cholesterol acyltransferase
AD	Activation domain
APLT	Aminophospholipid translocase
ApoA-I	Apolipoprotein A-1
ApoA-II	Apolipoprotein A-2
ApoA-IV	Apolipoprotein A-IV
ApoB-48	Apolipoprotein B-48
ApoB-100	Apolipoprotein B-100
ApoC-I	Apolipoprotein C-I
ApoC-II	Apolipoprotein C-II
ApoE	Apolipoprotein E
ATP	Adenosine triphosphate
BCθ	Biotinylated and protease (subtilisin Carlsberg)-nicked derivative of θ-toxin
BHK	Baby hamster kidney
BSA	Bovine serum albumin
CAD	Coronary artery disease
cAMP	Cyclic adenosine monophosphate
CAV1	Caveolin-1
CAV2	Caveolin-2
CAV3	Caveolin-3
CE	Cholesterol ester
CERT	Ceramide transfer protein
CETP	Cholesterol ester transfer protein
CHO	Chinese hamster ovary
COP	Coat protein
CS	Calf serum
CSD	Caveolin scaffolding domain
DBD	DNA binding domain
DMEM	Dulbecco's modified eagle's medium
DNA	Deoxyribonucleic acid
DRM	Detergent-Resistant Membrane
EDTA	Ethylene diamine tetracetic acid
EGF	Epidermal growth factor
EGFR	Epidermal growth factor receptor
EGTA	Ethylene glycol tetraacetic acid
ER	Endoplasmic reticulum

EYFP	Enhanced yellow fluorescent protein
FC	Free cholesterol
FFA	Free fatty acid
FOLCH	Chloroform methanol
FRAP	Fluorescence recovery after photobleaching
GFP	Green fluorescent protein
GLUT4	Glucose transporter 4
GM1	Monosialotetrahexosylganglioside
GPI	Glycosylphosphatidylinositol
HDL	High-density lipoprotein
HDL-C	High-density lipoprotein cholesterol
HEK	Human embryonic kidney
HEPES	4-(2-hydroxyethyl)-1-piperazineethanesulfonic acid
HL	Hepatic lipase
HMG-CoA	3-hydroxy-3-methyl-glutaryl-CoA
HPLC	High performance liquid chromatography
HSP-70	70 kilodalton heat shock protein
IDL	Intermediate-density lipoprotein
Insig-1	Insulin-induced gene 1
Insig-2	Insulin-induced gene 2
IP	Immunoprecipitation
IR	Insulin receptor
IRS-1	Insulin receptor substrate 1
kDa	Kilodalton
KO	Knockout
LBD	Ligand binding domain
LCAT	Lecithin cholesterol acyl transferase
LDL	Low-density lipoprotein
LDL-C	Low-density lipoprotein cholesterol
LDLR	Low-density lipoprotein receptor
LOX-1	Lectin-like oxLDL receptor
LPL	Lipoprotein lipase
LRP	LDLR related protein
LUV	Large unilamelar vesicle
LXR	Liver X receptor
MCD	Methyl β-cyclodextrin
MTP	Microsomal triglyceride transfer protein
NA	Numerical aperture
NADPH	Nicotinamide-adenine dinucleotide phosphate
NBD	Nucleotide binding domain
NBF	Nucleotide binding fold
NO	Nitric oxide
nSREBP	Nuclear sterol response element binding protein
Ox LDL	Oxidized LDL
PBS	Phosphate buffer saline
PC	Phosphatidylcholine

PDZ	Postsynaptic density protein-95, disk-large tumor suppressor protein, zonula occludens-1
PE	Phosphatidylethanolamine
PI3K	Phosphoinositide 3-kinase
P-IRS-1	Phosphorylated insulin receptor substrate 1
PLTP	Phospholipid transfer protein
PPARα	Peroxidase proliferator-activated receptor α
PS	Phosphatidylserine
PTV	Prechylomicron transport vesicles
RCT	Reverse cholesterol transport
RER	Rough endoplasmic reticulum
RIPA	Radioimmunoprecipitation
RPMI	Roswell Park Memorial Institute medium
RXR	Retinoic X receptor
S1P	Site-1 protease
S2P	Site-2 protease
SCAP	SREBP cleavage-activating protein
SD	Standard deviation
SDS-PAGE	Sodium dodecyl sulfate polyacrylamide gel electrophoresis
SE	Standard error
SER	Smooth endoplasmic reticulum
SM	Sphingomyelin
SR-A	Scavenger receptor A
SR-B1	Scavenger receptor B1
SRE	Sterol regulatory element
SREBP	Sterol response element binding protein
SRP	Signal recognition particle
SR-PSOX	Scavenger receptor recognizing phosphatidylserine
SUV	Small unilamelar vesicle
TC	Total cholesterol
TCA	Trichloroacetic acid
TD	Tangier Disease
Tf	Transferrin
TG	Triglyceride
TGN	Trans Golgi network
THP-1	Human acute monocytic leukemia cell line
TK	Thymidine kinase
TM	Transmembrane
TMD	Transmembrane domain
TRPC1	Stretch-activated channel short transient receptor potential channel-1
UAS	Upstream activating sequences
UPS	Ubiquitin-proteasome system
VLDL	Very low-density lipoproteins
W590S	Tryptophan590Serine
WT	Wild type

Chapter 1 Introduction

1.1 Cholesterol

1.1.1 Interactions with Phospholipids

Cholesterol is a biological molecule essential for the normal function of animal cells. Approximately 90% of total cellular cholesterol is found in the plasma membrane[1]. At the level of the plasma membrane, free cholesterol (FC) regulates membrane fluidity[2]. This is mainly due to the unique structural characteristics of cholesterol that facilitate its interaction with phospholipids in the membrane. According to one model by Bloch and others[3, 4], the flat α-face of cholesterol is optimally configured to interact with the *sn*-1 saturated fatty acyl group. At the same time, the methylated β-face is ideal for the interaction with the more flexible unsaturated fatty acyl chains in the *sn*-2 position of an adjacent phospholipid molecule. Additionally, a C-C double bond is present in the cholesterol α-face, which further enhances its interactions with proximal phospholipids[5]. The side chain of cholesterol is completely saturated and relatively unsubstituted, which maximizes the van der Waals interactions with phospholipids and ensures stability of the bilayer[3-5].

1.1.2 Caveolae: A Subclass of Lipid Rafts

In addition to maintaining rigidity of the plasma membrane, cholesterol also dictates the lateral micro-organizations, such as lipid raft microdomains[6]. Lipid rafts are operatively defined as membrane regions that remain insoluble in cold (4°C) Triton X-100, or detergent-resistant membranes (DRMs)[7]. Caveolae, a subclass of lipid rafts, were first identified by electron microscopy of thin sections back in the 1950s[8, 9]. Their morphology is quite

characteristic, and is described as round membrane invaginations that are typically 60-80 nm in diameter[10] (Fig. 1.1A and B). They have no obvious coat[11], as is commonly seen in clathrin-coated pits. Caveolae formation requires sphingolipids, cholesterol, and oligomerized caveolin proteins anchored to the actin cytoskeleton[12]. In some cell types, such as endothelial cells and adipocytes, caveolae represent over a third of the total plasma membrane surface[10]. Despite their striking morphology and abundance in many tissues, the precise function of caveolae has been debated to this day and remains largely unknown. It is hypothesized that they are involved in endocytosis, transcytosis, potocytosis, tumor suppression, calcium signaling, cholesterol transport and regulation. Caveolae also play a role in positive or negative regulation of Ras-, NO-, G-protein-coupled receptor- and growth-factor-mediated signaling[12-15]. It has been postulated that caveolae could serve as a cellular reservoir for sphingolipids and cholesterol or even plasma membrane itself, as flattening of caveolae would significantly increase the surface area of the plasma membrane[10]. Overall, caveloae represent morphologically distinct sphingomyelin (SM)-cholesterol-rich microdomains, stabilized by the caveolin protein family[10].

1.1.3 Caveolin Protein Family

The major protein components of caveolae are the caveolin proteins. Specifically, they are known to play a structural role in the stabilization of these invaginations[8]. The caveolins are 21 kDa integral proteins that can dimerize via their caveolin scaffolding domains (CSD) (Fig. 1.1C). There are three main family members: caveolin-1 (CAV1), caveolin-2 (CAV2) and caveolin-3 (CAV3). CAV1 and CAV2 exist as different isoforms, and are usually co-expressed in most non-muscle cell types, such as fibroblasts, endothelial

Figure 1.1

Plasma membrane caveolae and caveolin proteins. ***A*** *and* ***B,*** Electron micrographs of small invaginations called caveolae in the plasma membrane of adipocytes. ***C,*** An illustration of a caveola and its structural proteins, caveolins. Caveolin proteins oligomerize at their caveolin scaffolding domains **(CSD)** and are partially inserted in the plasma membrane. The N- and C-terminal domains both reside in the cytoplasm, while the C-terminal domain contains three palmitoylation sites. The bottom panel depicts clustered caveolae structures. (Images adopted from figure 1 of Parton and Simons. *Nature Reviews Molecular Cell Biology 8, 185-19.* 2007)

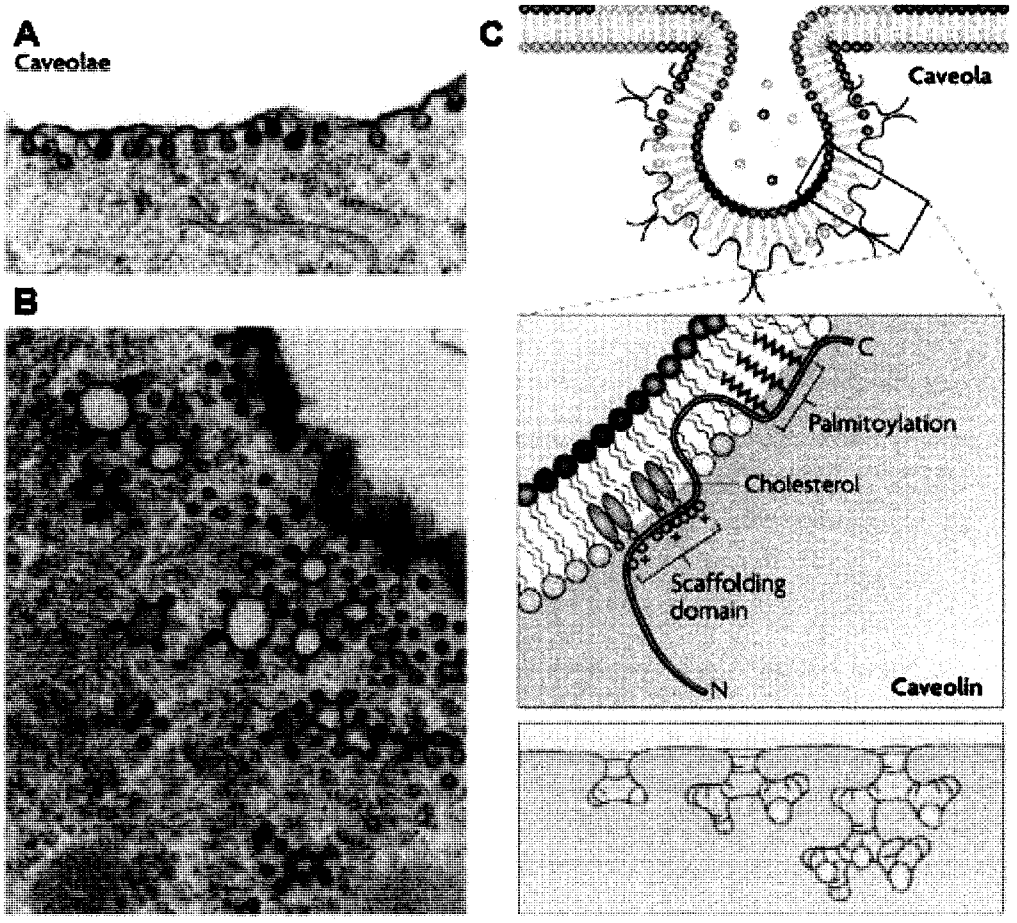
A
Caveolae
B
C
Caveola
C
Palmitoylation
Cholesterol
Scaffolding
domain
N
Caveolin

cells, and adipocytes. CAV3 is specific to skeletal, cardiac, and some smooth muscle cells[16, 17]. While most cell types contain caveolae, lymphocytes and some neuronal cells have been shown to lack caveolin, and therefore caveolae[18-20]. Interestingly, the expression of CAV1 or CAV3 alone can trigger caveolae formation, but not CAV2[9]. CAV2 participates in caveolae formation only when CAV1 is present. The formation of caveolae is dependent on the presence of plasma membrane cholesterol in tightly packed membrane regions. In fact, caveolin itself can bind 1-2 cholesterol molecules[21] and is palmitoylated in the C-terminal region[12] (Fig. 1.1C). The structure of caveolin proteins also contains a long putative intramembrane domain that is believed to anchor partially into the plasma membrane, flanked by cytosolic N- and C-terminal domains (Fig. 1.1C). It has been reported that a single caveolae invagination can contain ~144 molecules of caveolin[22] and ~20,000 molecules of cholesterol[23], along with plasma membrane enriched in glycosphingolipids and SM[10]. It is therefore not surprising that depletion of plasma membrane cholesterol leads to the disruption of caveolae[24]. Further evidence that caveolin proteins stabilize caveolae was found using a yeast two-hybrid screen. This screening identified the actin-binding protein filamin as a ligand for CAV1[25]. Correspondingly, if the actin cytoskeleton was reorganized, caveolae would subsequently redistribute[25]. The actin-anchoring of caveolin immobilizes caveolae structures, as demonstrated by fluorescence recovery after photobleaching (FRAP) of GFP-tagged CAV1. The mobile fraction of caveolin on the plasma membrane represents only 5-20% of the total membrane-associated caveolin protein[18].

In addition to the immobile caveolae-associated caveolin pool, there is an intracellular mobile pool of caveolin. This supports the idea that caveolin-associated vesicles are involved in the trafficking of proteins and/or lipids between multiple caveolin-associated

compartments, such as caveosomes or lipid droplets[18-20]. Interestingly, CAV1 in this intracellular mobile fraction has been suggested to bind cholesterol and form particles sharing the size[26] and buoyant density[27] of high density lipoprotein (HDL).

1.1.4 Caveolin-Dependent Formation of Caveolae

Caveolin proteins are synthesized as integral membrane proteins in the endoplasmic reticulum (ER), in a signal recognition particle (SRP)-dependent manner[28], and undergo subsequent oligomerization in this organelle[29]. The oligomerized caveolin proteins exit the ER in order to be transported to the Golgi, where they remain associated with the non-DRM fraction[30], as shown in Fig. 1.2. In the Golgi, a series of events occur leading to higher order oligomerization of caveolin, as well as association with lipid rafts. These modifications trigger the exit from the Golgi. This effectively shifts the newly formed caveolae rafts to the DRM fraction. Further evidence of this stems from the observation that specific quanta of GFP-tagged CAV1, that are similar in size to the mature caveolae seen at the plasma membrane, begin to appear at the Golgi exit sites of the trans Golgi network (TGN) and are trafficked directly to the plasma membrane[31]. In addition, antibodies that are specific for Golgi-localized CAV1 lose their ability to bind specific epitopes at the TGN. At the same time, CAV1 becomes recognizable to plasma membrane-specific CAV1 antibodies[32]. Interestingly, the exit of caveolin from the Golgi is accelerated when cholesterol is supplied[32], and inhibited by the depletion of glycosphingolipids[33]. These newly formed caveolin/caveolae structures shuttle to the plasma membrane (Fig. 1.2), and have been termed "exocytic caveolar carriers" by Parton and his group[10]. Many proteins have been

Figure 1.2

Caveolin-dependent formation of caveolae lipid rafts. The caveolin proteins are synthesized in the endoplasmic reticulum **(ER)** and are shuttled to the Golgi complex as detergent-soluble oligomers. Upon exit of the Golgi, the caveolin oligomers become associated with glycosphingolipid- and cholesterol-enriched lipid raft domains, marked by detergent-resistant membrane **(DRM)** association. Caveolin quanta are then shuttled directly to the membrane in caveolar carriers in a process dependent upon syntaxin-6, or by other poorly understood mechanisms. (Image adopted from figure 2 of Parton and Simons. *Nature Reviews Molecular Cell Biology 8, 185-19.* 2007)

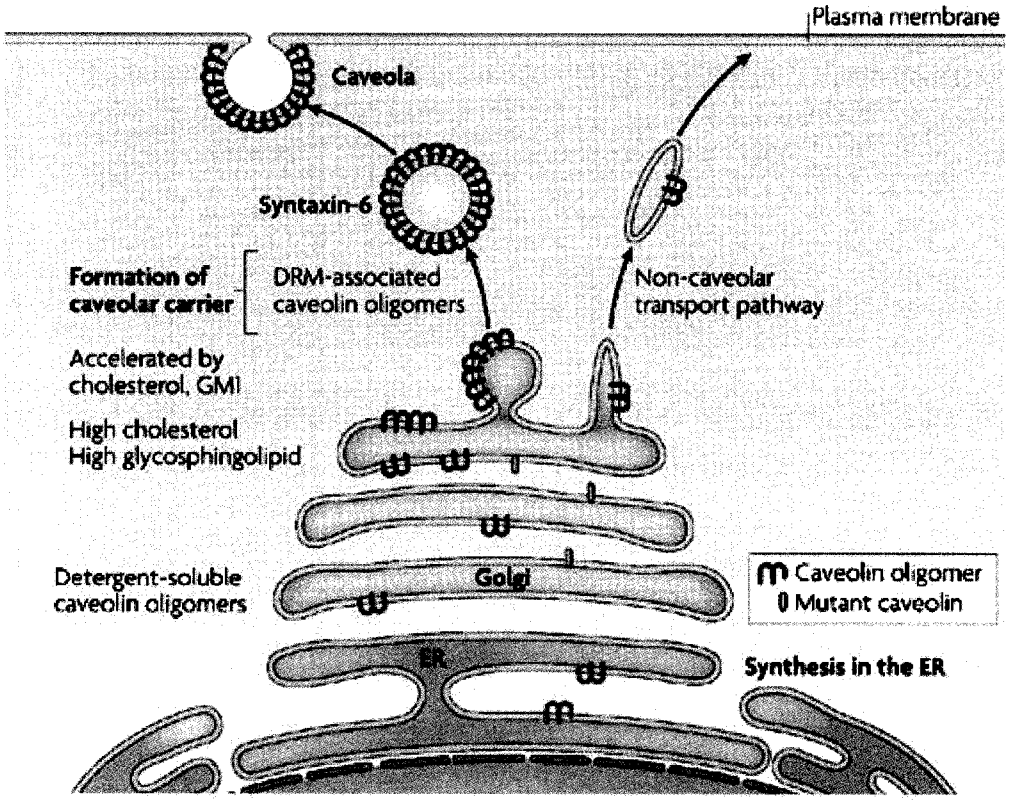
Plasma membrane
Caveola
Syntaxin-6
Formation of caveolar carrier
DRM-associated caveolin oligomers
Non-caveolar transport pathway
Accelerated by cholesterol, GM1
High cholesterol
High glycosphingolipid
Detergent-soluble caveolin oligomers
Golgi
Caveolin oligomer
Mutant caveolin
ER
Synthesis in the ER

shown to associate with these caveolar carriers, such as syntaxin-6, which ensures the proper delivery of CAV1, GPI-anchored proteins and GM1[34], although, GPI-anchored proteins do not require CAV1 for proper trafficking[35] (Fig. 1.2). Conversely, there are other proteins that depend on CAV1 for their trafficking to the plasma membrane. Those include dysferlin[36], the angiotensin receptor[37], the insulin receptor (IR)[38] and the stretch-activated channel short transient receptor potential channel-1 (TRPC1)[39, 40]. Whether CAV1 contributes to intracellular cholesterol trafficking or homeostasis is not clear at present.

1.1.5 Maintenance of Cellular Cholesterol Levels

Due to its critical importance in maintaining the cellular membrane and particularly in microdomain formation, cholesterol levels in cells are stringently regulated. With the exception of the liver and steroigenic tissues, somatic cells can not utilize cholesterol as a precursor for other products. The maintenance of cellular cholesterol levels is therefore mainly achieved by regulating biosynthesis and uptake. As cholesterol biosynthesis is extremely energy expensive, requiring 20 enzymes, 3 ATP and 7 molecules of reduced nicotinamide-adenine dinucleotide phosphate (NADPH), somatic cells have adopted an elegant scheme to coordinate cholesterol synthesis and uptake.

i) Regulation of Cholesterol Biosynthesis

Cholesterol biosynthesis is mainly regulated by a series of membrane-bound transcription factors known as sterol regulatory element-binding proteins (SREBPs). These transcription factors are comprised of three essential domains, namely the NH_2 domain, which contains the DNA binding bHLH-Zip region, the central domain containing two transmembrane (TM) projections separated by a short loop that enters the lumen of the ER,

and the C-terminal domain[41]. SREBPs are normally anchored to the ER membrane. Upon activation, SREBPs go through a series of proteolytic processes to release their DNA binding bHLH-Zip fragments, which act as transcriptional factors. There are three proteins responsible for initiating SREBP proteolytic processing[42]. The first is the SREBP cleavage-activating protein (SCAP) (Fig. 1.3A and B). SCAP binds SREBP through the C-terminal domain[41]. SCAP can also bind to two ER resident proteins designated as insulin-induced genes 1 and 2 (Insigs-1 and -2) (Fig. 1.3B). This forms a hetero-tetramer protein complex that retains SREBP in the ER. SCAP functions as the designated cholesterol sensor through its TM domains. In the event of cellular cholesterol shortage, SCAP changes its conformation and releases the Insigs, which can then be degraded by the ubiquitin-proteasome system (UPS)[43-45], as shown in Fig. 1.3B. This results in the exit of the SREBP/SCAP complex from the ER membrane to the Golgi apparatus via COPII-coated vesicles[46]. The Golgi houses two SREBP processing proteins known as Site-1 protease (S1P) and Site-2 protease (S2P)[41, 42](Fig. 1.3A). Upon entry of the SREBP/SCAP complex into the Golgi, membrane-bound S1P cleaves the SREBP protein at the small central loop connecting its two TM domains, thereby dividing SREBP in half. The N-terminal half of SREBP is then cleaved by the membrane-bound zinc metalloproteinase S2P, to release the bHLH-Zip domain from the Golgi membrane[41] (Fig. 1.3A). The free bHLH-zip domain, designated as nuclear SREBP (nSREBP), readily translocates to the nucleus. Once in the nucleus, it binds to nonpalindromic sterol response elements (SREs) in gene promoter/enhancer regions[41]. This results in the transcriptional activation of more than 30 genes dedicated to the synthesis and uptake of cholesterol, fatty acids, triglycerides,

Figure 1.3

Sterol-mediated proteolytic regulation of SREBP. ***A***, SCAP functions as a sterol sensor and a shuttle protein of SREBP. When sterol levels become depleted, the SREBP/SCAP complex shuttles to the Golgi complex via COPII vesicles. Upon entry into the Golgi, membrane-bound site-1 protease **(S1P)** cleaves the SREBP protein at the small central loop connecting its two TM domains, thereby dividing SREBP in half. The N-terminal half of SREBP is then cleaved by the membrane-bound site-2 protease **(S2P)**, thereby releasing the bHLH-zip domain from the Golgi membrane. The free bHLH-zip domain readily translocates to the nucleus. Once in the nucleus, it binds to nonpalindromic sterol response elements **(SREs)** in gene promoter/enhancer regions of genes involved in synthesis and uptake of cholesterol, fatty acids, triglycerides, phospholipids and NADPH. ***B***, SCAP can binds to two ER resident proteins designated as insulin-induced genes 1 and 2 **(Insigs-1 and -2)**, which retains the SREBP/SCAP complex in the ER. Following cholesterol depletion, the Insigs are released and SREBP/SCAP is free to shuttle to the Golgi. When cholesterol levels are replenished, sterol binding of SREBP/SCAP triggers a conformational change that causes the SREBP/SCAP complex to bind to the Insigs. This retains SREBP/SCAP in the ER. (*A*, Image was adopted from figure 1 of Horton *et al. J Clin Invest.109(9):1125-31.*2002. *B*, Image was adopted from figure 3 of Goldstein *et al. Cell.124(1):35-46.*2006)

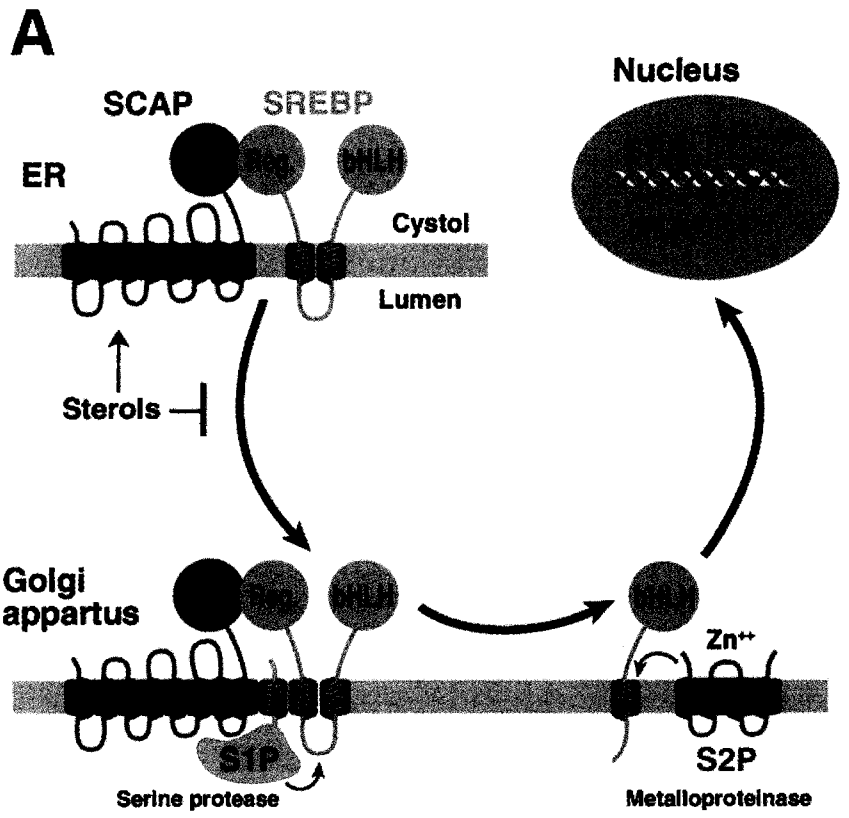
A
SCAP
SREBP
ER
Cystol
Lumen
Nucleus
Sterols
Golgi
appartus
Zn++
S1P
S2P
Serine protease
Metalloproteinase

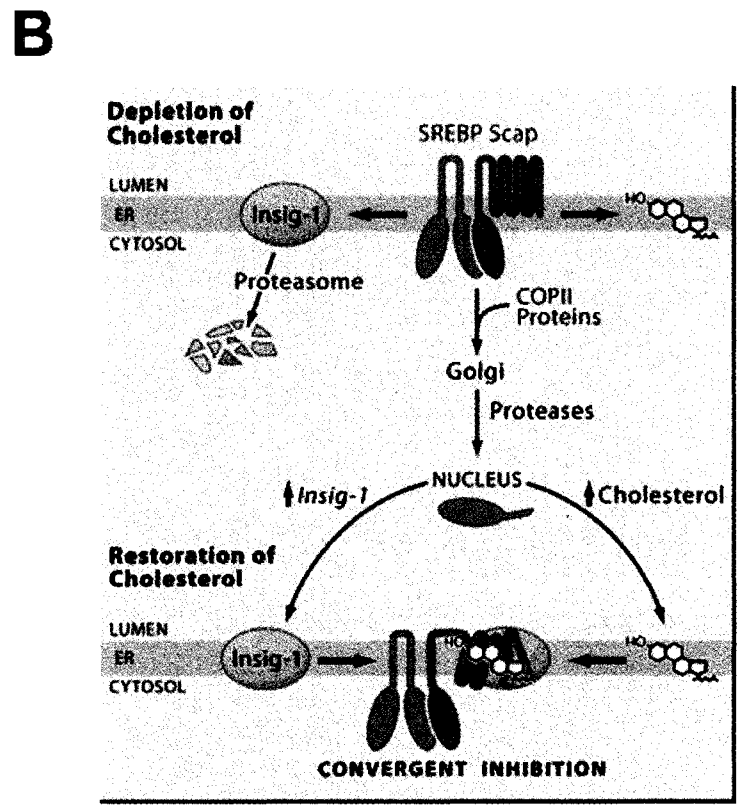
B
Depletion of
Cholesterol
SREBP Scap
LUMEN
ER
CYTOSOL
Insig-1
Proteasome
COPII
Proteins
Golgi
Proteases
Insig-1
NUCLEUS
Cholesterol
Restoration of
Cholesterol
LUMEN
ER
CYTOSOL
Insig-1
CONVERGENT INHIBITION

phospholipids and NADPH[47-50]. Conversely, when there is an excess of cholesterol, the sterol binds to SCAP[51], altering its conformation and causing the SREBP/SCAP complex to bind to Insigs[52](Fig. 1.3B). Consequently, this event inhibits the interaction of SCAP with the COPII coat proteins Sar1 and Sec23/24. As a result, the SREBP/SCAP complex is excluded from the COPII-coated vesicles departing the ER[46]. This effectively halts the transcriptional activation of the corresponding genes of cholesterol synthesis and uptake.

The rate-limiting enzyme of cholesterol biosynthesis in the ER, 3-hydroxy-3-methylglutaryl-CoA (HMG-CoA) reductase, is one of the major enzymes under the control of the SREBP regulation system[53]. HMG-CoA reductase readily catalyzes the conversion of HMG-CoA to mevalonic acid in response to cellular cholesterol depletion. Interestingly, the Insigs not only play a role in regulating SREBP transcriptional activity, but also control the posttranslational regulation of HMG-CoA reductase. In times of low sterol levels inside the cell, HMG-CoA reductase is active with a half-life exceeding 12 hours[53]. As cholesterol levels become elevated, sterols cause Insigs to bind the sterol-sensitive domain of HMG-CoA reductase, thereby marking it for ubiquitination and degradation[53] (Fig. 1.4). Interestingly, cholesterol is only a weak inducer of this degradation, while lanosterol, a precursor of cholesterol, is a potent inducer of HMG-CoA reductase degradation. A fraction of Insigs are bound to a complex consisting of an E3 ubiquitin ligase (gp78), an E2 ubiquitin-conjugating enzyme (Ubc7) and an ATPase (VCP). This Insig/ubiquitination complex rapidly binds HMG-CoA reductase in response to lanosterol binding, which quickly reduces the half-life of the reductase to less than 1 hour. Following ubiquitination of HMG-CoA reductase by Ubc7, it is extracted from the ER membrane by VCP and delivered to the proteasome for degradation[53] (Fig. 1.4). Taken together, Insigs stand at the junction

Figure 1.4

Regulation of HMG-CoA reductase degradation by Insigs. 3-hydroxy-3-methylglutaryl-CoA **(HMG-CoA)** reductase readily catalyzes the conversion of HMG-CoA to mevalonic acid in response to cellular cholesterol depletion, and is the rate-limiting enzyme of cholesterol synthesis. The degradation of HMG-CoA reductase is tightly controlled by the Insigs. During cholesterol accumulation, lanosterol causes HMG-CoA reductase to bind the Insigs. Insigs exist in a complex with a membrane-embedded E3 ubiquitin ligase **(gp78)**, an E2 ubiquitin-conjugating enzyme **(Ubc7)** and an ATPase **(VCP).** Following binding to HMG-CoA reductase, the enzyme is ubiquitinated by Ubc7, shuttled to the proteasome via VCP and the sterol geranylgeraniol and is degraded. (Image was adopted from figure 5 of Goldstein *et al. Cell.124(1):35-46.*2006)

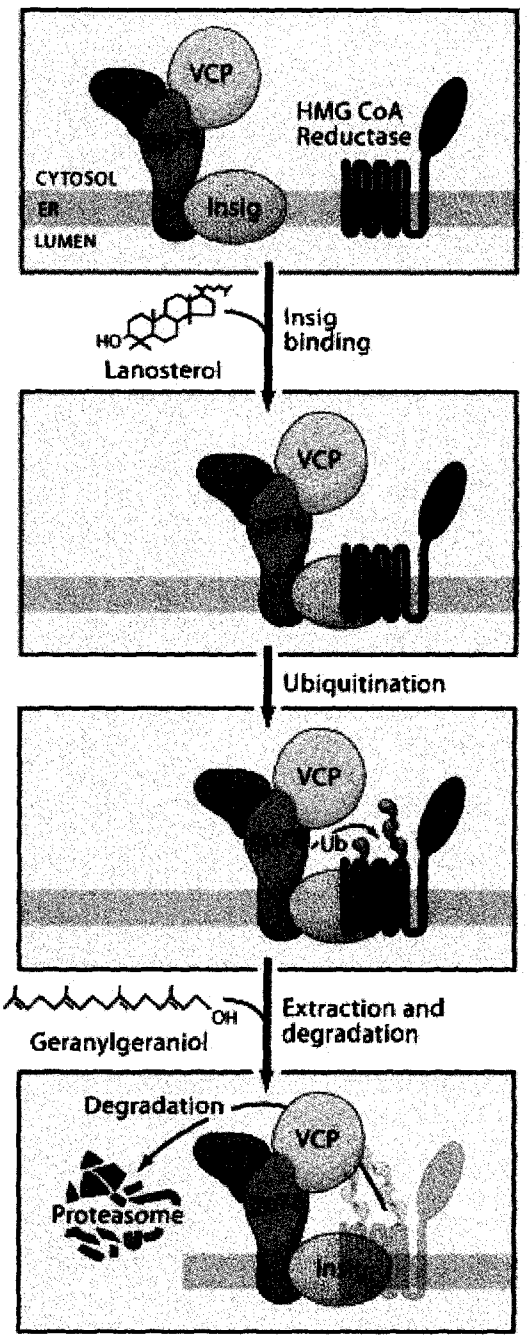
VCP
HMG CoA
Reductase
CYTOSOL
ER
LUMEN
Insig
HO
Lanosterol
Insig
binding
VCP
Ubiquitination
VCP
Ub
OH
Geranylgeraniol
Extraction and
degradation
Degradation
VCP
Proteasome

between the transcriptional and posttranscriptional regulatory mechanisms in order to assure cholesterol homeostasis.

ii) Regulation of Cholesterol Uptake

As mentioned above, another equally important function attributed to SREBP activation is the regulation of cholesterol uptake. The endogenous biosynthesis of cholesterol is expensive in terms of energy consumption. Animal cells must therefore efficiently utilize cholesterol from dietary sources present in the circulation. This is achieved mainly through the SREBP-induced upregulation of cell surface receptors. These receptors bind to plasma-derived cholesterol in the form of lipoproteins and facilitate the uptake cholesterol during times of cholesterol depletion. Once the cellular pool of cholesterol is replenished, SREBPs will downregulate receptor synthesis and thereby terminate cholesterol uptake.

1.1.6 Cholesterol Homeostasis in Humans

Plasma-derived cholesterol is transported through the circulation by lipoproteins. These complex particles generally consist of a core of neutral lipids, triglycerides (TG) and/or cholesteryl esters (CE), and a surface monolayer of amphipathic lipids i.e. phospholipids and FC[54]. In addition to the lipid components, lipoproteins also contain protein motifs named apolipoproteins. These apolipoproteins are crucial for the formation, conversion and clearance of lipoproteins. Plasma lipoprotein cholesterol is supplied through two major pathways: a) Intestinal dietary chylomicrons, and b) Hepatic synthesis/secretion of very low-density lipoproteins (VLDL). Both pathways involve the formation of

lipoproteins containing apolipoprotein B, or apoB. Human intestinal enterocytes synthesize N-terminal 48% of the full length gene (apoB-48), while hepatocytes synthesize the full length version, apoB-100[54]. During lipid absorption from the diet, cholesterol-derived bile acids serve to emulsify lipids so that they can be taken up from the intestinal lumen. Chylomicron formation has been suggested to occur through a two-step process[55] shown in detail in Fig. 1.5. First, apoB-48 is translated and lipidated with phospholipids and small amounts of TG in the rough ER (RER) by microsomal triglyceride transfer protein (MTP). This forms a primordial particle, which is then rapidly transported to the smooth ER (SER)[56]. This initial lipidation of apoB-48 is critical for the avoidance of premature degradation. Second, MTP mediates bulk lipidation of the primordial chylomicrons through the association with lipid droplets[55]. Following incorporation of apoA-IV, the nascent chylomicron particles are then packaged into prechylomicron transport vesicles (PTV) and shuttled to the *cis*-Golgi, a process believed to be the rate-limiting step of lipid absorption[57]. Once in the Golgi complex, the glycosylation status of apoB-48 is modified, apoA-I is incorporated, and the chylomicron is exocytosed from the basal membrane into the lymphatic system, eventually reaching the blood via the thoracic duct[55].

VLDL particles are believed to be produced in the hepatocytes in a similar two-step mechanism[54]. VLDL formation utilizes the full-length isoform, apoB-100, which contains the low-density lipoprotein receptor (LDLR) binding domain[54]. Again, apoB-100 is co-translationally lipidated with phospholipids and also TG by MTP. The lipid species that are incorporated into VLDL particles are formed mainly through *de novo* biogenesis. The availability of cholesterol and fatty acid species greatly affects the assembly/secretion of VLDL particles in the hepatocytes[58]. Once assembly is complete, VLDL particles are

Figure 1.5

The two-step model of chylomicron formation. Free fatty acids **(FFAs)** and monoacylglycerides **(MAG)** cross the brush border membrane and are translocated to the endoplasmic reticulum **(ER)** by fatty acid binding proteins **(FABP)**. First, apoB-48 is translated and lipidated with phospholipids and small amounts of dietary triglycerides **(TG)** in the rough ER **(RER)** by microsomal triglyceride transfer protein **(MTP)**. This forms a primordial particle, which is then rapidly transported to the smooth ER **(SER)**. Second, MTP mediates bulk lipidation of the primordial chylomicrons **(CV)** through association with lipid droplets. Following incorporation of apoA-IV, the nascent chylomicron particles are then packaged into prechylomicron transport vesicles **(PCTV)** and shuttled to the *cis*-Golgi. Once in the Golgi complex, the glycosylation status of apoB-48 is modified, apoA-I is incorporated, and the chylomicron is exocytosed from the basal membrane into the lymphatic system, eventually reaching the blood via the thoracic duct. (Image adopted from figure 1 of Black.*Am J Physiol Gastrointest Liver Physiol.293(3):G519-24.* 2007)

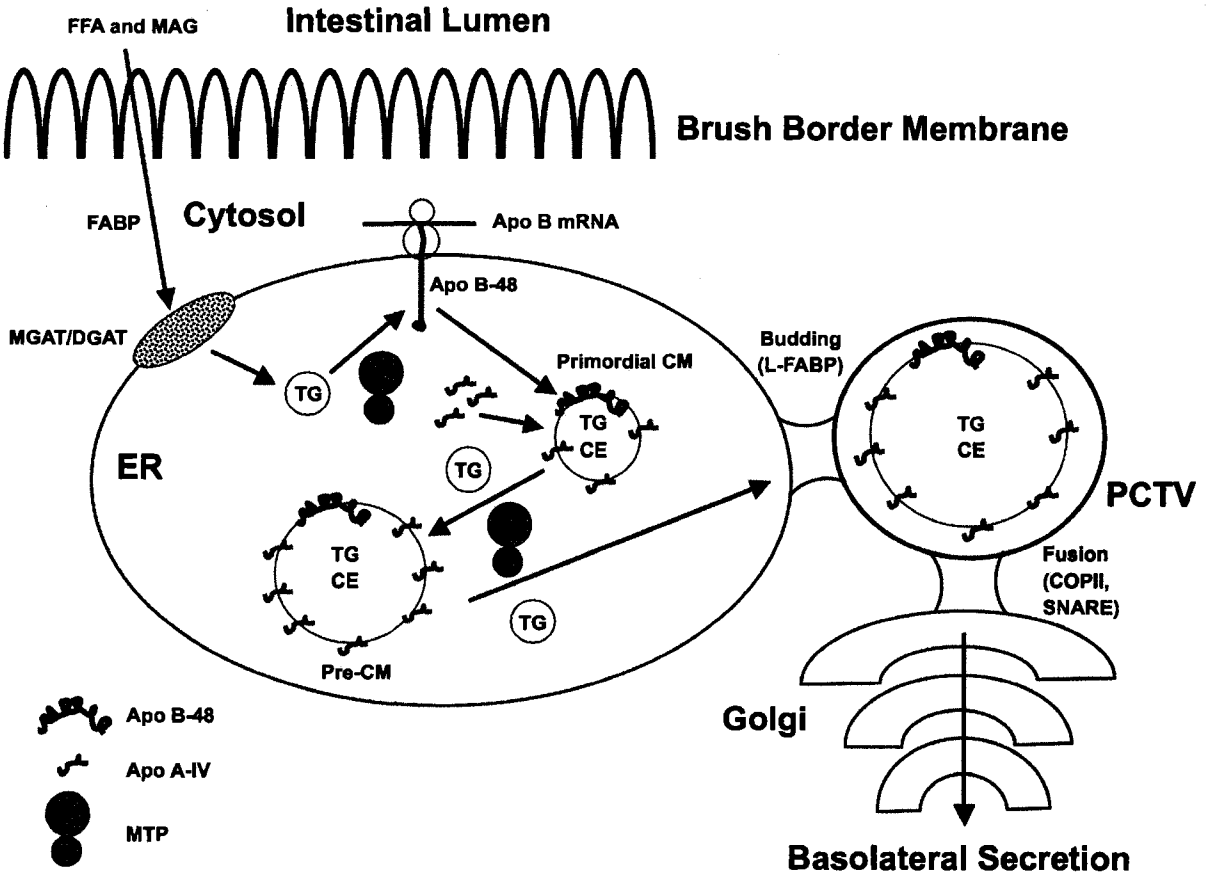
FFA and MAG
Intestinal Lumen
Brush Border Membrane
FABP
Cytosol
Apo B mRNA
Apo B-48
MGAT/DGAT
TG
Primordial CM
TG
CE
ER
TG
TG
CE
Pre-CM
TG
Budding
(L-FABP)
TG
CE
PCTV
Fusion
(COPII,
SNARE)
Golgi
Basolateral Secretion
Apo B-48
Apo A-IV
MTP

exocytosed into the plasma, where they deliver lipids, including cholesterol, to the peripheral tissues.

Once these lipoproteins have reached the plasma, they become enriched in apoC-I, apoC-II and apoE. In the case of chylomicrons, their apoA-I and apoA-IV content decreases progressively through exchange with HDL. The chylomicron and VLDL particles circulate in the plasma, where their TG core undergoes hydrolysis by endothelial-bound lipoprotein lipase (LPL)[55], and to a lesser extent by hepatic lipase (HL)[59]. This results in a transfer of free fatty acids (FFAs) to muscle cells and adipocytes for energy conversion and energy storage, respectively. This hydrolysis also produces relatively TG-deficient/cholesterol-rich chylomicron and VLDL remnants, known as β-VLDL particles. As β-VLDL particles are further remodeled, they form intermediate-density lipoproteins (IDL) and eventually low-density lipoproteins (LDL). LDL is the major source of cholesterol and lipids for peripheral tissues via the LDLR pathway that is regulated by the SREBPs[60].

Under normal physiological conditions, β-VLDL remnants, including IDL and LDL, are returned to the liver also through the LDLR pathway[59]. The hepatic uptake of remnants is mediated by apoB-100 and apoE through their binding to LDLR and LDLR related protein (LRP)[59]. This allows for the endocytosis of these particles by the receptor-mediated pathway[60]. The importance of LDLR was discovered through a human disease, familial hypercholesterolemia, where LDLR was mutated and thus dysfunctional. Affected individuals have extremely high levels of circulating LDL and VLDL[61]. The essential role of LDLR, as well as apoE, in maintaining plasma cholesterol levels has also been clearly demonstrated through transgenic animal models. ApoE KO mice showed defective remnant clearance and high plasma cholesterol[62, 63], similar to the LDLR KO animal[64]. Conversely,

infusion of apoE into cholesterol-fed rabbits was able to accelerate the clearance of β-VLDL from the plasma and enhance the uptake into hepatocytes[65].

1.1.7 Avoidance of Excess Cholesterol Accumulation

i) Intracellular Mechanism

Although somatic cells are equipped with molecular mechanisms, such as SREBPs, that tightly control cholesterol biosynthesis and uptake in order to avoid cholesterol accumulation, there are many situations in which unregulated cholesterol uptake occurs. For example, modified LDL can be taken up through scavenger receptors, a process which is not controlled by SREBP. Macrophages can also accumulate excess cholesterol through phagocytosis of apoptotic corpses. In order to avoid the toxic accumulation of FC, most cell types are capable of esterifying FC into CE. This reaction is mediated by the microsomal enzyme acyl-coenzyme A:cholesterol acyltransferase (ACAT)[66]. ACAT has two isoforms, ACAT-1 and ACAT-2. These isoforms are different with regard to their chromosomal gene locations, tissue-specific expression, and substrate specificity[67]. In humans, ACAT-1 is expressed in macrophages and most other cell types. ACAT-2, on the other hand, is expressed primarily in intestinal epithelial cells. In contrast, mice express only the ACAT-2 isoform[66]. The activity of ACAT is mostly driven by FC availability. When cellular FC is low, there is little ACAT activity and minimal conversion of FC to CE, while SREBPs are activated to increase both cholesterol synthesis and uptake. When cellular FC is high, the SREBP pathways shut down and ACAT is fully activated to convert the excess FC into storable CE. This stored cholesterol can supply the future demands of the cell, particularly during cellular division. However, for quiescent cells like those found in most non-

steroigenic or non-hepatic tissues, there is little need for the extensive storage of cholesterol. Under these circumstances, a specialized pathway termed reverse cholesterol transport (RCT) is required to remove excess cholesterol.

ii) Reverse Cholesterol Transport

In contrast to hepatic secretion of apoB-containing lipoproteins that supply cholesterol to the peripheral tissues, RCT is, as the name implies, a pathway that brings excess cholesterol from the peripheral tissues back to the liver where it can be excreted. The RCT process begins with the secretion of apoA-I, primarily by the liver and intestine[68]. Plasma apoA-I readily interacts with both hepatic and peripheral cells to become minimally lipidated with phospholipids and FC. This results in the formation of nascent HDL (Fig. 1.6A and B). Newly formed nascent HDL is a discoidal particle that begins to acquire additional cholesterol in the circulation through multiple mechanisms. First, as FC is slightly water-soluble (solubility in water is $\sim 10^{-8}$M), it can transfer from cell membranes to nascent HDL by an aqueous diffusion mechanism[69]. This is a bidirectional mechanism in which FC diffuses down its concentration gradient. FC can diffuse from the cell membranes, where the FC concentration is relatively high, to the discoidal HDL particles that are relatively FC-deficient[69]. Secondly, nascent HDL can acquire cholesterol through the association with a cell surface receptor, scavenger receptor class-B, type 1 (SR-BI). This is also a bidirectional, concentration gradient-driven process, therefore requiring higher FC in the cellular membrane relative to HDL[69]. In a third mechanism, HDL can become associated with plasma membrane domains formed by ATP-binding cassette transporter G-1 (ABCG1) to

Figure 1.6

Detailed overview of the reverse cholesterol transport pathway. ***A-C***, Phospholipids **(PL)** and free cholesterol **(FC)** are transferred from cells, such as macrophages, to apolipoprotein A-I **(apoA-I)** by ATP-binding cassette transporter A-1 **(ABCA1)** forming pre-β-HDL. Through the activity of lecithin cholesterol acyltransferase (LCAT), pre-β-HDL is converted to mature α-HDL. ***D***, Mature α-HDL is converted between α_3-HDL and α_2-HDL subspecies by LCAT, endothelial lipase **(EL)** and hepatic lipase **(HL)**. ***E***, Mature α-HDL continues to acquire FC from plasma membrane domains via ATP-binding cassettes G1/G4 **(ABCG1/G4).** ***F***, Indirect pathway of hepatic cholesterol uptake via cholesterol ester transfer protein **(CETP)**, which transfers cholesterol to low-density lipoproteins **(LDL)** and very low-density lipoproteins **(VLDL)**. LDL and VLDL are subsequently taken up via hepatic LDL receptors. ***G***, Direct pathway of hepatic cholesterol uptake via HDL binding to scavenger receptor class-B, type 1 **(SR-BI)**. The cholesterol is then converted to bile acids, and excreted. (Image adopted from figure 2 of Singh *et al. JAMA. 298(7):786-98.* 2007)

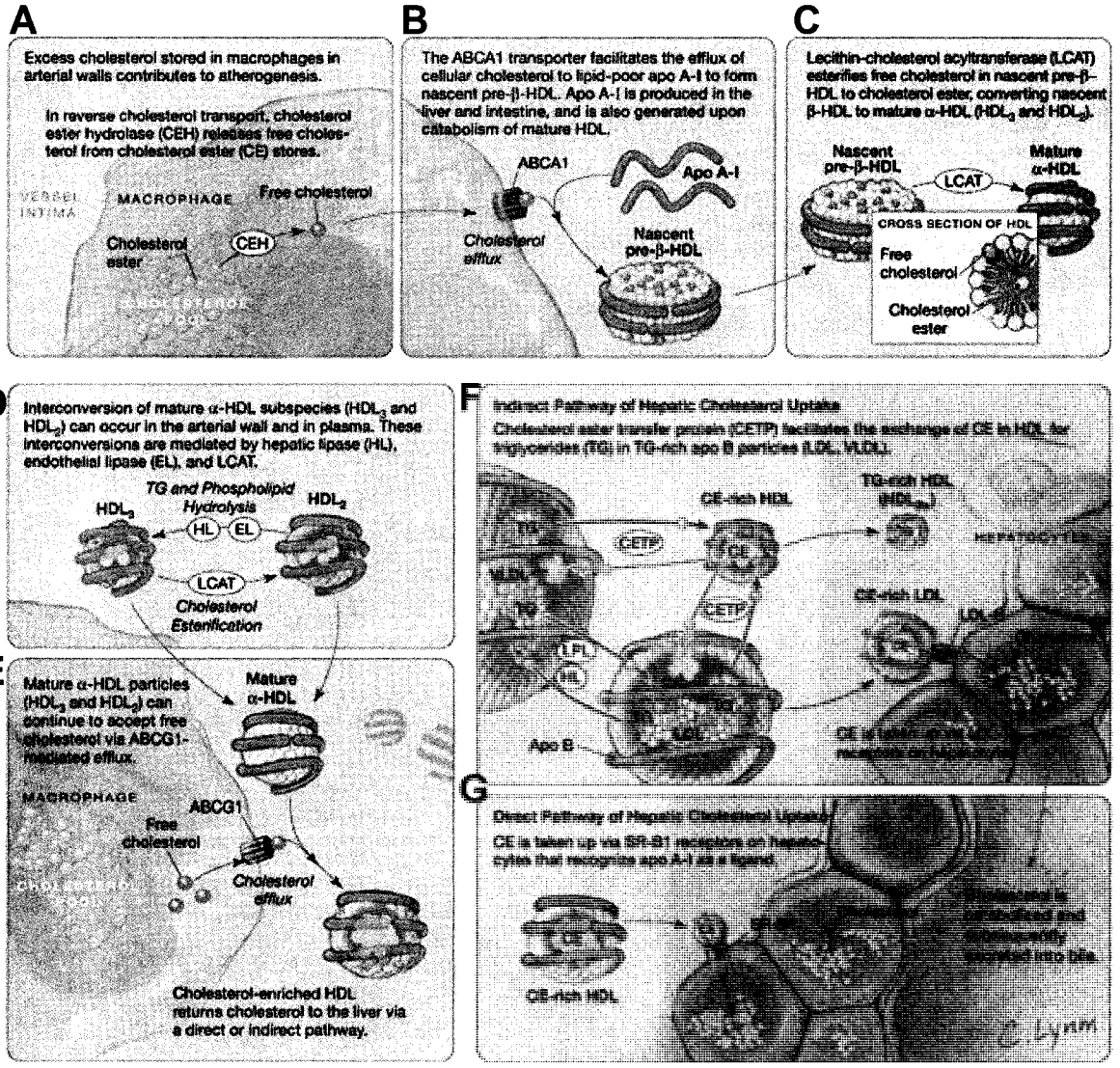
A
Excess cholesterol stored in macrophages in arterial walls contributes to atherogenesis.
In reverse cholesterol transport, cholesterol ester hydrolase (CEH) releases free cholesterol from cholesterol ester (CE) stores.
VESSEL INTIMA
MACROPHAGE
Free cholesterol
Cholesterol ester
CEH
B
The ABCA1 transporter facilitates the efflux of cellular cholesterol to lipid-poor apo A-I to form nascent pre-β-HDL. Apo A-I is produced in the liver and intestine, and is also generated upon catabolism of mature HDL.
ABCA1
Apo A-I
Cholesterol efflux
Nascent pre-β-HDL
C
Lecithin-cholesterol acyltransferase (LCAT) esterifies free cholesterol in nascent pre-β-HDL to cholesterol ester, converting nascent β-HDL to mature α-HDL (HDL3 and HDL2).
Nascent pre-β-HDL
LCAT
Mature α-HDL
CROSS SECTION OF HDL
Free cholesterol
Cholesterol ester
D
Interconversion of mature α-HDL subspecies (HDL3 and HDL2) can occur in the arterial wall and in plasma. These interconversions are mediated by hepatic lipase (HL), endothelial lipase (EL), and LCAT.
TG and Phospholipid Hydrolysis
HDL3
HDL2
HL
EL
LCAT
Cholesterol Esterification
E
Mature α-HDL particles (HDL3 and HDL2) can continue to accept free cholesterol via ABCG1-mediated efflux.
Mature α-HDL
MACROPHAGE
ABCG1
Free cholesterol
Cholesterol efflux
Cholesterol-enriched HDL returns cholesterol to the liver via a direct or indirect pathway.
F
Indirect Pathway of Hepatic Cholesterol Uptake
Cholesterol ester transfer protein (CETP) facilitates the exchange of CE in HDL for triglycerides (TG) in TG-rich apo B particles (LDL, VLDL).
CE-rich HDL
TG-rich HDL (HDL3)
CETP
VLDL
TG
CE-rich LDL
LDL
LPL
HL
Apo B
G
Direct Pathway of Hepatic Cholesterol Uptake
CE is taken up via SR-B1 receptors on hepatocytes that recognize apo A-I as a ligand.
CE-rich HDL

acquire cholesterol (Fig. 1.6E). Another transporter, ABCG4, has been shown to function similarly to ABCG1 in many cell types, but not in macrophages[70]. The evidence from Vaughan and Oram indicated that phospholipid-rich nascent HDL particles can acquire FC from the plasma membrane domains formed upon expression of ABCG1/G4. This association resulted in the remodeling of nascent HDL particles to larger, more cholesterol-rich HDL, or pre-β_2 HDL[71]. In addition, plasma lipid transfer proteins play a major role in HDL metabolism and RCT. Once HDL has acquired sufficient FC to become pre-β_2 HDL, it becomes associated with an enzyme, lecithin cholesterol acyltransferase (LCAT), that esterifies FC to CE, and subsequently transfers the CE to the core of HDL[72] (Fig. 1.6C). Largely due to the activity of LCAT, which is activated primarily by apoA-I, pre-β_2 HDL particles become larger, more spherical, CE-rich α_3-HDL particles. This action is also necessary in order to prevent FC reuptake by the cells. Continued acquisition of FC through the mechanisms described above lead to the formation of even larger α_1-HDL particles[73]. Importantly, α-HDL particles also serve as effective acceptors of FC from the domains formed by ABCG1/ABCG4.

HDL is then further remodeled by plasma lipid transfer proteins, such as cholesterol ester transfer protein (CETP) and phospholipid transfer protein (PLTP) (Fig. 1.6F). CETP is secreted primarily by the liver and mediates the net transfer of CE from HDL to apoB-containing lipoproteins (VLDL/LDL)[72]. PLTP mediates the net transfer of phospholipids from VLDL/LDL particles to HDL[74]. The overall formation of larger, spherical α-HDL particles allows for further hydrolysis of phospholipids and TG by HL, LPL and, most importantly, binding to the SR-BI receptor in the liver[73]. SR-BI mediates the selective uptake of CE from HDL to the hepatocytes, thus regenerating smaller α_3-HDL particles and

free apoA-I (Fig. 1.6G). This free apoA-I can then initiate a new cycle of the RCT process[73]. Cholesterol transferred from HDL to VLDL/LDL is also taken up by the liver through the LDLR pathway[72]. Cholesterol taken up into the hepatocytes is converted to bile acids by the rate-limiting enzyme 7α-hydroxylase[75]. These bile acids are then pumped into the bile by ABCG5/ABCG8[76, 77] and subsequently excreted, successfully completing the RCT cycle.

1.1.8 Atherosclerosis

The effectiveness of RCT is crucial to prevent cholesterol accumulation in peripheral tissues including arterial blood vessel walls. When RCT is compromised, the major consequence is atherosclerosis. Atherosclerotic coronary artery disease (CAD) is the leading cause of morbidity and mortality worldwide[78]. According to the 2004 report *Causes of Death, 2002*, released by Statistics Canada, cardiovascular disease claimed the lives of 74,626 Canadians in 2002. 54% of this death toll was attributed specifically to CAD. Atherosclerosis itself is defined as the inflammation-driven arteriole plaque formation and subsequent hardening of the arteries. In humans, approximately 66% of plasma cholesterol is transported by LDL, while ~20% is contained in HDL[2]. This becomes significant when we consider that LDL-cholesterol (LDL-C) is a major coronary risk factor in the general population[79], while HDL-cholesterol (HDL-C) is inversely related to CAD[80]. Through various mechanisms linked to oxidative stress, LDL particles can become oxidized (oxLDL) and can cross the intima of the aorta, coronary, carotid and/or cerebral arteries and enter the subendothelium[81]. While the uptake of native LDL is highly controlled through the transcriptional regulation of the LDLR, subendothelial macrophages readily uptake oxLDL

in an unregulated manner through the scavenger receptors[81]. These oxLDL receptors include scavenger receptors A (SR-A) and SR-BI, CD36, CD68, lectin-like oxLDL receptor (LOX-1) and the scavenger receptor that binds to phosphatidylserine (PS) (SR-PSOX)[82-85]. SR-A and CD36 are reported to be the primary receptors in the uptake of oxLDL[86]. The first step of atherosclerosis involves the dysfunction of the endothelium. This causes increased permeability to lipoproteins and other plasma constituents, the upregulation of endothelial adhesion molecules and migration of leukocytes into the artery wall[87] (Fig. 1.7A). The second step is marked by fatty-streak formation, which is the consequence of lipid-laden macrophage (foam cells) accumulation. Chemokines released by the foam cells further accelerate leukocyte chemotaxis and accumulation in the subendothelium, which installs a vicious cycle of foam cell formation[87] (Fig. 1.7B). Additionally, there is a steady increase in FC and a decrease in CE content as macrophages progress to foam cells in more advanced lesions[88]. Later stages of this second step lead to the secretion of multiple factors, which lead to the migration of smooth muscle cells into the intima[87] (Fig. 1.7B). As the fatty streaks grow and mature into intermediate and advanced lesions, they develop fibrous caps, which segregate the lesion from the arterial lumen. This marks the third step of plaque formation, stemmed by a healing or fibrous response to the injury[87]. The fibrous cap covers a combination of leukocytes, lipids and debris and can also contain a necrotic core as a result of apoptotic foam cells. During this stage, leukocyte chemotaxis continues leading to lesion growth at the extremities[87] (Fig. 1.7C). The final stage of atherosclerotic lesion formation is marked by unstable fibrous plaques, and is by far the most serious stage. At this point, the advanced lesion can develop thinning sections of the fibrous cap, which are susceptible to rupture or ulceration leading to thrombosis[87] (Fig. 1.7D). The continued influx and

Figure 1.7

Overview of the inflammatory response in atherosclerosis. ***A***, The first step of atherosclerosis involves the dysfunction of the endothelium. This causes increased permeability to lipoproteins and other plasma constituents, the upregulation of endothelial adhesion molecules and migration of leukocytes into the artery wall. ***B***, The second step is marked by fatty-streak formation, which is the consequence of lipid-laden macrophage (foam cells) accumulation. Chemokines released by the foam cells further accelerate leukocyte chomotaxis and accumulation in the subendothelium. Later stages of this second step lead to the secretion of multiple factors, which lead to the migration of smooth muscle cells into the intima. ***C***, The third step of plaque formation involves a healing or fibrous response to the injury. As the fatty streaks grow and mature into intermediate and advanced lesions, they develop fibrous caps, which segregate the lesion from the arterial lumen. ***D***, The continued influx and activation of macrophages at the lesion site is responsible for the thinning of the fibrous cap, due to metalloproteinase and other proteolytic enzymes released at the lesion site. This leads to hemorrhage from the vasa vasorum or from the arterial lumen. The end result is thrombus formation and occlusion of the artery. (Images *A-D* were adopted from figures 1-4 from Ross. *N Engl J Med.340(2):115-26.* 1999)

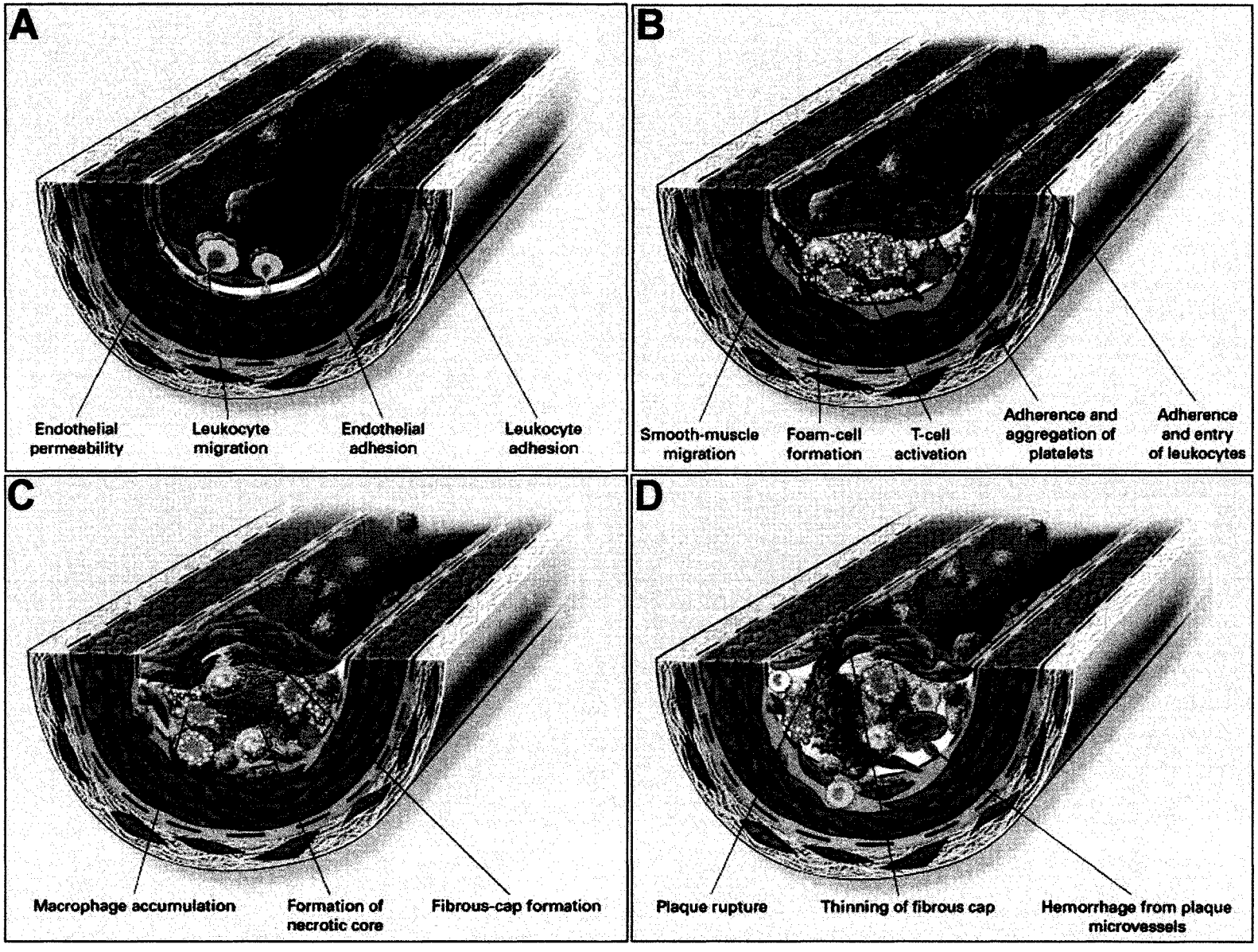
A
Endothelial permeability
Leukocyte migration
Endothelial adhesion
Leukocyte adhesion
B
Smooth-muscle migration
Foam-cell formation
T-cell activation
Adherence and aggregation of platelets
Adherence and entry of leukocytes
C
Macrophage accumulation
Formation of necrotic core
Fibrous-cap formation
D
Plaque rupture
Thinning of fibrous cap
Hemorrhage from plaque microvessels

activation of macrophages at the lesion site is responsible for the thinning of the fibrous cap, due to metalloproteinase and other proteolytic enzymes released at the lesion site. These enzymes degrade the matrix of the lesion, leading to hemorrhage from the vasa vasorum or from the arterial lumen. The dangerous end result is thrombus formation and occlusion of the artery[87] (Fig. 1.7D). In order to avoid the development of late stage atherosclerosis, it is essential to reduce the levels of LDL/oxLDL and to promote the mechanisms of RCT, particularly the transport of cholesterol from lipid-laden macrophages back to the liver. This cholesterol transport process is mediated by ATP-binding cassette tranporter A-1.

1.2 ATP-Binding Cassette Transporter A-1 (ABCA1)

1.2.1 Tangier Disease (TD)

During the early 1960s, Dr. Donald S. Fredrickson traveled to Tangier Island located in Chesapeake Bay. This small isle was situated 20 miles west of the eastern shore of Virginia, and was isolated both economically and socially from the mainland[89]. He was searching for additional cases of a strange illness that was discovered in a 5-year-old boy, native to the island. This mysterious disease was characterized by a striking phenotype involving large, yellowish-gray tonsils encompassing CE-loaded macrophages, splenomegaly, peripheral neuropathy and atherosclerosis. Most notably, he had an extreme deficiency in plasma apoA-I and HDL[90]. Not surprisingly, Dr. Fredrickson soon determined that a sister of the young boy shared the same phenotype, which led him to term the novel illness Tangier Disease (TD)[90].

Originally in the 1980s, a faulty conversion of pro-apoA-I to mature apoA-I, either through a defect in the converting enzyme or mutation in apoA-I, was believed to cause

TD[91], but this explanation was later disregarded following a series of studies[92, 93]. The field of TD research then shifted focus towards the determination of a dysfunctional HDL receptor. This resulted in the discovery of over 40 different HDL-binding partners, all of which were not found to be missing or dysfunctional in TD[89]. It was not until the mid-1990s that four different groups reported that Tangier cells were specifically impaired in their ability to efflux cholesterol and phospholipids, not to HDL, but to lipid-poor apoA-I, such as pre-β-HDL[94-97]. Interestingly, Hara and Yokoyama had shown previously that lipids could be effluxed to lipid-poor apoA-I, but physiological significance was not established until the link to TD was uncovered[98]. Once it was determined that the conversion of apoA-I to nascent HDL was defective in TD, four years would pass before Rust and colleagues mapped the genetic defect in TD to chromosome 9q31, in 1998[99]. In 1999, three independent groups published the long awaited news that the mutated protein in TD was the ATP-binding cassette (ABC) transporter 1 (later termed ABCA1)[100-102].

1.2.2 Structure and Topology of ABC Proteins and ABCA1

ABCA1 is part of a highly conserved superfamily known as the ABC transporter proteins. There are currently 48 known ABC transporter genes in the human genome that transport a dynamic range of substrates including lipids, amino acids, carbohydrates, vitamins, ions, glucuronide conjugates and xenobiotics[103]. Based on structural homology, these transporters have been further categorized into 7 subclasses referred to as ABC A-G[104, 105]. They all contain ATP-binding domains, also known as nucleotide-binding folds (NBFs)[106, 107] (Fig. 1.8). These transporters thus can potentially use the energy released from

Figure 1.8

Structure and topology of ABCA1. ABCA1 contains two ATP-binding domains, also known as nucleotide-binding folds **(NBF)**, each containing Walker A and B motifs, and a signature C motif. There are also two transmembrane **(TM)** domains each formed by six α-helices. ABCA1 contains two large extracellular loop domains, one in the N-terminal region and a second following the first NDF. Overall, ABCA1 is a full transporter 2261 amino acids in length and 240 kDa in size. (Image adopted from figure 1 of Singaraja *et al. Arterioscler. Thromb. Vasc. Biol. 23;1322-1332.* 2003)

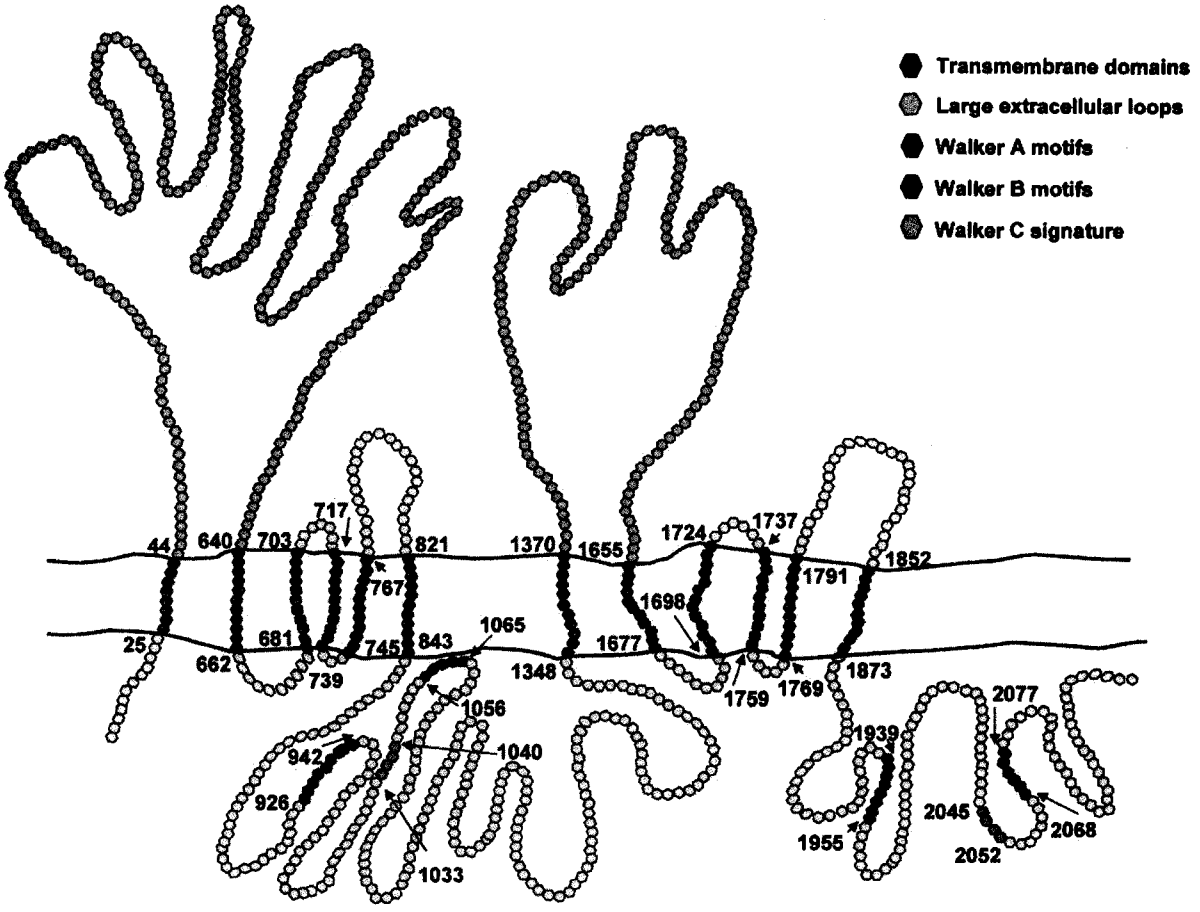
Transmembrane domains
Large extracellular loops
Walker A motifs
Walker B motifs
Walker C signature
44
640
703
717
767
821
1370
1655
1724
1737
1791
1852
25
662
681
739
745
843
1065
1348
1677
1698
1759
1769
1873
1056
1040
942
926
1033
1939
2077
2045
2068
1955
2052

ATP hydrolysis to pump or flip substrates across the intracellular and/or plasma membranes[103]. The NBFs contain Walker A and Walker B motifs separated by 90-120 amino acids (Fig. 1.8). There is also a third sequence of interest located just upstream of the Walker B motif, known as the signature (C) motif[108]. In addition, there is a TM domain (TMD) composed of 6-11 α-helices, which allows for the proteins to embed in the membrane. Some functional ABC proteins are full transporters, in which the single gene encodes two NBFs and two TMDs[109]. Alternatively, some are half-transporters with one NBF and one TMD that can form homo-dimers with each other or hetero-dimers with a different ABC half-transporter[110]. The ABCA-subfamily is comprised only of full transporters, ranging from 1543-5058 amino acids in size. ABCA1 is the prototypic member of this subfamily and contains two TMDs each formed by six α-helices and two large extracellular domains, resulting in a transporter of 2261 amino acids in length and 240 kDa in size (Fig. 1.8).

1.2.3 ApoA-I/ABCA1-Mediated FC Efflux

In 1994, over three decades after the initial discovery of TD, the ABCA1 and ABCA2 proteins were simultaneously cloned by Luciani in the laboratory of Giovanna Chimini[111]. At the time of discovery, the function of both proteins was unknown, yet it was observed that cholesterol-loading of cells led to the up-regulation of the ABCA1 gene[112]. It is now widely accepted that ABCA1 is required for the initial transfer of phospholipids and cholesterol to lipid-poor apoA-I, but the mechanism by which this occurs is largely unknown. Nevertheless, the apoA-I/cell association correlates with ABCA1 expression, as does the subsequent apoA-I-mediated cholesterol efflux[113].

Based on these observations, one theory suggests that ABCA1 can act as a membrane receptor for apoA-I to form a high-affinity protein complex (Fig. 1.9A). Evidence for this stemmed from cross-linking experiments, in which apoA-I could be coprecipitated with ABCA1 after cross-linking[114-116]. In addition, Fitzgerald *et al.* examined 5 different naturally occurring missense mutations in the large N-terminal and central extracellular loop domains of ABCA1 (Fig. 1.8) and found that 4 of the 5 mutants were defective in apoA-I-induced efflux as well as cross-linking to apoA-I[115]. However, it is difficult to consider ABCA1 as a typical surface receptor for apoA-I. First of all, ABCA1-mediated cholesterol efflux can be triggered by all exchangeable apolipoproteins, such as apoA-I, apoA-II, apoA-IV, apoE, and apoC, that share little primary sequence homology. Secondly, various synthetic amphipathic helical peptides made with all –L or all –D amino acids are equally effective in mediating cholesterol efflux[117-119]. Finally, it has been shown recently that of all apoA-I bound to ABCA1-expressing cells, only 10% can be coprecipitated with ABCA1[120]. Current evidences, therefore, do not seem to support the receptor hypothesis. In addition, an ABCA1 mutant with a point mutation in the N-terminal loop, W590S, can in fact be efficiently cross-linked to apoA-I, yet fails to trigger cholesterol efflux[115]. This further suggests that, even if apoA-I binds to ABCA1 briefly, such binding alone is not sufficient to promote lipid efflux or explain ABCA1 function[115].

An alternative model suggests that apoA-I first associates with specific lipid domains generated by a fully functional ABCA1 transporter on the plasma membrane (Fig. 1.9B). Evidence for this model stems from the fact that disruption of ATPase activity leads to deficient apoA-I binding to the cell surface[121]. Also, ABCA1 has been shown to impact the

Figure 1.9

Proposed models of apoA-I-mediated cholesterol efflux. ***A,*** The receptor theory involves the direct binding of apoA-I in order to form a high-affinity complex. ABCA1 then transfers phospholipids **(PL)** and cholesterol **(C)** directly to apoA-I, thus forming nascent HDL. ***B,*** The indirect model of apoA-I-mediated cholesterol efflux involves the association of apoA-I with specialized lipid domains, presumably formed by ABCA1. ApoA-I then acquires PL and C from these lipid domains in order to form nascent HDL. ***C,*** The hybrid theory involves the initial tethering of helix 10 of apoA-I to the plasma membrane in close proximity to ABCA1. ApoA-I then moves laterally along the membrane in order to bind to ABCA1. ABCA1 then transfers PL and C to apoA-I, forming nascent HDL.

A) Direct binding of apoA-I to ABCA1

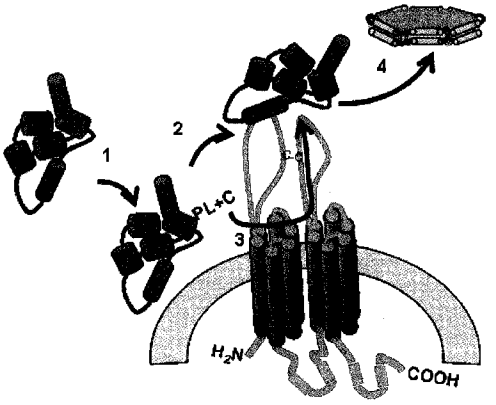

B) Association of apoA-I with lipid domains

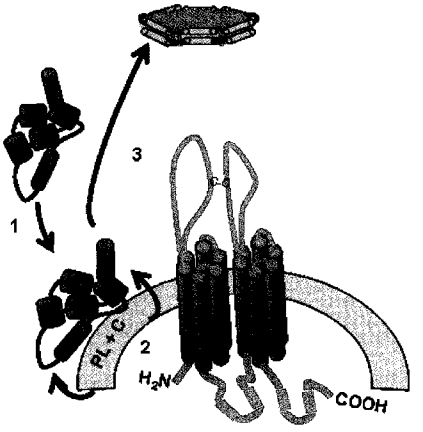

C) Hybrid theory of apoA-I-mediated efflux

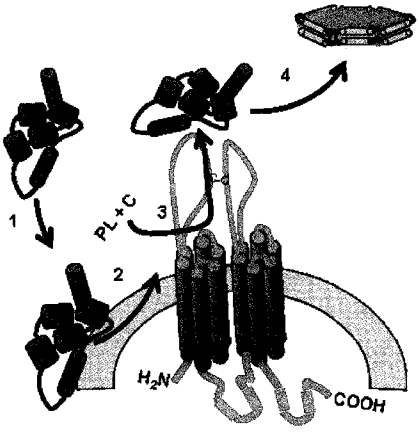

plasma membrane morphology[116, 122], as well as release FC from specific domains[123]. In support of this model, mutagenesis studies have shown that apoA-I lipid affinity correlates positively with its capacity to trigger ABCA1-mediated FC efflux[123]. Additionally, when cells are cooled to 4°C, a process known to facilitate the formation of lipid rafts and limit the lateral diffusion, no measurable cross-linking of apoA-I with ABCA1 is detected[115]. In order to reconcile both models, a hybrid model of apoA-I binding has also been put forward (Fig. 1.9C). Herein, the helix 10 of apoA-I initially tethers the apolipoprotein to a specific lipid domain formed by functional ABCA1. ApoA-I then diffuses laterally across the plasma membrane in order to form a productive complex with ABCA1, resulting in lipidation and the formation of nascent HDL[124].

In addition to the models attempting to explain apoA-I binding, multiple models exist in order to elucidate how ABCA1 might mediate the formation of nascent HDL. One of them is known as the "one-step" model, in which phospholipids and FC are released together from the membrane to apoA-I[125, 126]. This simultaneous model proposes that the apoA-I/cell interaction generates vesiculation and solubilization of plasma membrane domains, through which apoA-I can acquire both phospholipids and cholesterol at the same time. This model is supported by the kinetic studies of phospholipid and FC efflux, especially at early time points. In fact, in the first 10 minutes of efflux, both species were shown to be released at similar rates[127]. Further studies have supported a model of retroendocytosis, in which simultaneous release of cholesterol and phospholipids occurs through intracellular lipidation of endocytosed apoA-I, followed by exocytosis of nascent HDL particles[128, 129].

A "two-step" model has also been suggested. This sequential model implies that ABCA1 would first promote the lipidation of apoA-I through the transfer of phospholipids. This would effectively form pre-β nascent HDL. Phospholipid-enriched HDL would then acquire FC from lipid domains on the plasma membrane[130]. In support of this model, conditioned medium containing phospholipidated apoA-I can trigger FC efflux from vascular endothelial cells deficient in ABCA1[130]. In further experiments using HEK293 cells, cholesterol depletion by cyclodextrin effectively reduced FC efflux to apoA-I, but phospholipid efflux remained unaffected[131]. Despite a rich array of various models, each with their share of experimental support, the precise mechanisms by which ABCA1 mediates the efflux of phospholipids and FC to apoA-I remain elusive.

1.2.4 Expression and Regulation

The transcriptional regulation of *ABCA1* is controlled by a variety of mechanisms. These include the nuclear orphan receptors, liver X receptors (LXR) α or β and retinoid X receptor (RXR)[69]. Induction of these systems can occur alone or in combination, in which case, the effect is additive[132]. Oxysterols, such as 27-, 22(R)-, and 20(S)-hydroxycholesterol can stimulate *ABCA1* transcription through the LXR[132-134], while 9-*cis*-retinoic acid regulates the transcription through the RXR[132]. Cholesterol loading also causes potent upregulation of *ABCA1* transcription, likely mediated by oxysterols through the LXR/RXR[132, 134]. Furthermore, peroxidase proliferator-activated receptor α (PPAR-α) and fibric acids increase *ABCA1* transcription in an LXR-dependent manner[135, 136]. *ABCA1* expression is also strongly induced by cAMP in mouse macrophage cell lines, such as RAW264 and J774 cells[137]. Interestingly, some calcium channel blockers have been shown

to induce the expression of *ABCA1* through a mechanism that is independent of the LXR/RXR system[138]. Importantly, the ability of apoA-I to acquire cellular lipids correlates positively with the *ABCA1* mRNA levels modulated by the aforementioned systems[139]. It is also worth noting that multiple transcripts of *ABCA1* have been detected. A recent study has shown that various liver *ABCA1* transcripts may be regulated differently in hepatocytes through LXR/RXR and SREBP-2 systems, perhaps serving as a counter-balance control of *ABCA1* expression[75].

ABCA1 is also posttranslationally regulated. ABCA1 was found to be distributed on the plasma membrane surface and in the late endosomal compartments by a study using GFP-ABCA1, presumably cycling between these two regions[128]. ABCA1 has also been observed in the Golgi compartment and in lysosomes[128, 140, 141], although it is not clear whether those locations are its final destination. In the absence of active cholesterol efflux, ABCA1 is rapidly degraded by calpain-mediated proteolysis with a half-life of around 2 hours[142, 143]. The presence of apoA-I or other exchangeable apolipoproteins protects ABCA1 from degradation[142]. Additionally, apoA-I binding leads to the phosphorylation of ABCA1, which is believed to be responsible for the stabilization of ABCA1 on the cell surface[144]. Interestingly, synthetic helical peptides that trigger cholesterol efflux also prevent ABCA1 degradation[145].

ABCA1 was found to bind Lin7, α1- and β2-syntrophins through its C-terminal postsynaptic density protein-95, disk-large tumor suppressor protein, zonula occludens-1 (PDZ) domain[146, 147]. While the physiological relevance of Lin7 and β2-syntrophin is unclear, it has been shown that α1-syntrophin binding stabilizes ABCA1 and increases efflux activity in α1-syntrophin-transfected cells[147]. A study that co-purified ABCA1 and its

binding partners by an affinity column further confirmed the aforementioned ABCA1 binding proteins as well as a novel binding partner, β1-syntrophin. β1-syntrophin was also found to stimulate cholesterol efflux, redistribute ABCA1 and protect the transporter from degradation in mouse hepatocytes and THP-1 cells[148]. Interestingly, syntrophins are a part of a dystrophin glycoprotein complex that binds actin filaments. ABCA1 may be effectively anchored to the actin meshwork, which could protect it from degradation.

1.2.5 Tissue-Specific Contributions to Plasma HDL

Cellular ABCA1 expression and function lead to the physiological formation of HDL in the plasma. Using transgenic mice, the relative contributions of ABCA1-derived HDL from major ABCA1-expressing tissues was analyzed. When ABCA1 was overexpressed specifically in the liver and macrophages under the control of the apoE promoter, there were elevated levels of plasma HDL, pre-β HDL and apoA-I[149, 150]. Similar results were also observed when the overexpression was targeted specifically to the liver. Conversely, using liver- and intestine-specific ABCA1 knockout mice, it was later determined that the liver contributes ~80% of plasma HDL, while the intestine contributes ~20%, respectively[151, 152]. In comparison, macrophage ABCA1 contributed rather insignificantly to the plasma HDL levels. ABCA1 function in macrophages, however, is extremely important in terms of preventing atherogenesis. Macrophage-specific ABCA1 KO mice had severely accelerated atherosclerosis even though there was little change in circulating HDL levels[89].

1.3 Rationale for Research

ABCA1 was originally reported to be a PS "floppase" that transfers PS from the inner to outer leaflet of the plasma membrane in an ATP-dependent manner[153, 154]. Further studies deemed this event as functionally relevant as apoA-I has been shown to preferentially bind PS-rich membranes[155]. This process is believed to be facilitated by the formation of an aqueous chamber by the two TMDs[156]. In mammalian cells, phospholipids are asymmetrically distributed with phosphatidylcholine (PC) and SM mainly on the outer leaflet and PS and phophatidylethanolamine (PE) on the inner leaflet. It is not entirely known what purpose such an asymmetry serves or how it is achieved. In the case of PS, however, it is known that its predominant inner leaflet distribution is governed by an aminophospholipid translocase (APLT) that flips PS from the outer to the inner leaflet of the plasma membrane by hydrolyzing ATP. ABCA1 is thought to play a regulatory role by dynamically flopping PS to the outer leaflet. However, a recent study investigated the translocation of PS in multiple cell lines either expressing or lacking ABCA1, and found no evidence that ABCA1 plays any identifiable role as a translocase, scramblase, or regulator of either of those proteins in hematopoietic or fibroblast cells[157]. This argues against a possible role for ABCA1 in regulating the transbilayer PS distribution as previously suggested[158]. Although it remains possible that ABCA1 may regulate the PS distribution through a highly dynamic mechanism technically difficult to detect, available observations do not provide sufficient support for such a hypothesis. Nevertheless, ABCA1 expression has consistently been associated with membrane shape changes[159], a phenomenon commonly seen following the redistribution of lipids between the two leaflets of a bilayer membrane. According to the bilayer-couple theory[159, 160], the shape of a membrane can be controlled by regulating the

relative surface areas of the two leaflets. By modulating the relative numbers of phospholipids in each leaflet, cells could potentially control the relative leaflet surface areas, and thus dynamically determine the actual membrane shape[160]. For example, if phospholipids are flopped from the inner to outer leaflet, there would be an increase in the relative number of phospholipids on the outer leaflet, therefore forcing the membrane to bulge outward, a process favouring membrane blebbing or shedding. On the other hand, if phospholipids were flipped from the outer to inner leaflet, it would favour membrane invagination, or endocytosis. Interestingly, it has been shown in various labs, including our own, that the expression of functional ABCA1 decreases endocytosis in human fibroblasts and macrophages[161, 162].

An interesting model has recently been proposed by Michael Phillips and his group, which integrates key findings from the literature as well as their own laboratory[163]. They suggest that the translocation of lipids to the outer leaflet results in lateral compression of outer leaflet phospholipids. Concomitantly, there is expansion and decreased phospholipid packing in the inner leaflet due to a net depletion of phospholipids. This creates strain in the plasma membrane, which can be relieved by outward bending of the membrane, or exovesiculation. Several groups, including our own, have observed plasma membrane protrusions in ABCA1-expressing cells[116]. Such membrane protrusions could have a functional significance in terms of cholesterol efflux. ApoA-I binding to model membranes was recently found to be highly sensitive to membrane curvature, independent of any imbedded proteins. It was shown that apoA-I prefers the high curvature small unilamelar vesicles (SUV), compared to the low curvature large unilamelar vesicles (LUV) with identical phospholipid compositions[163]. Plasma membrane protrusions, as proposed, could

disorder the lipid packing of the outer leaflet and create space between the phospholipid polar headgroups. Consequently, this could allow for the insertion of amphipathic α-helices, such as apoA-I, and thereby cholesterol efflux.

ABCA1 has been shown to influence several plasma membrane functions, such as phagocytosis, endocytosis and microvesiculation[164-167] . These findings strongly imply that intrinsic ABCA1 activity significantly influences the physical aspects of the plasma membrane. Vaughan and Oram have reported that ABCA1 can increase the pool of plasma membrane cholesterol available to the enzyme cholesterol oxidase. This occurs in the absence of apolipoproteins such as apoA-I[168]. In addition, the cholesterol removed by apoA-I, but not by HDL, was derived exclusively from these domains[168]. Michael Phillips' group has proposed the loosening of lipid packing through exovesiculated plasma membrane regions formed by ABCA1. Taken together, it is likely that cholesterol present in the more loosely packed membrane regions is more accessible to enzymatic oxidation[169, 170]. Currently, it is unknown whether ABCA1 modulates the lipid raft/non-raft partition of the plasma membrane and, consequently, how this may affect apoA-I-mediated cholesterol efflux. We hypothesize that functional ABCA1 can actively disrupt plasma membrane lipid raft microdomains, therefore making cholesterol more readily available and subsequently facilitating cellular apoA-I association and cholesterol efflux.

Chapter 2 Materials and Methods

2.1 Materials - Cell culture media and reagents were obtained from Invitrogen. Mifepristone, methyl-β-cyclodextrin (MCD), and Triton X-100 were purchased from Sigma. The cholesteryl ester (CE) and total cholesterol (TC) analysis kits were obtained from VWR International (West Chester, PA). The polyclonal antibody against ABCA1 was obtained from Novus Biological Inc. (Littleton, CO). The polyclonal and monoclonal anti-caveolin-1 antibodies were obtained from BD Transduction Laboratories. Polyclonal anti-Akt antibody (C-20) was from Santa Cruz Biotechnology (Santa Cruz, CA), and polyclonal anti-phospho-Akt (Ser-473) was from Cell Signaling Technology (Beverly, MA). The total anti-IRS-1 antibody was obtained from Upstate Biochemicals (Lake Placid, NY). Fluorescent secondary antibodies (Alexa 488 and Alexa 594) and $DiIC_{18}$ were purchased from Molecular Probes (Eugene, OR). The EYFP-caveolin-1 construct used was formed by C-terminal fusion of the EYFP protein to caveolin-1. It is important to note that EYFP-caveolin-1 was reported to traffic similarly to caveolin-GFP, which traffics to plasma membrane caveolae indistinguishably from untagged caveolin-1[32]. EYFP-caveolin-1 was originally obtained from Dr. Robert G. Parton (University of Queensland, Brisbane, Australia). 3-isobutyl-1-methylxanthine was obtained from Sigma-Aldrich (St. Louis, MO). Dexamethasone was obtained from Steraloids Inc. (Newport, RI). Human insulin, recombinant (yeast), was purchased from Roche Diagnostics (Switzerland).

2.2 Cell culture— Baby hamster kidney (BHK) cells stably expressing either an empty vector (Mock), WT or A937V ABCA1 under the control of a mifepristone-inducible Gene-switch promoter were prepared as described previously[168]. To facilitate morphological

analysis, we further subcloned ABCA1- or A937V mutant-expressing cells and chose colonies that expressed equal levels of ABCA1 among individual cells. BHK cells were maintained in DMEM plus 10% fetal bovine serum (FBS) and 1% penicillin/streptomycin (P/S) at 37 °C in a 5% CO_2 incubator (HERA Cell 150, Heraeus). Incubation of BHK cells for 18-20 hours in DMEM with 1 mg/ml BSA and 10 nM mifepristone successfully induced ABCA1. Mock and A937V-ABCA1 mutant cells were treated identically to WT ABCA1-expressing cells.

3T3-L1 preadipocytes, kindly supplied by Dr. Alexander Sorisky (Ottawa Health Research Institute) were grown in monolayer culture in 35 mm dishes with low glucose DMEM supplemented with 10% calf serum (CS) and 1% P/S at 37°C in a 5% CO_2 incubator. Two days post-confluence, 3T3-L1 fibroblasts were triggered to differentiate into adipocytes in low glucose DMEM supplemented with 10% FBS, 1% P/S, 0.5 mM 3-isobutyl-1-methylxanthine, 0.25 μM dexamethasone, and 1 μM insulin for 2 days. The medium was then replaced with low glucose DMEM supplemented with 10% FBS, 1% P/S and 1 μM insulin for 2 days. On days 4 and 6, the medium was replaced with low glucose DMEM supplemented with 10% FBS and 1% P/S. On day 8, 3T3-L1 adipocytes were ready for experimentation/harvest, with more than 85% of cells exhibiting an adipocyte morphology. To generate hypertrophic adipocytes, 3T3-L1 preadipocytes were differentiated into adipocytes using the same protocol as mentioned above except that low glucose DMEM was substituted with supplemented RPMI 1640 medium (10% FBS, 1% P/S, 10 mM HEPES, 100 mM Na pyruvate, 0.05 mM β-mercaptoethanol, pH 7.15).

2.3 GeneSwitch™ system for ABCA1 induction—The inducible gene expression system used here was a modified version of the mifepristone-inducible mammalian expression system originally developed by Wang and al, 1994 [171]. This system involves the co-transfection of an inducible expression plasmid, pGene/V5-His, and a regulatory plasmid, pSwitch. The pGene/V5-His plasmid is comprised of a hybrid promoter containing GAL4 upstream activating sequences (UAS) and the adenovirus E1b TATA box, as well as the gene of interest. The pSwitch plasmid encodes Gal4 UAS, a thymidine kinase (TK) promoter for basal transcription, as well as a fusion protein consisting of three components: yeast Gal4 DNA binding domain (DBD), truncated human progesterone receptor ligand binding domain (hPR-LBD), and the human p65 activation domain (AD) from NF-kβ. Upon incubation with mifepristone, which is an inhibitor of the human progesterone receptor, the hPR-LBD is bound and a conformational change of the fusion protein occurs. This allows the fusion protein to dimerize, and become transcriptionally active. The ligand-bound fusion protein homodimer can then bind the GAL4 UAS of both the pSwitch and pGene/V5-His plasmids, resulting in transcription of the fusion protein itself as well as that of the gene of interest, respectively. ABCA1 and A937V cells contain the Wt-ABCA1 and A937V-ABCA1 genes in the pGene/V5-His plasmid, respectively, while Mock control cells contain no insert in this plasmid.

2.4 Cholesterol efflux—BHK cells were incubated in normal growing media (DMEM plus 10% fetal calf serum) with 0.5 μCi/ml [^{3}H]cholesterol for 2 days to label cellular cholesterol to equilibrium. The cells were then switched to DMEM with 1 mg/ml BSA and 10 nM mifepristone for 18-20 h. To measure cholesterol efflux, cells were incubated with 10

μg/ml apoA-I for 4 h at 37 °C. The medium was collected, centrifuged to remove detached cells, and counted for ^{3}H. Cells were lysed with NaOH (0.5 N) overnight and counted for ^{3}H. Cholesterol efflux was calculated as the percentage of total [^{3}H]cholesterol released into the medium. For methyl-β-cyclodextrin-induced cholesterol efflux, cells were also labeled with 0.5 μCi/ml [^{3}H]cholesterol for 2 days, followed by 18-20 h of incubation with 1 mg/ml BSA and 10 nM mifepristone. The cells were then incubated with 5 mM MCD either at 37 °C for 1 min or on ice for the indicated times. The medium was collected, centrifuged, and counted for [^{3}H]cholesterol. Cell-associated [^{3}H]cholesterol was measured from NaOH lysates as mentioned above. Efflux was again calculated as the percentage of total [^{3}H]cholesterol released into the medium.

2.5 Immunofluorescent staining of ABCA1 and endogenous CAV1—WT ABCA1-, A937V mutant-, and Mock-expressing BHK cells were incubated for 18-20 hours in DMEM containing 1 mg/mL BSA and 10 nM mifepristone. The cells were then fixed with 4% paraformaldehyde and permeabilized with 0.1 mg/ml saponin. For ABCA1 staining, subsequent antibody incubations were performed using a primary polyclonal antibody against ABCA1 followed by an Alexa-488 goat anti-rabbit secondary antibody. Confocal fluorescent images were taken using a Nikon TE2000 inverted fluorescent microscope with C1 confocal attachment and a 60x (numerical aperture: 1.4) oil-immersion objective. Images from WT ABCA1-, A937V mutant- and Mock-expressing cells were taken under identical microscopy conditions and settings. For the staining of endogenous CAV1, cells, following permeabilization, were subsequently incubated with a plasma membrane-specific mouse monoclonal antibody against CAV1 followed by an Alexa-488 goat anti-mouse secondary

antibody. Confocal fluorescent images of the basal membrane were taken using a Nikon TE2000 inverted fluorescent microscope with a 60x (numerical aperture: 1.4) oil-immersion objective and the 488 nm line of an argon ion laser. 3T3-L1 adipocytes were immunostained for CAV1 using the same protocol and microscopy equipment. For CAV1 and ABCA1 co-localization experiments, an Alexa-594 secondary antibody and the 594 nm line of a HeNe laser were used for ABCA1 visualization, while the Alexa-488 goat anti-mouse secondary antibody and the 488 nm line of an argon ion laser were again used for the visualization of caveolin-1.

2.6 EYFP-CAV1 transfection of BHK cells—In order to visualize plasma membrane caveolae and the CAV1 distribution, WT ABCA1-, A937V mutant-, or Mock-BHK cells were transiently transfected with EYFP-CAV1 using Lipofectamine 2000. Briefly, BHK cells were transfected with EYFP-CAV1 cDNA for 4 hours at 37°C, in serum-free DMEM, using Lipofectamine 2000. The DNA to Lipofectamine 2000 ratio used was 0.25 μg cDNA:1 μL Lipofectamine 2000 per 35mm well. The transient transfectants were then incubated 18-20 hours in DMEM with 1mg/mL BSA plus 10 nM mifepristone

2.7 Cholesterol depletion and loading of BHK cells—MCD was used to deplete cholesterol from EYFP-CAV1-transfected WT ABCA1 and Mock BHK cells. Cells were incubated with either 0.5 mM or 2.5 mM MCD for 30 minutes at 37°C. For cholesterol enrichment, a Cholesterol/MCD complex was formed at a ratio of 8:1 in medium 1 (150 mM NaCl, 5 mM KCl, 1 mM $CaCl_2$, 1 mM $MgCl_2$, 2 g/L glucose, and 20mM HEPES, pH 7.4) containing 7.5 μM cholesterol and 60 μM MCD. The solution was vortexed and then sonicated (Branson Sonifier 450) until clarified. The resulting solution was incubated

overnight at 37°C in order to maximize the formation of the cholesterol/MCD complex. The complex solution was then centrifuged using a TLA 120.2 rotor and an Optima TLX Ultracentrifuge at 21,000g for 20 minutes before use. EYFP-CAV1 transfected BHK cells were incubated with the complex for 30 minutes at 37°C to load the cells with cholesterol.

2.8 Cy3-Transferrin labeling of EYFP-CAV1-transfected cells—WT ABCA1-, A937V mutant- and Mock-BHK cells were grown in 35-mm glass-bottom dishes and transfected with EYFP-CAV1 as described above. All cell lines were then incubated in DMEM with 1 mg/ml BSA and 10 nM mifepristone for 18-20 hours. The cells were placed on ice and washed with ice-cold PBS. For staining of transferrin (Tf) receptor on the cell surface, cells were incubated with 80 ng/ml of Cy3-Tf in medium 1 for 30 min on ice and then washed 2x with ice-cold PBS and fixed with 4% paraformaldehyde for 10 min on ice. Cy3-Tf and plasma membrane EYFP-CAV1 fluorescence images were taken on a Nikon TE2000 using a 16-bit cooled digital camera (Cascade 512B EM, Photometrics).

2.9 Fluorescence recovery after photobleaching (FRAP)—EYFP-CAV1-transfected WT-ABCA1- and Mock-BHK cells were grown on glass cover slips to subconfluency. The photobleaching of a defined square region of the basal plasma membrane was conducted using the 488 nm line of a Bio-Rad MRC 1024 laser-scanning confocal microscope at full laser power (100%). Fluorescence recovery was monitored by imaging whole cells at low laser power (3-10%). Recovery was measured as the fluorescence intensity of the photobleached region / fluorescence intensity of a non-bleached section of basal membrane with time.

2.10 Filipin staining of cellular FC—Filipin staining of cellular FC was performed as described previously[172]. Briefly, all three BHK cell lines were fixed with 4% paraformaldehyde for 1 hour at room temperature. The cells were then incubated in PBS containing 10% calf serum (CS), and 1.5 mg/mL glycine for 10 minutes at room temperature. The cells were then stained with PBS containing 10% CS and 0.05 mg/mL filipin for 2 hours at room temperature. Light was avoided during incubation in the presence of filipin. FC distribution was analyzed using a Nikon TE2000 microscope with a 60x (1.4 NA) objective and a 16-bit cooled digital camera with a UV filter set.

2.11 Cholesterol mass determination—Cellular lipids were extracted by organic solvent and dried under an N_2 atmosphere. The dry samples were directly resuspended by vigorous vortexing in 500 µl of the Free Cholesterol E reagent supplied with the cholesterol mass determination kit (Wako Chemicals, Richmond, VA). The samples were then incubated for 10 min at 37°C, and the absorbance was determined at a wavelength of 600 nm. The Triton X-100-extractable cholesterol fraction was calculated as % cholesterol as follows: (Triton X-100-soluble fraction)/(Triton X-100-soluble fraction + Triton X-100-insoluble fraction)

2.12 Subcellular [^{3}H]-cholesterol distribution—WT ABCA1-, A937V mutant- and Mock-BHK cells were grown to 80% confluence in 20-cm plates (two for each cell line) and radiolabeled with 0.5 µCi/ml [^{3}H]-cholesterol for 24 hours. Cells were then incubated in DMEM with 1 mg/ml BSA and 10 nM mifepristone for 18-20 hours. The following procedures were carried out at 4°C. Plates were washed twice with 3 ml of ice-cold buffer A (250 mM sucrose, 2.0 mM EDTA, 40 mM Tricine, pH 7.8). The cells were then scraped,

collected in 3 ml of buffer A and pelletted by centrifugation at 1,000 x *g* for 5 min in a Beckman Coulter Allegra 6R centrifuge. The pellets were the resuspended in 1 ml of buffer A, and then homogenized with a Dounce homogenizer (20 strokes). Homogenates were transferred to 1.5-ml Eppendorf tubes and centrifuged at 1000 x *g* for 10 min in a Fischer Scientific accuSpin MicroR centrifuge to remove nuclei. The postnuclear supernatant fractions were collected and buffer A was added to a final volume of 2 ml. These 2-ml postnuclear supernatant fractions were layered on top of a 45-10% continuous sucrose gradient in SW41 tubes, and subjected to centrifugation at 137,000 x *g* for 20 h at 4°C. 12 fractions were collected from each tube (1 ml each). Equal volumes of each fraction were analyzed by SDS-PAGE, followed by immunoblotting, for the following cellular markers: CAV1 (plasma membrane), hsp-70 (cytosol), and calnexin (endoplasmic reticulum). [^{3}H]Cholesterol levels in each fraction were analyzed by mixing 300 µl of sample with 2 ml of scintillation liquid, and radioactivity was detected using a Beckman Coulter LS 6500 multipurpose scintillation counter.

2.13 Triton X-100 extraction—Mifepristone-induced 75% confluent BHK cells grown in 6-well plates were washed twice with ice-cold PBS and chilled on ice for 30 min in DMEM containing 10 mM HEPES, pH 7.4. The medium was then replaced with 1 ml/well DMEM/HEPES in the presence or absence 1% Triton X-100 and further incubated on ice for 30 min. The medium was then collected, and the first wash with 500 µl of ice-cold PBS was combined with the medium. Lipids were then extracted overnight at 4°C by adding 4 volumes of Folch solution (chloroform/methanol (2:1)). The organic phase was collected and evaporated under N_2 atmosphere. Lipids were also extracted twice from cells in 1 ml/well of a 3:2 hexane:isopropanol solution, and the organic phase was evaporated under N_2

atmosphere as described previously. For labeling FC and CE, cells were labeled for 48 h with 1 μCi/ml [^{3}H]cholesterol. After Triton X-100 treatment, tritiated samples were separated by high-performance thin layer chromatography (Whatman) using a 80:20:6.7:1 hexane:ether:methanol:acetic acid mixture as the elution system. For ^{3}H-labeled phospholipids, half-confluent cells were labeled for 24 h with 1 μCi/ml [^{3}H]choline and the elution system was composed of chloroform:methanol:acetic acid:formic acid:water (35:15:6:2:1). Spots corresponding to CE, FC, PC, and SM were scraped and counted in a β-scintillation counter.

2.14 DiIC$_{18}$ cold Triton X-100 extractability—Cold Triton X-100 extractability of surface-bound DiIC$_{18}$ on the plasma membrane was performed as described previously[173]. Cells were transferred from growth medium to medium 1. DiIC$_{18}$ was transferred as monomers from fatty acid-free BSA carriers[174]. In some of the experiments, DiIC$_{18}$ solubilized in ethanol was directly added to labeling medium at 37°C. In each case, cells were labeled with DiIC$_{18}$ for 20 s at 37°C, rinsed with ice-cold medium 1, and then incubated on ice with ice-cold Triton X-100 (1%) for 30 min. Triton X-100-resistant membranes were visualized by imaging DiIC$_{18}$ using a standard rhodamine filter set. Images were quantified by manually outlining each cell using the ImageJ software, and measuring fluorescent intensity from entire cell area. This is the fraction of DiIC$_{18}$ remaining after Triton X-100 treatment (insoluble fraction, F_i). To extrapolate the DiIC$_{18}$ fluorescent intensity before Triton X-100 treatment in the same cell, we randomly sampled several regions of interest from areas excluding any visible holes and determined average of fluorescent intensities from these regions of interest. We used this to calculate the fluorescent intensity before Triton X-100 treatment from the entire cell area, or total DiIC$_{18}$

(F_t). The percentage of $DiIC_{18}$ extracted by Triton X-100 (F_s) in each individual cell was then calculated as: $F_s = (F_t - F_i) \times 100/F_t$. For each data point, more than 50 individual cells were analyzed and pooled to produce an average and standard error of the mean (S.E.).

2.15 Detergent-free purification of caveolae membrane—The procedure used was based on an established protocol by Smart *et al.*[175]. WT ABCA1-, A937V mutant- and Mock-BHK cells were grown to 80% confluence in 20-cm plates (five per cell line), and incubated in DMEM with 1 mg/ml BSA and 10 nM mifepristone for 18-20 hours to induce ABCA1 expression. The following steps were carried out at 4°C. Plates were washed twice with 3 ml of ice-cold buffer A (250 mM sucrose, 2.0 mM EDTA, 40 mM Tricine, pH 7.8). Cells were then scraped, collected in 3 ml of buffer A and pelletted by centrifugation at 1000 x *g* for 5 min in a Beckman Coulter Allegra 6R centrifuge. The pellets were resuspended in 1 ml of buffer A and homogenized with 20 strokes using a Dounce homogenizer. Homogenates were transferred to 1.5-ml Eppendorf tubes and centrifuged at 1000 x *g* for 10 min to remove nuclei. After collection of supernatants, the pellets were resuspended in 1 ml of buffer. The homogenization and centrifugation steps were repeated as described. Postnuclear supernatants from both homogenizations were combined (2 ml total), layered onto 23 ml of 30% Percoll, and then centrifuged in a Ti-70 rotor at 86,000 x g_{max} for 30 min using a Beckman Coulter Optima L-90K Ultracentrifuge. The Percoll gradient was then collected in 2-ml fractions, including the 2-ml plasma membrane band. The plasma membrane fractions were transferred to glass test tubes and sonicated on ice three times in succession for 10 s on setting 3 of a Branson Sonifier 450. The sonicated plasma membrane fractions were then combined with 1.84 ml of 50% Optiprep and 160 µl of buffer A, and placed in the bottom of SW41 tubes. After vortexing, a 6-ml continuous 20-10% Optiprep

gradient was layered above the 4-ml plasma membrane preparations. The gradients were then centrifuged at 52,000 x *g* for 90 min in a Beckman SW41 rotor and Beckman Coulter Optima L-90K Ultracentrifuge. 10 fractions were then collected, 1-ml each, and protein was trichloroacetic acid (TCA)-precipitated. The pellets were then dissolved in sample/loading buffer and analyzed by SDS-PAGE (60 µl loading volume) and probed for CAV1 and clathrin by immunoblotting.

2.16 Determination of Akt activation—The procedure used was based on a protocol developed by Pike *et al.*[176]. Briefly, WT ABCA1-, A937V mutant- and Mock-expressing BHK cells were grown to 80% confluence in 20-cm plates, followed by incubation in DMEM with 1 mg/ml BSA and 10 nM mifepristone for 18-20 hours. This effectively serum-starved the cells during the 18-20 hour incubation. Cells were then stimulated with 50 ng/ml of epidermal growth factor (EGF) for 5 min. The cells were washed twice with 5 ml of ice-cold PBS. Once again, all of the following steps were carried out at 4°C. Cells were washed twice with 3 ml of ice-cold radioimmune precipitation assay (RIPA) buffer (150 mM NaCl, 10 mM Tris, pH 7.2, 0.1% SDS, 1% Triton X-100, 1% deoxycholate, 5 mM EDTA), scraped and collected in 3 ml of RIPA buffer supplemented with 100 µM orthovanadate, 20 nM *p*-nitrophenylmethylsulfonyl fluoride, 1 µg/ml leupeptin. Cells were pelletted by centrifugation at 1000 x *g* for 5 min in a Beckman Coulter Allegra 6R centrifuge. The pellets were resuspended in 1 ml of RIPA buffer, and then homogenized with a Dounce homogenizer (20 strokes). Homogenates were transferred to 1.5-ml Eppendorf tubes and centrifuged at 1000 x *g* for 10 min. The supernatants were collected, and aliquots were assayed for protein content using the Lowry method. Equivalent amounts of protein were mixed with SDS loading buffer and analyzed by SDS-PAGE and immunoblotting. Phospho-Akt (activated) was

probed using a goat polyclonal antibody recognizing phosphorylated Akt1 (Ser-473). Total Akt was probed using a goat polyclonal antibody against Akt1 (C-20). The degree of Akt activation was expressed as a ratio of phospho-Akt1/total Akt1, determined by densitometry of the resulting protein bands.

2.17 ^{125}I-ApoA-I association—Purified plasma apoA-I (Biodesign) solubilized in 4 M guanidine-HCl was dialyzed extensively against PBS buffer. ApoA-I was iodinated with 125-iodine by IODO-GEN® (Pierce) to a specific activity of 2800 cpm/ng of apoA-I, dialyzed, and used within 48 hours. Mifepristone-induced BHK cells were washed two times with DMEM and incubated for 30 min at 37°C in DMEM containing 10 μg/ml ^{125}I-apoA-I. The medium was removed, cells were washed three times with ice-cold PBS, chilled on ice for 30 min in DMEM plus 10 mM HEPES, pH 7.4, and cold Triton X-100 extraction was performed. Cells were lysed with 0.5 N NaOH, and the protein concentration was determined using the Lowry method. Radioactivity found in the medium and in the cells was determined by gamma counting.

2.18 Triacylglycerol extraction of 3T3-L1 adipocytes—On day 8 of differentiation, the normal and hypertrophic adipocytes grown on 35 mm dishes were washed twice with 1 ml PBS. Lipids were extracted using 2 ml of a 2:3 mixture isopropanol and heptane for 30 minutes at room temperature. Extraction solution was transferred to glass culture tubes, and cellular lipids were extracted once more using 1 ml of isopropanol:heptane for 15 minutes. Extraction solution was combined with the first extraction in glass culture tubes. Samples were dried for 1 hour in a Speed Vac (SC 110A, Savant). 600 μl of isopropanol to the dried TG extracts and standards. 150 μl of

saponification reagent (10 g KOH, 75 ml H_2O and 25 ml isopropanol) was then added to each tube followed by vortexing, and samples were incubated for 10 minutes at room temperature. This was followed by adding 300 µl of sodium metaperiodate reagent (65 mg sodium periodate, 6 ml of glacial acetic acid, 70 ml of dH_2O, 7.7 g of anhydrous ammonium acetate, and adjusted to 100 ml with H_2O) to each sample and standard before vortexing. 300µl of acetyl acetone reagent (0.4 ml of 2,4 pentadione in 100 ml isopropanol) was then added followed by vortexing. Glass tubes were covered with 2 layers of parafilm and placed in a 65°C water bath for 15 minutes. Samples and standards were then cooled and the absorptions were read at 410 nm.

2.19 Acute insulin stimulation of 3T3-L1 adipocytes—On day 8 of differentiation, medium from both normal and hypertrophic adipocytes was replaced with low glucose DMEM supplemented with 1% P/S and 0.5% CS. Following 16-20 hour serum-starvation, the medium was removed. Adipocytes were washed with 1 ml KRH (125 mM NaCl, 4.8 mM KCl, 2.6 mM $CaCl_2 2H_2O$, 1.2 mM $MgSO_4$, 25 mM HEPES and 5.6 mM Dextrose/Glucose) and incubated in 1 ml of KRH for 15 minutes at 37°C. 10 µl of vehicle (2 mg BSA/ ml KRH) or 10 µl of insulin treating solution (100 µM stock) was added to control and insulin treatment dishes, respectively, for 5 minutes at 37°C. KRH was then removed and adipocytes were lysed on ice with 200 µl of 1X Laemmli buffer [1 ml 2X Laemmli buffer (4% SDS, 20% Glycerol, 120 mM Tris pH 6.8, 0.004% Bromophenol Blue), 280 µl H_2O, 200 µl 500 mM NaF, 200 µl 50 mM Na pyrophosphate, 200 µl 50 mM EGTA, 20 µl 100 mM Na orthovanadate and 100 µl β-mercaptoethanol]. Adipocytes were then scraped and transferred to chilled microfuge tubes using a 26G1/2 syringe. The samples were boiled for 5 minutes, transferred to 1.5-ml Eppendorf tubes and centrifuged at max speed for 10

minutes to remove lipids. Protein concentrations were determined by Lowry assay, and equivalent amounts of protein were separated on 7.5% SDS-PAGE. Immunoblotting analyis was performed using anti-phosphotyrosine, anti-IRS-1, anti-pSer473-Akt, and anti-Akt/PKB antibodies.

Chapter 3 Results

3.1 WT-ABCA1 is expressed and functional in induced BHK cells

We hypothesized that ABCA1 functions on the plasma membrane by actively modulating lipid raft microdomains and non-raft regions in order to prime cells for apoA-I-mediated cholesterol efflux. In order to control for any non-target mifepristone-induced effects, we used a cell line containing the same induction system but lacking an insert in the plasmid (Mock)[168]. BHK cells do not normally express ABCA1, but upon 18-20 hour mifepristone induction of our ABCA1 stable transfectants, ABCA1 protein was detected (Fig. 3.1A). The ABCA1 protein level in our BHK cells was comparable to that of cAMP-induced RAW264 macrophages and ~5-fold higher than that in human THP-1 macrophages induced with 22(R)-hydroxycholesterol and 9-*cis*-retinoic acid, as determined by immunoblot (data not shown). We also used a third cell line stably transfected with a mutant form of ABCA1, A937V-ABCA1 (A937V). A937V comprises a naturally occurring mutation in its first ATP-binding domain and is defective in apoA-I-mediated cholesterol efflux. As shown in Fig. 3.1A, A937V was expressed at a similar level to WT-ABCA1. As expected, once induced by mifepristone, WT-ABCA1 BHK cells produced efficient cholesterol efflux to apoA-I (Fig. 3.1B), comparable to RAW264, which typically efflux ~15% of their cholesterol in 4 hours[129]. As expected, A937V and Mock cells failed to efflux cholesterol to apoA-I (Fig. 3.1B). These efflux results were indicative that our induced expression of WT-ABCA1 in the BHK cells was fully functional.

Figure 3.1

Characterization of BHK cells with inducible ABCA1 expression. ***A***, ABCA1 expression in Mock, ABCA1 and ABCA1 mutant, A937V, before (lane 1-3) and after overnight incubation with 10 nM mifepristone (lane 4-12). Cytosolic protein Hsp70 serves as a loading control. Ratio of ABCA1 and Hsp70 represents relative level of ABCA1 expression among the cell lines (error bars are standard deviations). ***B***, ApoA-I mediated [^{3}H]cholesterol efflux. [^{3}H]cholesterol labeled cells were incubated with mifepristone overnight and cholesterol efflux was measured after 4 h incubation with or without apoA-I (10 μg/ml). Error bars represent standard deviations of triplicate wells.

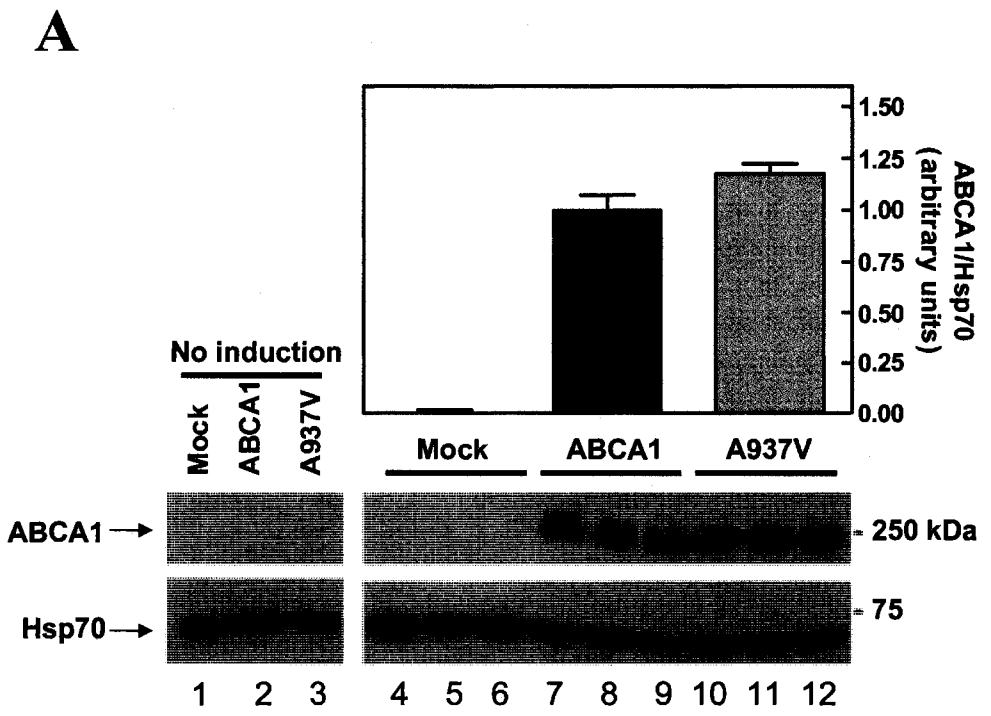
A
1.50
1.25
1.00
0.75
0.50
0.25
0.00
ABCA1/Hsp70 (arbitrary units)
No induction
Mock
ABCA1
A937V
Mock
ABCA1
A937V
ABCA1
250 kDa
Hsp70
75
1 2 3 4 5 6 7 8 9 10 11 12

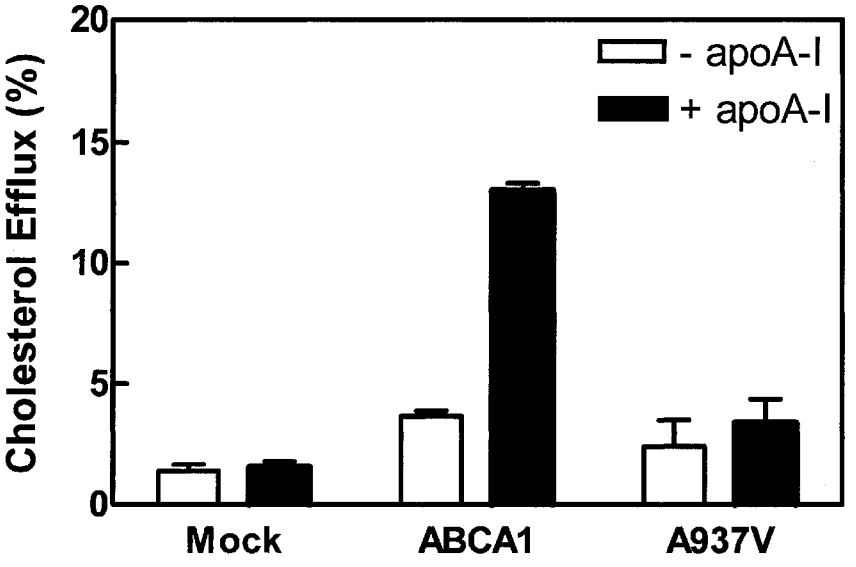
B
Cholesterol Efflux (%)
20
15
10
5
0
- apoA-I
+ apoA-I
Mock
ABCA1
A937V

3.2 WT-ABCA1 and A937V are similarly expressed and distributed

Previously, ABCA1 was found to localize on the plasma membrane and in the late endosomes/lysosomes using GFP-tagged ABCA1[128]. In order to characterize the WT-ABCA1 and A937V cellular distributions, which may not be identical to GFP-ABCA1, we immunostained cells using a polyclonal antibody against ABCA1. We found that WT-ABCA1 was localized mainly to the plasma membrane. Single images taken of the basal plasma membrane showed that WT-ABCA1 was nicely decorating the general area of the plasma membrane (Fig. 3.2, first row), while Mock cells produced little staining, confirming the specificity of our antibody. We also took sequential images along the z-axis covering the entire cell volume. We then projected these z-axis images onto a single image to represent the total WT-ABCA1 distribution throughout the cell volume (Fig. 3.2, second row). It was apparent that WT-ABCA1 primarily decorated the plasma membrane as well as membrane projections, as reported previously using GFP-tagged ABCA1[131, 165]. Importantly, the expression level and distribution of A937V were indistinguishable from WT-ABCA1. This indicated that the mutant protein was synthesized normally and was able to traffic to the plasma membrane. WT-ABCA1 was also shown to be present in intracellular structures (Fig. 3.2, second row), that had the characteristics of the ER and Golgi. In order to determine whether WT-ABCA1 found in these intracellular structures represented the shuttling of WT-ABCA1 to the plasma membrane along the biosynthesis pathway, we briefly inhibited general protein synthesis with cycloheximide. As suspected, when the biosynthesis of WT-ABCA1 was inhibited, WT-ABCA1 expression was only seen on the plasma membrane (Fig. 3.2, fourth row). This demonstrated that these WT-ABCA1-containing intracellular structures only transiently housed WT-ABCA1 protein during its

Figure 3.2

ABCA1 expression level and distribution. ***A***, ABCA1 distribution in Mock, ABCA1, and A937V cells. Cells were immunostained using an anti-ABCA1 antibody. Single slices of images (*first* and *third rows*) or a series of Z-sections (*second* and *fourth rows*) were taken throughout the cell volume using confocal fluorescent microscopy and then projected to a single plane. Some of the cells were also treated with cycloheximide for 2 h before immunostaining (*third* and *fourth rows*).

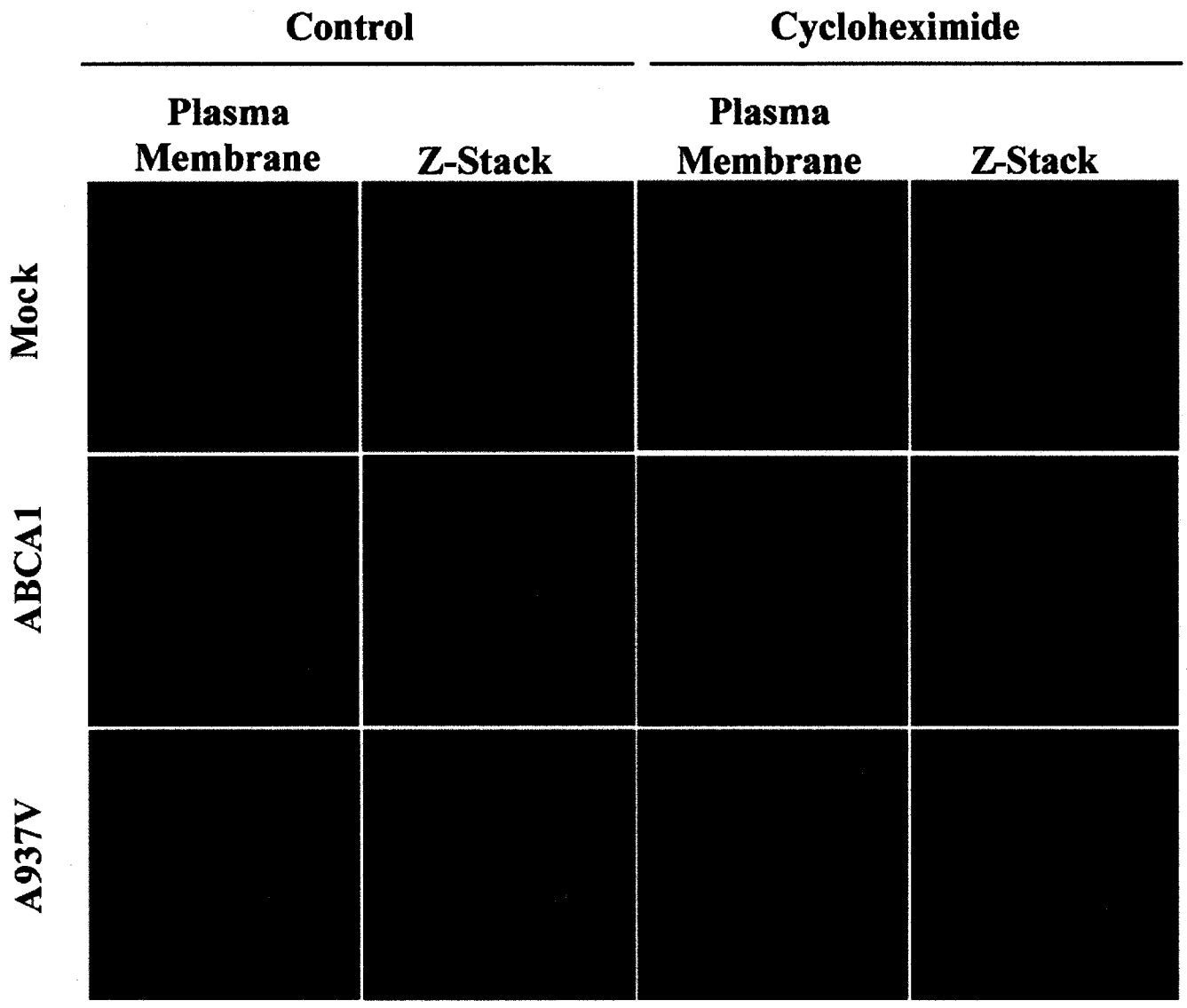
Control
Cycloheximide
Plasma Membrane
Z-Stack
Plasma Membrane
Z-Stack
Mock
ABCA1
A937V

biosynthesis and trafficking to the plasma membrane. Once again, A937V was found only on the plasma membrane when cells were treated with cycloheximide, identical to WT-ABCA1.

3.3 Cholesterol levels and distribution are identical in all cell types

We also examined FC levels in both WT-ABCA1 and Mock BHK cells and found that the total FC mass was equivalent between the two cell lines (4.56 ± 0.77 μg/mg of protein versus 4.87 ± 0.88 μg/mg of protein). The equal measure of total FC indicated a similar mass content between the cell lines, but it lacked distributional information. Abnormal sequestration of FC to an intracellular compartment in WT-ABCA1-expressing cells could significantly diminish the FC on the plasma membrane, yet would remain undetected in total cholesterol mass analysis. Therefore, we performed filipin staining in order to visualize the relative FC levels and distribution between all three cell lines. We found that the filipin staining patterns were comparable in Mock, WT-ABCA1 and A937V cells (Fig. 3.3), indicating that WT-ABCA1 expression did not substantially alter the subcellular distribution of FC. Furthermore, we analyzed the cholesterol cellular distribution in all three cell types biochemically by cell fractionation. As shown in Fig. 3.4, the plasma membrane peaked in fraction 7, marked by CAV1. As expected, this peak had the highest content of cholesterol. The fractionation and cholesterol distribution were very similar among all three cell types, which was consistent with our microscopy observations. However, WT-ABCA1-expressing cells seemed to contain slightly less cholesterol in the ER (fractions 9 and 10), marked by calnexin, which could indicate an increase in cholesterol

Figure 3.3

Filipin staining of FC in BHK cells. Mock, ABCA1, and A937V cells were stained with 0.05 mg/mL filipin for 2 hours at room temperature and fluorescent images were taken under identical conditions.


Mock
ABCA1
A937V

Figure 3.4

Cellular cholesterol distribution analysis by cell fractionation. [^{3}H]Cholesterol-labeled cells were fractionated as described under "Materials and Methods." Each fraction was analyzed by ^{3}H counts and protein markers: Hsp70 for the cytosol (peaked at *fractions 3* and *4*), CAV1 for the plasma membrane (peaked at *fraction 7*) and calnexin for the endoplasmic reticulum (peaked at *fraction 9*). *Error bars* are the standard errors of the mean from two independent experiments.

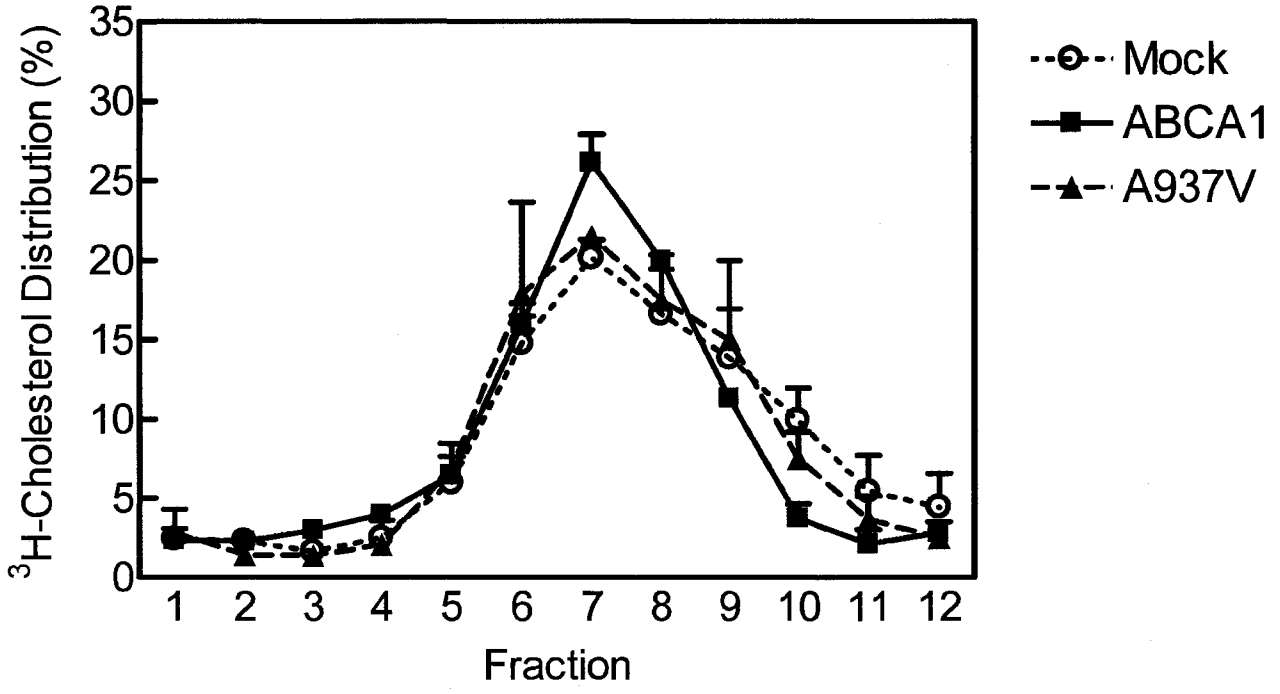
35
30
25
20
15
10
5
0
^{3}H-Cholesterol Distribution (%)
1 2 3 4 5 6 7 8 9 10 11 12
Fraction
Mock
ABCA1
A937V

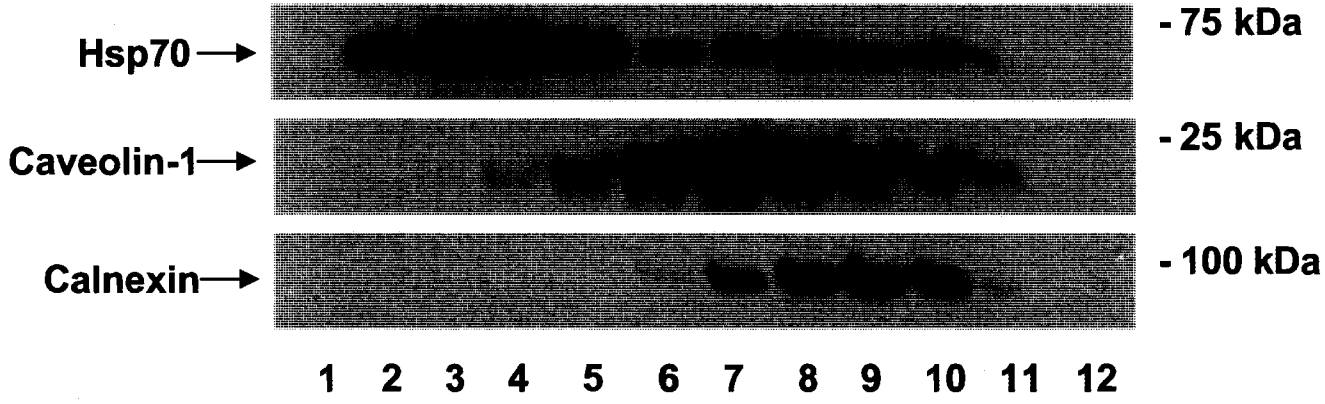
Hsp70
Caveolin-1
Calnexin
- 75 kDa
- 25 kDa
- 100 kDa
1 2 3 4 5 6 7 8 9 10 11 12

mobility from internal membranes to the plasma membrane. Collectively, it was determined that the majority of WT- and A937V-ABCA1 was expressed on the plasma membrane and its expression did not cause significant cholesterol redistribution.

3.4 Functional ABCA1 disrupts plasma membrane microdomains

In order to determine whether ABCA1 expression affects the raft/non-raft partitioning of the plasma membrane, we analyzed FC mass in the tightly packed membrane microdomains (rafts), as well as in the loosely packed regions (non-rafts). We first performed this characterization employing the solubility in cold Triton X-100, which is a widely used criterion to define lipid raft microdomains. Mock, WT-ABCA1 and A937V cells were incubated in cold Triton X-100 (1%) for 30 minutes. Non-raft regions of the plasma membrane were solubilized (Triton X-100-soluble fraction), therefore releasing non-raft cholesterol into the detergent media. Conversely, lipid raft membrane regions remained cell-associated (Triton X-100-insoluble fraction). FC levels in each fraction were quantified by mass analysis. In Mock cells, ~40% of total FC was present in the non-raft, Triton X-100-soluble fraction (Fig. 3.5A), which was consistent with previous reports by others that the majority of plasma membrane FC is Triton X-100-insoluble[173, 177]. Interestingly, in WT-ABCA1 cells, >60% of total FC was present in the Triton X-100-soluble fraction. In parallel, we also used [^{3}H]cholesterol to label the total cellular cholesterol pool, followed by cold Triton X-100 extraction. Again, we determined that WT-ABCA1 cells contained significantly more [^{3}H] FC in the Triton X-100-soluble fraction relative to Mock cells (Fig. 3.5B). In addition, WT-ABCA1 did not increase the Triton X-100 solubility of [^{3}H]CE

Figure 3.5

Distribution of FC and phospholipids. BHK cells induced to express either empty vector (*Mock*), ABCA1 (*ABCA1*), or ABCA1 mutant A937V (*A937V*) were subjected to 1% cold Triton X-100 extraction for 30 min on ice. ***A***, free cholesterol contents in the media (Triton X-100-soluble) and in the cell (Triton X-100-insoluble) were analyzed by a colorimetric kit as described under "Materials and Methods." The results are presented as percentage Triton X-100-soluble free cholesterol of total free cholesterol (Triton X-100-soluble plus insoluble). ***B***, cells labeled with [^{3}H]cholesterol overnight were treated with 1% cold Triton X-100 on ice for 30 min. Cellular lipids in Triton X-100-insoluble fraction or in Triton X-100-soluble fraction were extracted and separated by TLC, and radioactivity associated with free cholesterol was counted. Results are presented as percentage Triton X-100-soluble ^{3}H-free cholesterol. ***C*** and ***D***, Mock, ABCA1, and A937V cells were radiolabeled with 1 μCi/ml [^{3}H]choline for 24 h, chilled on ice for 30 min prior to 1% Triton X-100 extraction at 4 °C. Lipids were extracted from media and cells and separated by thin-layer chromatography. Radioactivity associated with sphingomyelin (***C***) and phosphatidylcholine (***D***) was determined by β-scintillation counting. Results are expressed as mean ± S.D. of triplicate wells. *, $p < 0.05$; #, $p < 0.025$.

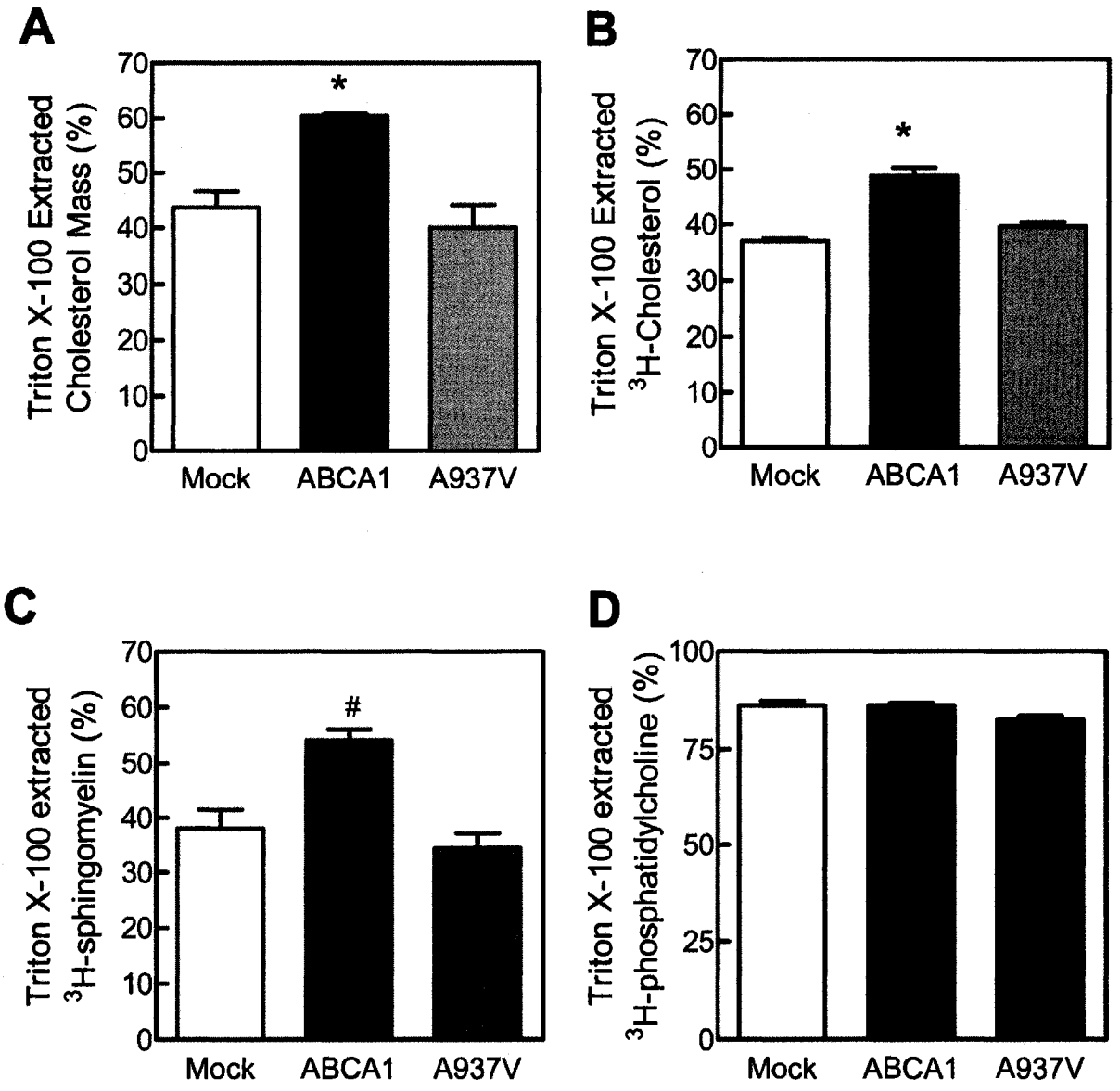
A
Triton X-100 Extracted Cholesterol Mass (%)
70
60
50
40
30
20
10
0
*
Mock
ABCA1
A937V
B
Triton X-100 Extracted ^{3}H-Cholesterol (%)
70
60
50
40
30
20
10
0
*
Mock
ABCA1
A937V
C
Triton X-100 extracted ^{3}H-sphingomyelin (%)
70
60
50
40
30
20
10
0
#
Mock
ABCA1
A937V
D
Triton X-100 extracted ^{3}H-phosphatidylcholine (%)
100
75
50
25
0
Mock
ABCA1
A937V

(data not shown). This was indicative of WT-ABCA1 being able to expand the non-raft FC pool without modifying total cholesterol mass or the subcellular distribution as shown in Fig. 3.3 and Fig. 3.4. The FC redistribution to the Triton X-100-soluble fraction occurred in the absence of the physiological cholesterol acceptor apoA-I and thus in the absence of active cholesterol efflux. Such a redistribution, therefore, could be driven by the intrinsic activities of WT-ABCA1. Alternatively, it is also possible that protein overexpression *per se* could disrupt plasma membrane microdomains, particularly with a protein consisting of 12 TMDs. In order to address this issue, we again took advantage of the A937V cell line. Interestingly, the cold Triton X-100-soluble fraction of cholesterol in A937V cells was identical to that of Mock cells (Fig. 3.5A and B), which suggested that the redistribution of FC from lipid rafts to non-raft membrane domains requires a fully-functional ABCA1 protein.

3.5 Functional ABCA1 increases non-raft SM without affecting PC

It has been suggested that WT-ABCA1 can generate phospholipid-rich microdomains though its postulated lipid-flipping activity. This modulation of the inner/outer leaflet phospholipid distribution could play a major role in the general lipid packing of the plasma membrane. Upon analysis, we found that the Triton X-100 solubility of [^{3}H]SM, a major lipid raft component, was also significantly increased in WT-ABCA1 cells (~50%) relative to Mock cells (Fig. 3.5C). At the same time, the expression of WT-ABCA1 had no effect on the distribution of [^{3}H]PC, a major component of non-raft domains, relative to Mock cells (Fig. 3.5D). Again, we analyzed the effect of A937V expression on the plasma membrane in comparison to WT-ABCA1 and Mock cells. It was

confirmed that the A937V-mutant was unable to redistribute [^{3}H]SM, consistent with its incapability to redistribute cholesterol, relative to WT-ABCA1 (Fig. 3.5C).

3.6 WT-ABCA1 decreases the general packing of the plasma membrane

In order to further explore the intrinsic activity of functional ABCA1, we examined the effect of WT-ABCA1 on the general packing of the plasma membrane. In order to selectively visualize the plasma membrane of WT-ABCA1 and Mock cells, we performed 20 second pulse-labeling of both cell lines using $DiIC_{18}$, a fluorescent phospholipid analog[173] (Fig. 3.6A and B). As expected, cold Triton X-100 extracted the non-raft portion of the plasma membrane, which, upon visualization, resulted in swiss-cheese-like remnants of fluorescent membrane: the detergent-resistant lipid raft portion of the plasma membrane. Interestingly, we observed that WT-ABCA1-expressing cells contained a greater amount of plasma membrane holes following Triton X-100 solubilization, relative to Mock cells (Fig. 3.6C and D). In order to quantify the degree of plasma membrane solubilization, we measured the total area of the plasma membrane that was extracted by cold Triton X-100 in individual cells, and pooled the data obtained from a large number of cells. We found that cold Triton X-100 was able to extract twice the amount of plasma membrane in WT-ABCA1 cells, compared to Mock cells (Fig. 3.6E), similar to our biochemical analysis. This effectively demonstrated that, in addition to cholesterol and SM, the plasma membrane as a whole showed increased cold Triton X-100 extractability in WT-ABCA1 cells. In summary, the aforementioned results support the idea that WT-ABCA1 redistributes lipids from lipid raft to non-raft plasma membrane domains.

Figure 3.6

Characterization of cold Triton X-100 extractability of $DiIC_{18}$. ABCA1 and Mock cells were incubated with mifepristone overnight. Cells were first labeled with $DiIC_{18}$ at 37 °C for 20 s (***A*** and ***B***), washed, and extracted with 1% Triton X-100 on ice for 30 min (***C*** and ***D***). Cells were imaged by fluorescence microscopy. For quantification in ***E***, each cell was outlined manually, and $DiIC_{18}$ fluorescent intensities before and after Triton X-100 extraction were calculated as described under "Materials and Methods." For each data point, results from >50 cells were pooled and presented as the mean ± S.E.

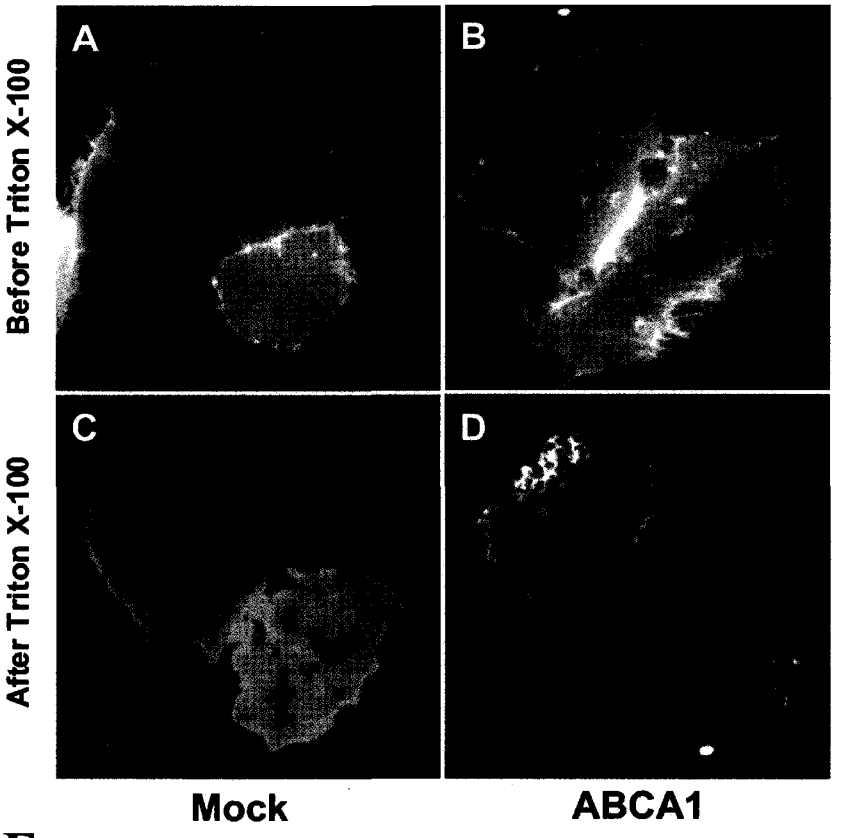
A
B
C
D
Before Triton X-100
After Triton X-100
Mock
ABCA1

E

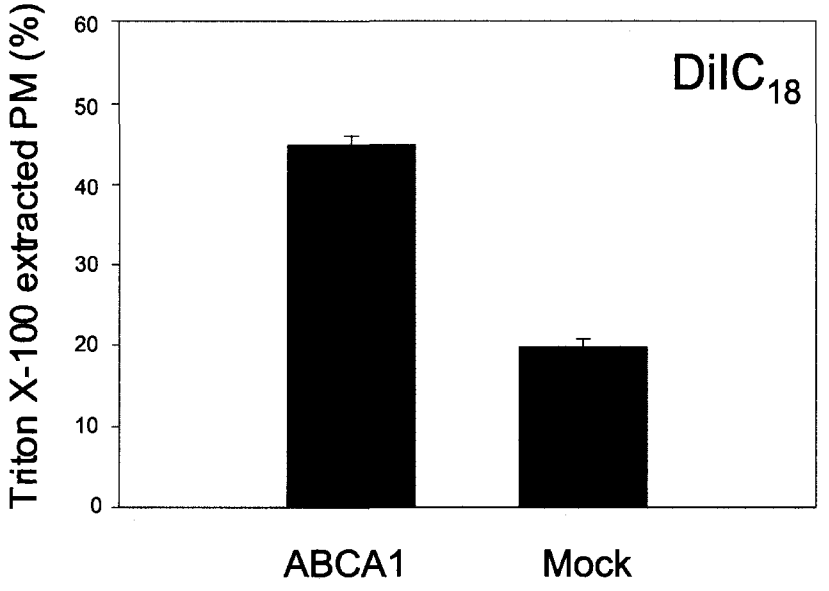
Triton X-100 extracted PM (%)
60
50
40
30
20
10
0
DiIC18
ABCA1
Mock

3.7 Functional ABCA1 disperses CAV1 on the plasma membrane

To this point, we have employed Triton X-100 insolubility, a commonly used operational definition of lipid rafts, in order to characterize the effect of functional WT-ABCA1 on the plasma membrane. Although this method is highly informative, it does involve some limitations and possible unconfirmed artifacts. In order to address this issue, we sought to couple our detergent solubility analyses with multiple detergent-free approaches. As mentioned in the introduction, CAV1 is a well known lipid raft/caveolae marker whose intracellular localization is highly sensitive to the cellular cholesterol content, as well as the lipid organization of the plasma membrane[178, 179]. We therefore transiently transfected Mock, WT-ABCA1 and A937V cells with EYFP-CAV1 to visualize their respective EYFP-CAV1 distributions. The actual role of CAV1 in terms of cholesterol efflux has been highly inconsistent among various cell models tested to date[180], therefore it was important to first examine the effect of EYFP-CAV1 transfection on ABCA1-mediated cholesterol efflux in our BHK cell model. Importantly, we determined that the transient transfection of EYFP-CAV1 had no effect on cholesterol efflux from WT-ABCA1-expressing BHK cells (WT-ABCA1, 4.35 ± 0.2%; WT-ABCA1/EYFP-CAV1, 4.12 ± 0.02%) (data not shown). According to this result, we were convinced that EYFP-CAV1 expression had no effect on the intracellular mobility of cholesterol in the transfected BHK cells. Following the transfection of EYFP-CAV1, we performed morphological characterization of EYFP-CAV1 using confocal microscopy. In Mock cells, the EYFP-CAV1 distribution was punctate and clustered, especially along the cellular boundaries of the membrane (Fig. 3.7A). This is characteristic of the reported CAV1 plasma membrane distribution[181]. Through further characterization at higher magnification, EYFP-CAV1

Figure 3.7

ABCA1 expression disperses EYFP-CAV1 on the plasma membrane. EYFP-CAV1 was transiently expressed in either Mock (***A*** and ***C***) or ABCA1 (***B*** and ***D***) cells. EYFP-CAV1 distribution was observed by confocal microscopy. ***E***, the EYFP-CAV1 appearance, namely diffused or punctate, was used to score a large number of cells in ABCA1 and Mock clones. Results are presented as percentages of each phenotype in ABCA1 or Mock cells.

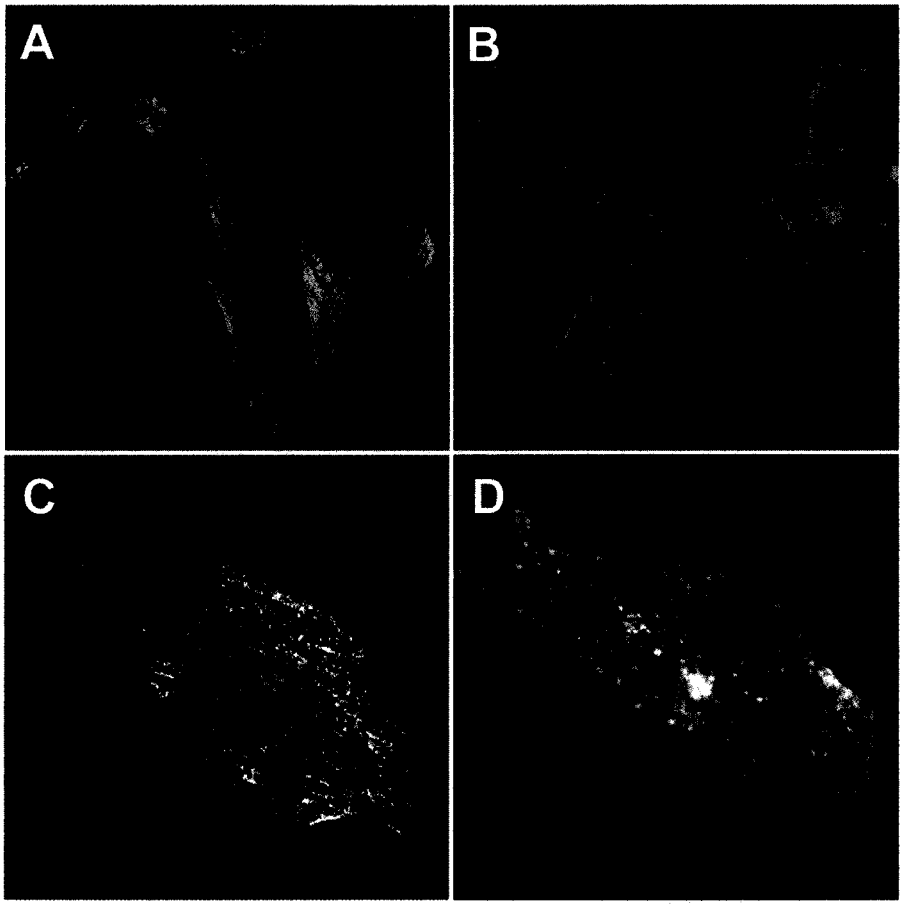
A
B
C
D
Mock
ABCA1

E

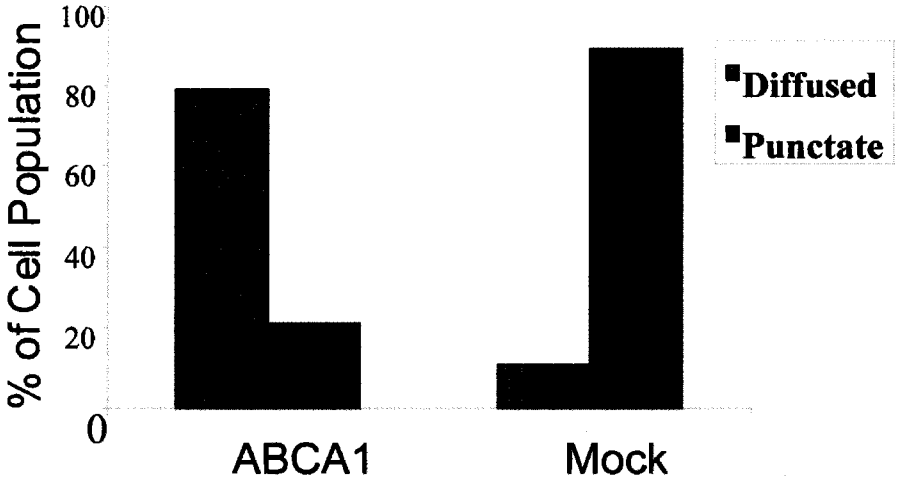
% of Cell Population
100
80
60
40
20
0
ABCA1
Mock
Diffused
Punctate

was observed to decorate cable-like structures in Mock cells (Fig. 3.7C), presumably along the actin filaments as described previously[12]. In contrast, WT-ABCA1-expressing cells strikingly distributed EYFP-CAV1 in a dispersed manner across the general area of the plasma membrane, almost exclusively lacking clustered caveolae-like structures (Fig. 3.7B and D). We subsequently scored the cell populations of both cell types according to their EYFP-CAV1 distribution (clustered versus dispersed/diffused). We found that ~80% of WT-ABCA1-expressing cells had a dispersed/diffused EYFP-CAV1 distribution on the plasma membrane, in contrast to Mock cells, where nearly all cells showed the punctate EYFP-CAV1 distribution (Fig. 3.7E). In addition, the endogenous distribution of CAV1 was examined in non-transfected cells by immunofluorescence, using a monoclonal anti-CAV1 antibody. The distribution was identical to that of EYFP-CAV1 (not shown). It is also important to note that the EYFP-CAV1 distribution in non-induced WT-ABCA1 cells, which lack WT-ABCA1 expression, was indistinguishable from the distribution in Mock cells. The clustered EYFP-CAV1 distribution only became dispersed across the plasma membrane upon 18-20 hour induction of WT-ABCA1 expression (not shown). Additionally, when we treated cells with apoA-I for 4 hours, there was no visible effect on the EYFP-CAV1 distribution in either Mock or WT-ABCA1 cells (data not shown).

In order to provide further evidence that the redistribution of CAV1 indeed resulted from intrinsic WT-ABCA1 activity, we characterized EYFP-CAV1-transfected cells co-stained for ABCA1 using immunofluorescence. In this case, we were able to take advantage of the fact that there were some variations within our cell line in terms of WT-ABCA1 expression. We found that the dispersion of EYFP-CAV1 on the plasma membrane occurred only in cells expressing WT-ABCA1 (Fig. 3.8A and B, cells *a* and *b*). As shown (Fig. 3.8A

Figure 3.8

Effect of ABCA1 expression on EYFP-CAV1 distribution. BHK cells expressing either WT-ABCA1 or A937V were transfected with EYFP-CAV1 and immunostained against ABCA1. Fluorescent images for ABCA1 (***A*** and ***C***) and EYFP-CAV1 (***B*** and ***D***) were taken from the identical fields of cells with confocal fluorescent microscopy under identical instrument settings. Cells ***a*** and ***b*** express detectable levels of ABCA1, while cells ***c*** and ***d*** express very little.

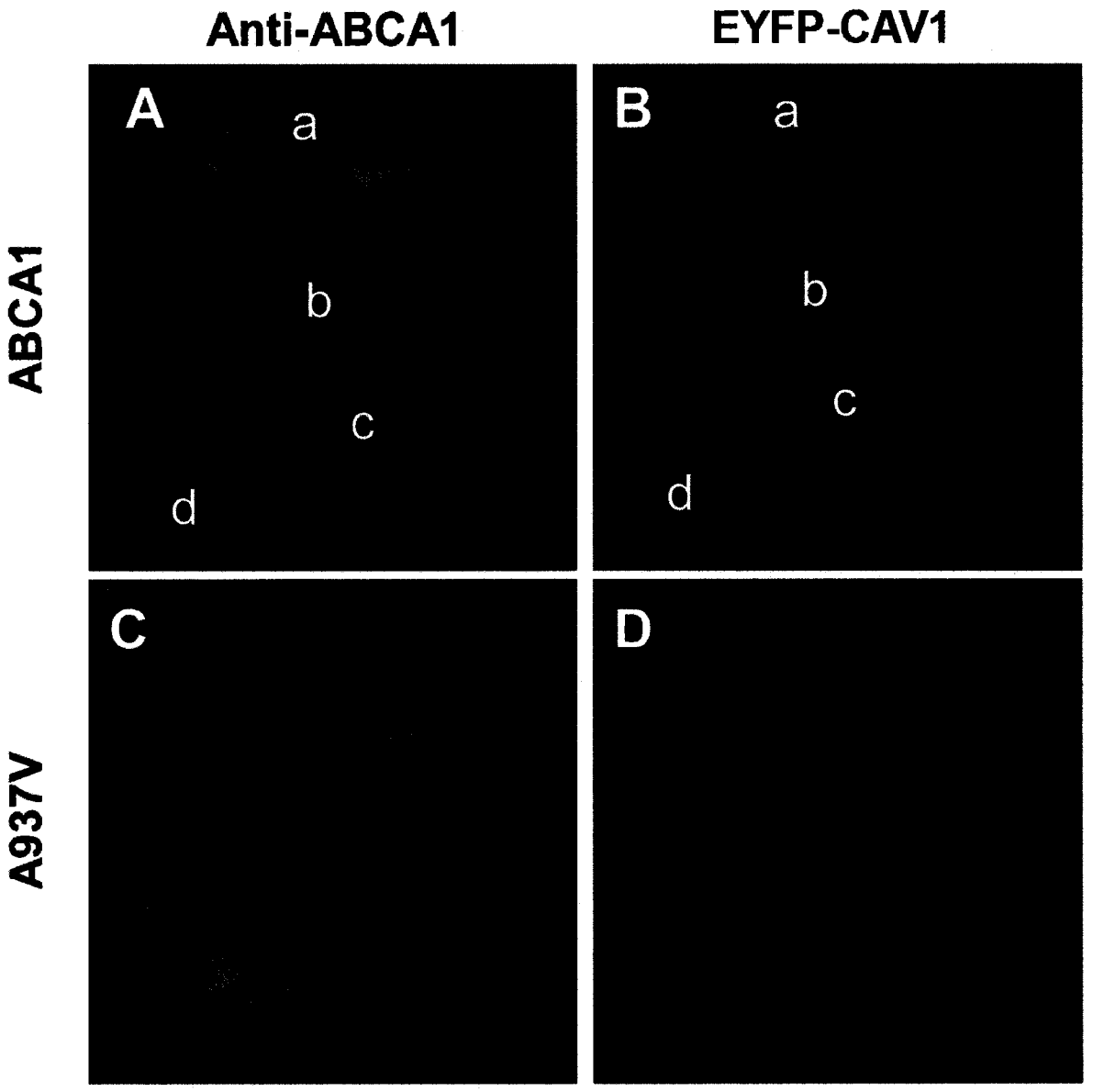
Anti-ABCA1
EYFP-CAV1
ABCA1
A937V
A
a
b
c
d
B
a
b
c
d
C
D

and B, cells *c* and *d*), two neighboring cells that failed to express WT-ABCA1 expressed EYFP-CAV1 as punctate and clustered structures on the plasma membrane, similar to Mock cells (Fig. 3.7C). Interestingly, while A937V expression and distribution was similar to that of WT-ABCA1 (Fig. 3.8C), A937V cells failed to disperse EYFP-CAV1 on the plasma membrane and retained the punctate and clustered EYFP-CAV1 distribution (Fig. 3.8D) as observed in Mock cells. This result was consistent with the observed inability of A937V-expressing cells to redistribute lipids and disrupt lipid rafts (Fig. 3.5).

While we were confident that the different EYFP-CAV1 distributions were caused by modifications in lipid packing by WT-ABCA1, it remained possible that a different membrane topology could influence the appearance of membrane proteins such as EYFP-CAV1. For example, if membrane ruffling was occurring more frequently in Mock and A937V cells, EYFP-CAV1 residing in ruffles would appear brighter and more clustered, while EYFP-CAV1 covering flatter membrane sections would appear to be more diffused. In order to exclude the possibility of membrane ruffling, we stained for a second plasma membrane protein, transferrin (Tf) receptor, using Cy3-transferrin (Cy3-Tf). If membrane ruffling was indeed occurring, the distribution of Cy3-Tf would match that of EYFP-CAV1, therefore appearing clustered in Mock and A937V cells. We, however, found that Cy3-Tf was distributed evenly across the plasma membrane in all cell lines (Fig. 3.9). This indicated that the membrane morphology was similar in all cell lines, and that the redistribution of EYFP-CAV1 had been caused by changes in the intrinsic properties of the membrane, such as lipid packing.

Figure 3.9

Plasma membrane labeling with Cy3-Transferrin. Mock, WT-ABCA1 and A937V cells were transiently transfected with EYFP-CAV1 as described in "Materials and Methods". EYFP-CAV1 transfected cells were incubated with 80 ng/ml of Cy3-transferrin for 30 min on ice in order to evenly label the plasma membrane trasferrin receptor.

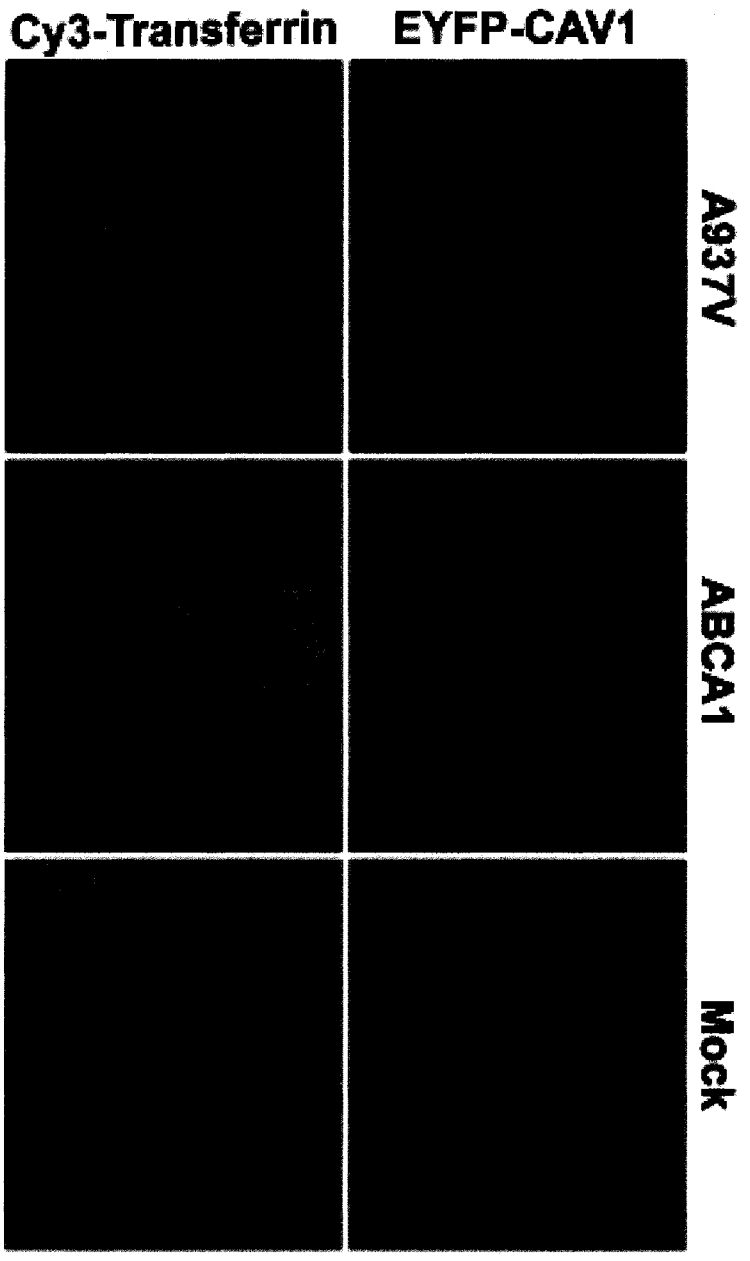
Cy3-Transferrin
EYFP-CAV1
A937V
ABCA1
Mock

3.8 Effect of cellular cholesterol modulation on EYFP-CAV1

In order to validate our assumption of caveolae disruption by WT-ABCA1, we took advantage of cellular cholesterol modulation, which is a previously established means of disrupting caveolar structures[10]. In fact, cholesterol depletion by 30 minute incubation with MCD is known to deplete >60% of cellular cholesterol, and subsequently disrupt lipid rafts. Using this cholesterol depletion method, we successfully dispersed EYFP-CAV1 from clusters to the general area of the plasma membrane in Mock cells (Fig. 3.10A to C). This same treatment had little effect on the EYFP-CAV1 distribution in WT-ABCA1, which remained diffused across the membrane (Fig. 3.10B and D). Conversely, when we exogenously loaded cholesterol into WT-ABCA1 cells using a cholesterol-MCD complex, a treatment known to enforce lipid raft formation, we were able to shift EYFP-CAV1 from the general membrane area into punctate clusters (Fig. 3.10B to F). This same treatment had little effect on Mock cells, in which the EYFP-CAV1 remained in punctate clusters (Fig. 3.10A and E). Overall, our results obtained regarding the distribution of CAV1 in live cells support the idea that WT-ABCA1 re-organizes the lipid raft/non-raft partition of the plasma membrane.

3.9 EYFP-CAV1 mobility is unaffected by WT-ABCA1

The distribution of CAV1 is known to be sensitive to various cellular elements, most notably the levels of plasma membrane cholesterol, as well as the anchoring of CAV1 to the actin cytoskeleton. As described above, we determined that there were no differences in terms of FC mass or subcellular cholesterol distribution among the cell types. We therefore examined whether the actin anchoring of EYFP-CAV1 was altered upon dispersion in

Figure 3.10

EYFP-CAV1 redistribution by cholesterol modulation. Mock (***A***) and WT-ABCA1 (***B***) cells were transfected with EYFP-CAV1 and the resulting distributions were analyzed under identical instrument settings. EYFP-CAV1 images were taken in Mock (***C***) and WT-ABCA1 (***D***) cells treated with 2.5 mM MCD in order to deplete cholesterol and disrupt caveolae. EYFP-CAV1 images were also taken in Mock (***E***) and WT-ABCA1 (***F***) cells treated with cholesterol:MCD complex in order to enrich cholesterol and facilitate caveolae formation.

Mock
ABCA1
Untreated
Cholesterol Depletion
Cholesterol Enrichment
A
B
C
D
E
F

WT-ABCA1 cells using FRAP, which is a classic method for the analysis of protein mobility on the plasma membrane. As shown by FRAP analysis, EYFP-CAV1 remained extremely immobile in both clustered and dispersed distributions, as indicated by the lack of fluorescence recovery (Fig. 3.11A and B). This suggested that EYFP-CAV1 remained tightly anchored in both the clustered Mock cell distribution and in the dispersed WT-ABCA1 EYFP-CAV1 distribution. According to these results, we therefore concluded that a shift in lipid packing conditions in WT-ABCA1-expressing cells, such as a significant expansion of non-raft membrane domains, hindered CAV1 from forming caveolae clusters, since the assembly of caveolae is highly-dependent on tightly packed lipid raft domains. In order to accomplish this outcome, WT-ABCA1 likely disrupts lipid rafts resulting in a redistribution of CAV1 from punctate clusters to the general area of the plasma membrane and a depletion of plasma membrane cholesterol from caveolae domains[182]. This redistribution of CAV1 on the plasma membrane was, therefore, consistent with our biochemical analysis (Fig. 3.5).

3.10 WT-ABCA1 disrupts caveolae according to non-detergent analysis

In the case that the altered CAV1 distribution in WT-ABCA1-expressing cells is indeed due to the reorganization of membrane lipids, the floatation properties of CAV1 should also be modified. The floatation properties of CAV1 constitute a second commonly used, detergent-free method of lipid raft characterization. We therefore performed Optiprep gradient floatation on Mock, WT-ABCA1 and A937V cells to analyze their respective CAV1 floatation distribution across 10 density fractions (Fig. 3.12A). We found that the

Figure 3.11

EYFP-CAV1 mobility in clustered and dispersed distributions. Mock and WT-ABCA1 cells were transfected with EYFP-CAV1 and placed on a confocal microscope stage. ***A***, photobleaching of a defined square region of the basal plasma membrane was conducted using the 488 nm line of a Bio-Rad MRC 1024 laser-scanning confocal microscope at full laser power (100%). Fluorescence recovery was monitored by taking images of whole cells at low laser power (3-10%). ***B***, recovery was measured as the fluorescence intensity of the photobleached region / fluorescence intensity of a non-bleached section of basal membrane with time.

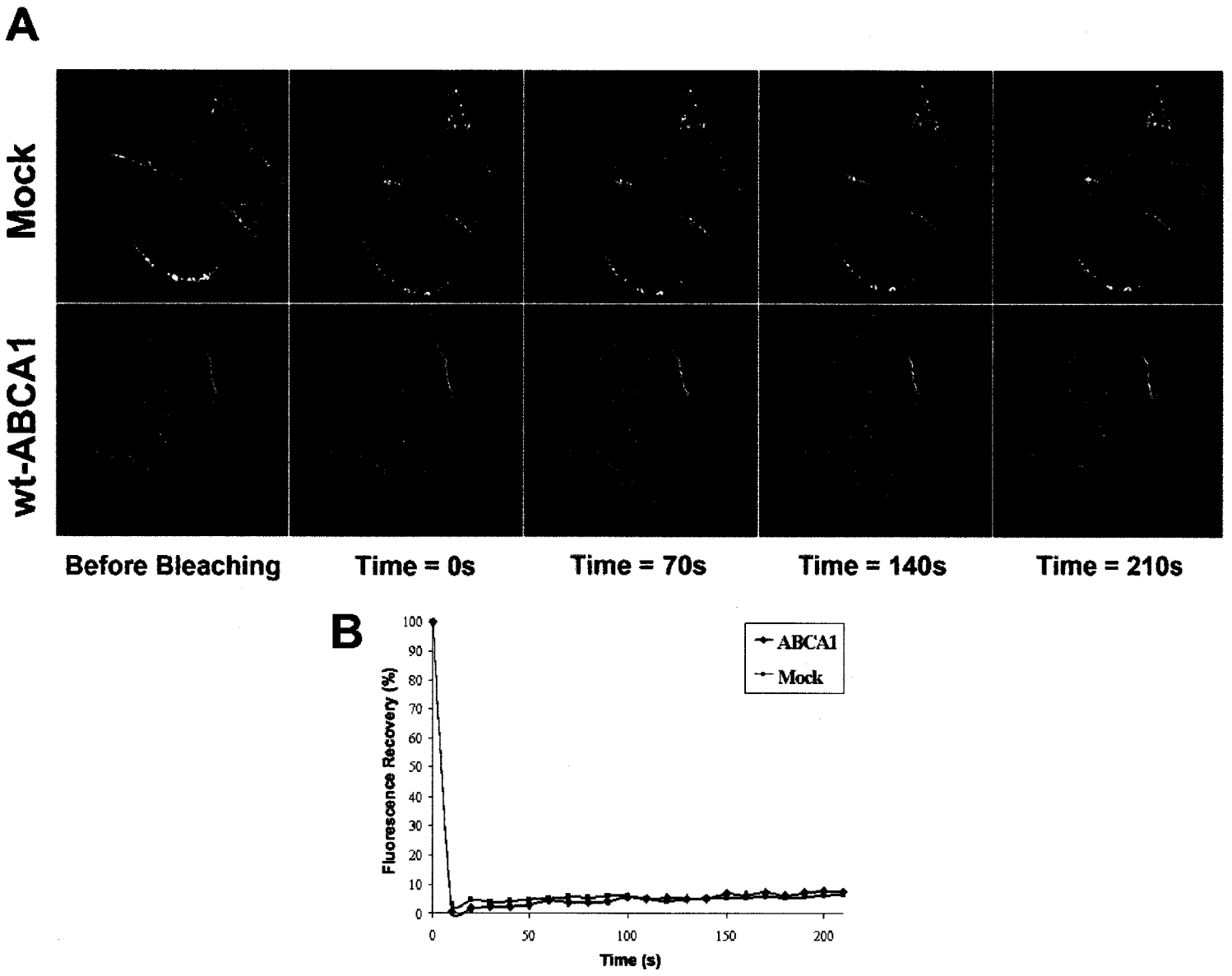
A
Mock
wt-ABCA1
Before Bleaching
Time = 0s
Time = 70s
Time = 140s
Time = 210s
B
ABCA1
Mock
Fluorescence Recovery (%)
Time (s)
0
10
20
30
40
50
60
70
80
90
100
0
50
100
150
200

Figure 3.12

Endogenous CAV1 distribution by non-detergent-based Optiprep ultracentrifugation. Mock, ABCA1, and A937V cells were induced overnight with mifepristone, and membrane fractions were isolated as described under "Materials and Methods." ***A***, a 60-µl aliquot of each gradient fraction was analyzed by electrophoresis followed by immunoblotting for either CAV1 or clathrin. ***B***, immunoblots from Mock, ABCA1 and A937V cells were scanned and analyzed. The amount of CAV1 in non-raft fractions (*7-9*) was pooled together and presented here as the percentage of the total caveolin. *Bars* are the average from two independent experiments, and *error bars* are standard deviations.

A

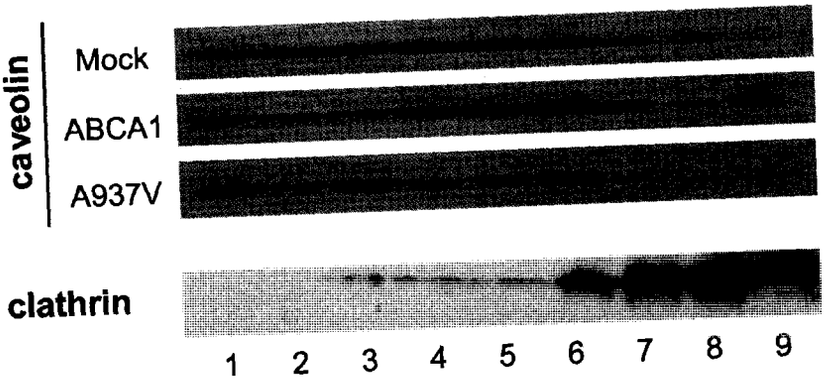
caveolin
Mock
ABCA1
A937V
clathrin
1 2 3 4 5 6 7 8 9

B

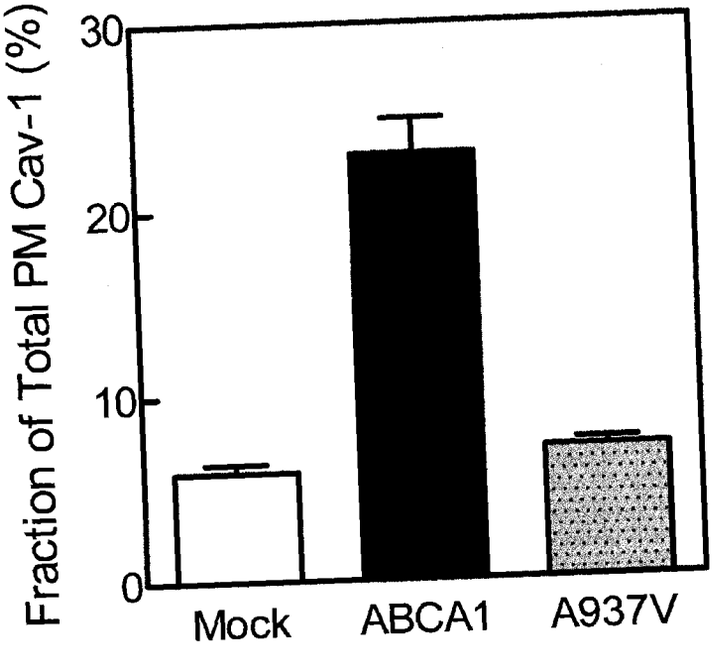
Fraction of Total PM Cav-1 (%)
30
20
10
0
Mock
ABCA1
A937V

majority of CAV1 was present in fractions 1-6, typical of a lipid raft marker. There was also a minor portion of CAV1 (~5%) present in fractions 7-9, which co-localized with the non-raft marker clathrin, in Mock and A937V cells. Interestingly, there was a shift in the CAV1 distribution in WT-ABCA1 cells, which contained 20% more non-raft CAV1 relative to Mock and A937V cells. There was also no significant difference in the floatation results of CAV1 between Mock and A937V cells (Fig. 3.12B). We could therefore conclude that the CAV1 floatation, using a non-detergent-based gradient, was in agreement with our live cell microscopy observations.

3.11 WT-ABCA1 disrupts EGF-mediated Akt activation

A major postulated function of lipid rafts involves their role as specialized signaling platforms on the plasma membrane. In order to examine whether WT-ABCA1-mediated non-raft expansion and lipid raft disruption is able to influence cell signaling events, we characterized EGF-induced Akt phosphorylation, which is a process known to be sensitive to plasma membrane microdomains[183]. As shown in Fig. 3.13, 5 minute EGF stimulation of Mock cells resulted in subsequent Akt phosphorylation, as detected by anti-phospho(Ser-473)-Akt antibody (Fig. 3.13A). In contrast, very little Akt phosphorylation was detected in WT-ABCA1-expressing cells (Fig. 3.13A). In A937V-expressing cells, EGF stimulation led to subsequent Akt activation, similar to that in Mock cells (Fig. 3.13A). As the total amounts of Akt were similar in all three cell lines (Fig. 3.13A), we calculated the ratio of Ser-473-phosphorylated Akt to total Akt (Fig. 3.13B), which was indicative of a specific impairment in Akt activation by WT-ABCA1 activity. It is evident that EGF signaling is modulated by ABCA1 expression, likely through the interruption of the raft microdomains.

Figure 3.13

EGF-induced Akt phosphorylation. Mock, ABCA1, and A937V cells were induced and serum-starved overnight before 5 min 50 ng/ml EGF treatment. Cell lysates were collected and analyzed for phosphorylated Akt or total Akt (***A***). The ratio of phosphorylated Akt over total Akt is presented in ***B***. *Error bars* are standard deviations among triplicate lanes.

A

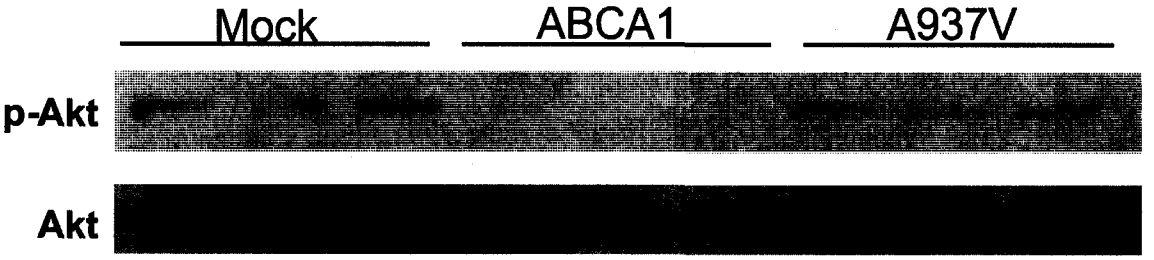
Mock
ABCA1
A937V
p-Akt
Akt

B

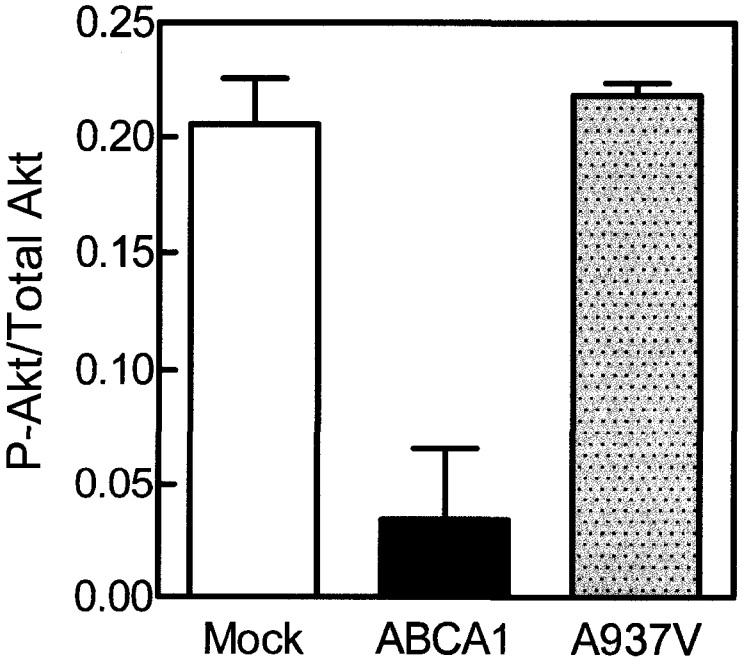
0.25
0.20
0.15
0.10
0.05
0.00
P-Akt/Total Akt
Mock
ABCA1
A937V

3.12 WT-ABCA1 increases cholesterol availability to MCD

In addition to the impairment of lipid-raft-dependent cell signaling events, an increase in loosely packed non-raft plasma membrane domains could also result in an increased availability of cellular cholesterol to extracellular acceptors. In order to investigate this possibility, we performed MCD cholesterol extraction at 37°C and 0°C. It has been previously determined by others that a short pulse (1 minute) with 5 mM MCD at 37°C can extract cholesterol specifically from the plasma membrane without any significant involvement of intracellular transport. Through our own analysis, we confirmed the extreme potency of MCD, as 1 minute MCD treatment at 37°C resulted in the extraction of >30% [^{3}H]cholesterol from Mock and WT-ABCA1 cells alike (Fig. 3.14A). This was encouraging to us for two major reasons. First, it provided us with further evidence that there was no apparent difference in terms of plasma membrane total cholesterol content between Mock and WT-ABCA1 cells. Second, this observation was consistent with previous reports that at the physiological temperature of 37°C, the MCD-mediated cholesterol efflux process is independent of ABCA1 function[95, 117, 184]. The high potency of MCD at this temperature could very easily override any native mechanisms of intrinsic WT-ABCA1 activity, such as the observed non-raft domain expansion. In order to overcome this high potency, we performed the MCD-mediated cholesterol efflux at 0°C. We made this modification in order to enforce the formation of lipid rafts on the plasma membrane, as Triton X-100 can only distinguish lipid rafts from non-raft domains at 0°C. Additionally, by lowering the temperature, the potency by which MCD extracts cholesterol could be diminished, thus allowing the participation of intrinsic WT-ABCA1 plasma membrane activities. Upon performing the MCD-mediated cholesterol efflux experiments on ice, it was indeed apparent

Figure 3.14

Apolipoprotein-independent cholesterol extraction and apoA-I binding. ***A*** and ***B***, cells labeled with [^{3}H]cholesterol for 2 days were treated with MCD (5 mM) for either 1 min at 37 °C (***A***) or on ice for the indicated times (***B***). [^{3}H]Cholesterol in the media and cell-associated cholesterol were measured and presented as percentage of media [^{3}H]cholesterol of total [^{3}H]cholesterol (Triton X-100-insoluble plus Triton X-100-soluble fractions). All the data are the means ± S.D. of triplicates. ***C***, Mock- and ABCA1-expressing BHK cells were incubated for 30 min at 37 °C in DMEM containing 10 μg/ml ^{125}I-apoA-I. Cells were washed, chilled on ice for 30 min, and cold Triton X-100 extraction was performed. Radioactivity found in the medium (*Triton-soluble*), corresponding to non-rafts, and in the cells (*Triton-insoluble*), corresponding to rafts, was determined by gamma counting. Results are expressed as mean ± S.D. of triplicate wells.

A

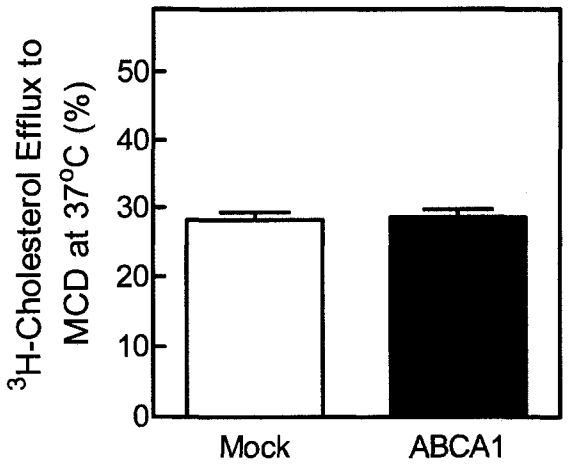
^{3}H-Cholesterol Efflux to MCD at 37°C (%)
50
40
30
20
10
0
Mock
ABCA1

B

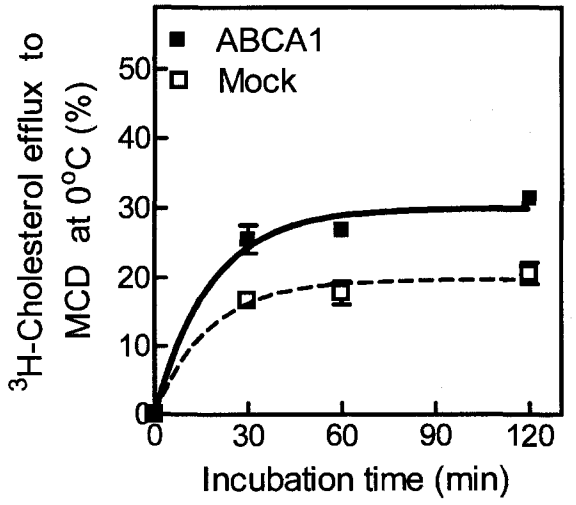
^{3}H-Cholesterol efflux to MCD at 0°C (%)
ABCA1
Mock
50
40
30
20
10
0
0
30
60
90
120
Incubation time (min)

C

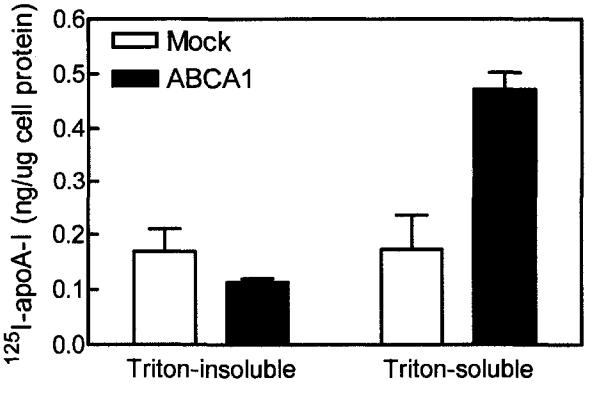
^{125}I-apoA-I (ng/ug cell protein)
Mock
ABCA1
0.6
0.5
0.4
0.3
0.2
0.1
0.0
Triton-insoluble
Triton-soluble

that the potency of MCD had decreased substantially even during prolonged incubation times. Interestingly, MCD (5 mM) was able to extract 40-50% more cholesterol from WT-ABCA1-expressing cells relative to Mock cells at all time points examined (Fig. 3.14B). Similar results were obtained using 10 mM MCD (data not shown). Taken together, these results suggested that the intrinsic activities of WT-ABCA1 on the plasma membrane increase the accessibility of cholesterol for extraction, once again consistent with the increased non-raft pool of cholesterol and lipids.

3.13 ApoA-I associates with non-raft domains formed by WT-ABCA1

The ability of WT-ABCA1 to increase the prominence of non-raft domains on the plasma membrane could have physiologically important functional consequences in terms of cholesterol efflux. Previous studies have shown that the physiological cholesterol acceptor apoA-I acquires lipids primarily from non-raft membrane domains[185], and, therefore, an expanded non-raft membrane pool could favour apoA-I cell association and lipidation. In order to explore this possibility, we analyzed which membrane domain apoA-I would associate with preferentially. We performed this experiment by incubating Mock and WT-ABCA1 cells with ^{125}I-apoA-I for 30 minutes, at 37°C, followed by subsequent cold Triton X-100 extraction. We found that apoA-I preferentially associated with non-raft membrane microdomains in WT-ABCA1-expressing cells (Fig. 3.14C), while there was no detectable preferential apoA-I association in Mock cells. This provides strong evidence for the intrinsic activities of WT-ABCA1 playing a role in facilitating the association of apoA-I with non-raft microdomains. Taken together, the amalgamation of our results suggests that a functional ABCA1 transporter, with an intact NBD/NBF, facilitates the functional proximity

of phospholipids, FC, and apoA-I in loosely packed lipid microdomains of the plasma membrane. It is highly probable that this is achieved through the expansion of plasma membrane non-raft microdomains by the intrinsic activities of WT-ABCA1.

3.14 Caveolae disruption in hypertrophic adipocytes

In the current study, we have provided evidence for caveolae/lipid raft disruption by WT-ABCA1 in BHK cells. We have also shown that this disruption of lipid rafts results in impaired lipid raft-dependent signaling, such as EGF-stimulated activation of Akt through the EGFR pathway. For this reason, we sought to investigate the consequences of similar lipid raft disruption in a second cellular model. Caveolae have been postulated to act as mechanosensors, which could serve as a store of sphingolipids and cholesterol, as well as a plasma membrane reservoir. Therefore, cells that routinely expand in size could rely on the flattening of caveolae in order to satisfy their demands for increased plasma membrane area. Adipocytes serve as an excellent example, as they expand in size in order to accommodate increasing lipid stores. We therefore used 3T3-L1 preadipocytes in order to address this issue, as this cell line is one of the most well-characterized and reliable models of adipocyte differentiation[186].

We utilized the standard 8-day differentiation protocol in order to obtain fully differentiated 3T3-L1 adipocytes. Dr. Sorisky's group has developed an RPMI-based medium, which results in the differentiation of hypertrophic 3T3-L1 adipocytes, relative to those differentiated using standard DMEM medium. Following the 8-day differentiation period, we analyzed the morphology of both DMEM-differentiated (normal) and RPMI-differentiated (hypertrophic) adipocytes. The hypertrophic adipocytes contained much larger

lipid droplets (Fig. 3.15B) compared to those found in the normal adipocytes (Fig. 3.15A), presumably due to increased lipid storage. Through analysis of TG content, a common determinant of adipocyte cell size, it was determined that RPMI-differentiated adipocytes were indeed hypertrophic, containing higher levels of TG per protein mass (Fig. 3.16).

We then examined endogenous CAV1 in both normal and hypertrophic adipocytes using immunofluorescent staining and confocal microscopy. CAV1 was present on the basal membrane in both normal (Fig. 3.15C) and hypertrophic adipocytes (Fig. 3.15 D), yet to a lesser extent in the hypertrophic adipocytes. We proceeded to examine the cytosolic region just above the basal membrane in both normal and hypertrophic adipocytes. In normal adipocytes, we observed the large clustered structures known as caveolae rosettes, which are common to fully differentiated adipocytes (Fig. 3.15E). Interestingly, these caveolae rosette structures were absent in hypertrophic adipocytes (Fig. 3.15F). This was indicative of caveolae disruption in the hypertrophic adipocytes, which could be attributed to the flattening of caveolae on the membrane in response to increasing cell size or cholesterol redistribution.

Caveolin/caveolae are known to be important in IR activation, as well as glucose uptake. We postulated that the observed disruption of caveolae rosettes in hypertrophic adipocytes could result in impaired insulin signaling-dependent processes. We therefore analyzed the insulin-dependent activation of insulin receptor substrate 1 (IRS-1) as well as the subsequent downstream activation of Akt (Fig. 3.17). Total levels of phospho-IRS-1 (P-IRS-1) and total IRS-1 were increased in hypertrophic adipocytes, relative to normal adipocytes (Fig. 3.17). However, when the extent of insulin activation was evaluated through ratio of P-IRS-1 to total IRS-1, it was found that insulin activation was reduced

Figure 3.15

Morphology and CAV1 analysis in 3T3-L1 adipocytes. 3T3-L1 preadipocytes were grown to confluency and triggered to enter eight-day differentiation two days post-confluency. 3T3-L1 cells differentiated in DMEM resulted in normal adipocytes, ***A***, while cells differentiated in supplemented RPMI medium became hypertrophic, ***B***. Adipocytes were stained for CAV1, and confocal images were taken of the basal membrane (***C*** and ***D***) and cytosolic middle sections (***E*** and ***F***) of normal and hypertrophic adipocytes, respectively.

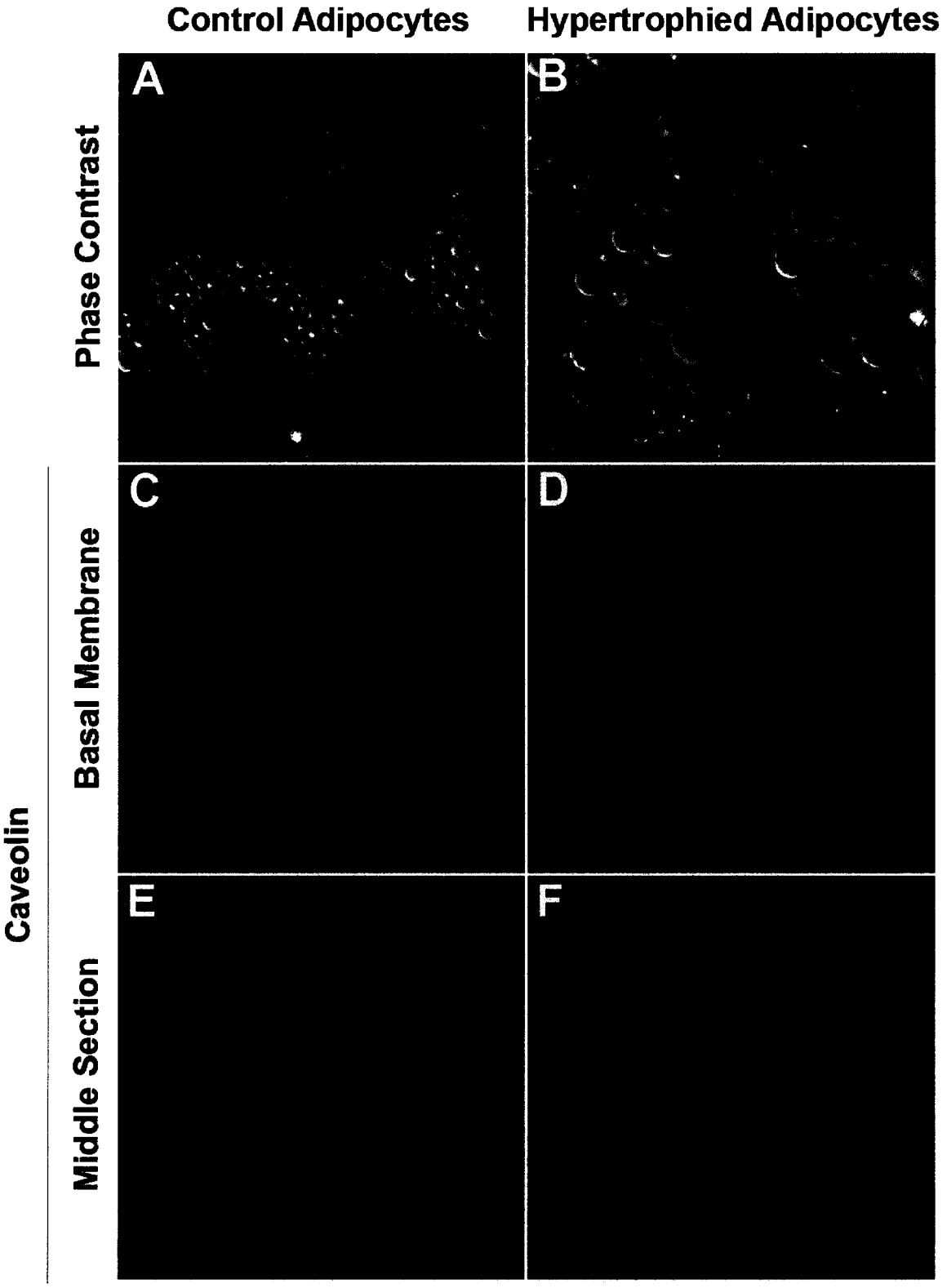
Control Adipocytes
Hypertrophied Adipocytes
Phase Contrast
Caveolin
Basal Membrane
Middle Section
A
B
C
D
E
F

Figure 3.16

Analysis of TG content in 3T3-L1 adipocytes. TG was extracted twice (30 min and 15 min) from normal and hypertrophic adipocytes with a 2:3 isopropanol:heptane mixture. TG content was quantified by colourimetric analysis. Adipocyte cell size was measured through ratio of total TG to protein levels in normal and hypertrophic adipocytes. Figure is representative of two independent experiments, and results are expressed as mean ± S.D. of two wells.

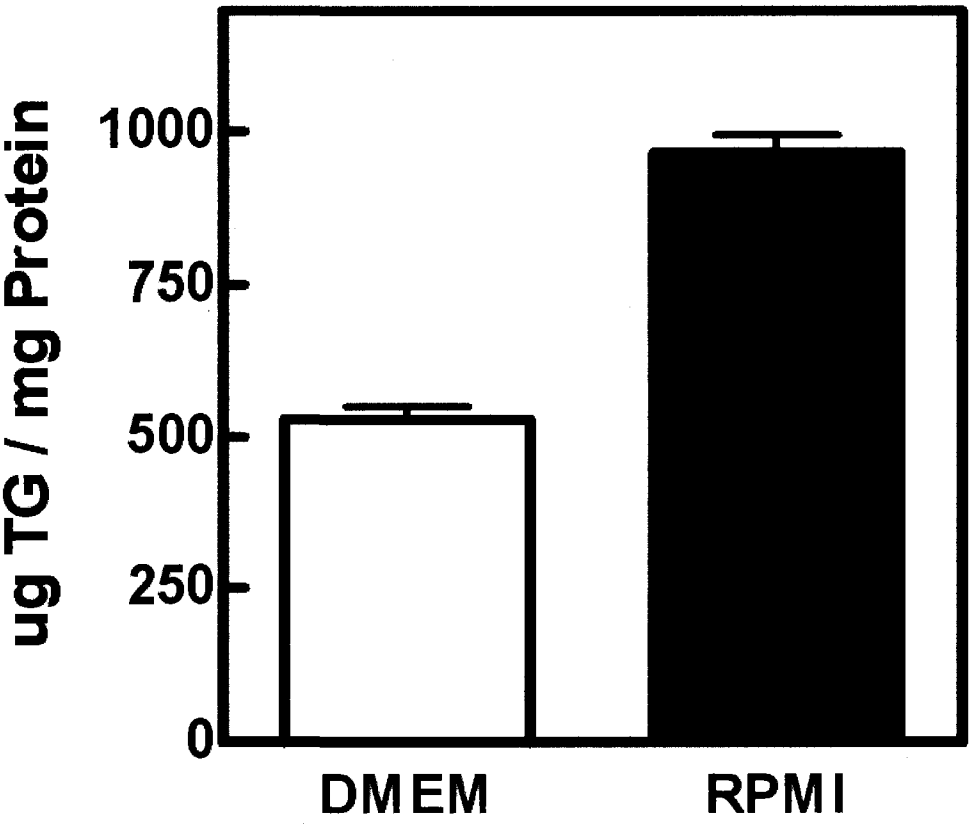
ug TG / mg Protein
1000
750
500
250
0
DMEM
RPMI

Figure 3.17

Acute insulin stimulation of 3T3-L1 adipocytes. Fully differentiated normal and hypertrophic 3T3-L1 adipocytes were serum-starved for 16-20 hours followed by treated with 10 µl of vehicle or insulin (100 µM stock).Cells were then lysed, homogenized and equal amounts of protein were loaded on SDS-PAGE. Insulin stimulation was analyzed by immunoblotting using anti-phosphotyrosine, anti-IRS-1, anti-pSer473-Akt, and anti-Akt/PKB antibodies.

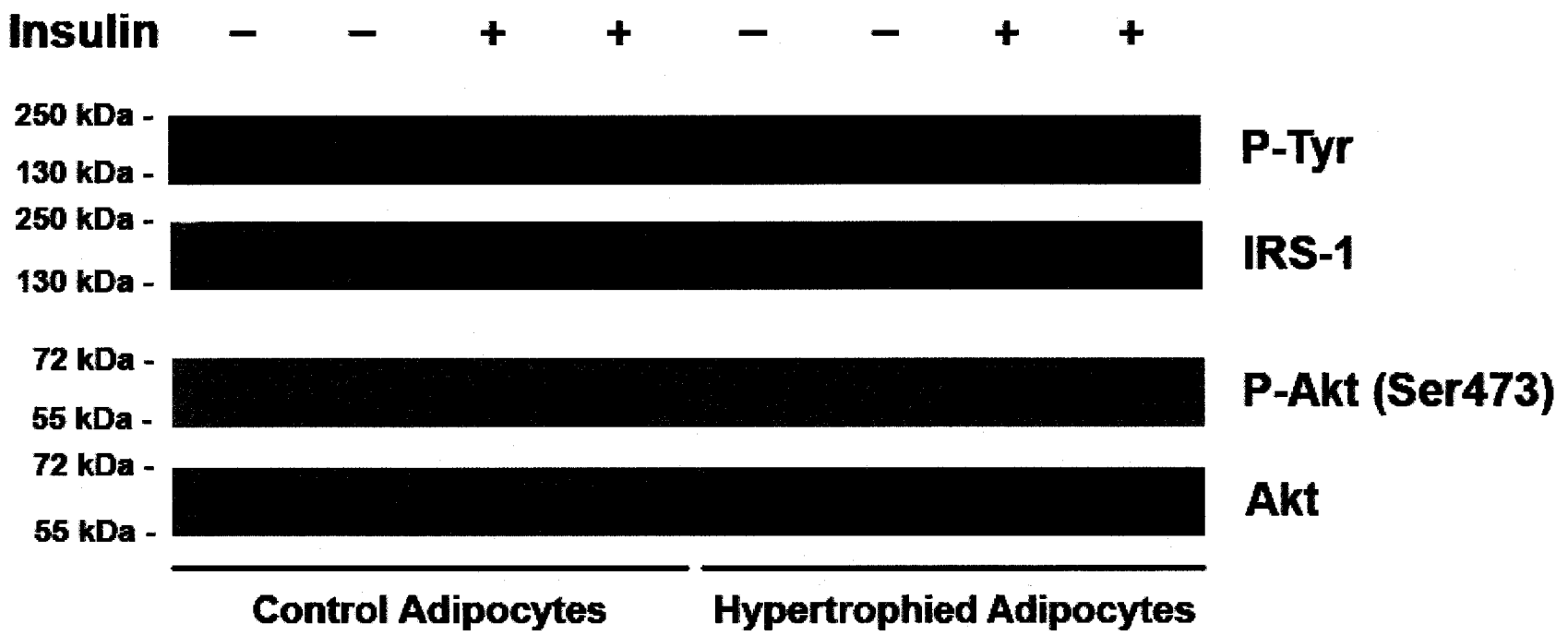
Insulin
– – + + – – + +
250 kDa -
130 kDa -
P-Tyr
250 kDa -
130 kDa -
IRS-1
72 kDa -
55 kDa -
P-Akt (Ser473)
72 kDa -
55 kDa -
Akt
Control Adipocytes
Hypertrophied Adipocytes

slightly in the hypertrophic adipocytes, relative to normal adipocytes. Similarly, phospho-Akt and total Akt levels were both increased in hypertrophic adipocytes, relative to normal. Ratio analysis of phospho-Akt to total Akt indicated a similar Akt activation in both hypertrophic and normal adipocytes (ratios not shown). These observed trends are reflective of preliminary data, and further investigation is required.

Chapter 4: Discussion

Throughout this study, we provided multiple lines of evidence indicating that functional ABCA1 actively alters the general packing of the plasma membrane, by generating more loosely packed non-raft microdomains. First, WT-ABCA1 increased the Triton X-100 solubility of cholesterol and SM. Second, fluorescence microscopy using $DiIC_{18}$ revealed an increased percentage of the plasma membrane area that was solubilized by Triton X-100 in WT-ABCA1-expressing cells. Third, upon expression of WT-ABCA1 in BHK cells, normally clustered caveolin was dispersed across the plasma membrane, which is associated with the disruption of caveolae. Consistent with this microscopy analysis, we found that WT-ABCA1 expression increased the amount of CAV1 in non-raft fractions obtained by non-detergent-based Optiprep gradient ultracentrifugation. Fourth, ~50% more cholesterol was available to cold MCD extraction from WT-ABCA1-expressing cells, relative to Mock. In addition to biophysical changes in the membrane, WT-ABCA1 expression also modulated EGF-mediated Akt activation, consistent with the known sensitivity of Akt activation to microdomain organizations. Most importantly, we determined that the observed membrane remodeling by ABCA1 was dependent on an intact nucleotide-binding domain. ABCA1 with a mutation in its first NBF, A937V-ABCA1, was unable to redistribute cholesterol, SM, or CAV1. A937V also failed to influence EGF-mediated Akt activation. These observations collectively demonstrate that, through its ATPase-related functions, WT-ABCA1 reorganizes the plasma membrane and generates more non-raft microdomains. The loosely packed non-raft domains likely facilitate the cell association of apoA-I and, consequently, lipid acquisition by apoA-I to form nascent HDL particles.

The results presented here may serve to clarify previous studies involving ABCA1 activity[168, 185]. It has been shown in these studies that, while HDL is able to remove cholesterol from raft domains, lipid-free apoA-I acquires cholesterol from a distinct membrane source, likely non-raft domains. Additionally, in both human fibroblasts and BHK cells, ABCA1 expression was found to enhance the efficiency of cholesterol oxidase, likely due to improved enzyme accessibility to cholesterol in the membrane. Exogenous cholesterol oxidase was able to convert more cholesterol into cholestenone in ABCA1-expressing cells, relative to Mock BHK cells. As only a fraction of plasma membrane cholesterol is vulnerable to this enzymatic oxidation, this process is thought to depend on the lipid environment surrounding the cholesterol molecules. Cholesterol present in loosely packed plasma membrane domains is more accessible to cholesterol oxidase[169, 170]. Our results suggest that the higher percentage of cholesterol accessible to enzymatic oxidation in ABCA1-expressing cells may reflect an increased availability of FC in what we may now call non-raft microdomains. Interestingly, FC removed by lipid-poor apoA-I in ABCA1-expressing cells was derived exclusively from this cholesterol oxidase-sensitive membrane pool[168, 185]. Those results therefore support the concept presented here that ABCA1-mediated expansion of non-raft microdomains facilitates the cell association of apoA-I and subsequent lipid efflux.

Throughout the years, significant advancements have been made in our understanding of biological membranes, particularly the plasma membrane. We no longer simply regard the plasma membrane as a fluid mosaic with homogenously distributed lipids. Instead, we essentially consider the plasma membrane as a quilt containing many heterogeneous patches, namely microdomains[187]. At the same time, our understanding of

this complex lateral heterogeneity within the plasma membrane is very far from complete. It is accepted, however, that microdomains can be operatively defined by their respective detergent solubility[188]. ABCA1 appears to be localized to detergent-soluble non-raft fractions[185]. The mechanism by which ABCA1 expands these non-raft microdomains remains unclear, but likely represents some intrinsic functions of ABCA1, as these membrane remodeling events occurred in the absence of apoA-I. This is consistent with the cholesterol oxidase study by Vaughan and Oram, which was also performed in the absence of apolipoproteins[168]. It is possible that ABCA1 could influence membrane lateral organization simply through the integration of its twelve TMDs and subsequent partitioning to non-raft domains. However, as the A937V mutant is localized similarly to the plasma membrane, yet fails to impact the microdomains, this explanation seems unlikely. Alternatively, WT-ABCA1 may actively flip phospholipids and FC from the inner to outer leaflet, leading to disruption of membrane microdomains.

Although our study presented here used BHK cells that were forced to overexpress exogenous ABCA1, our conclusions are well-supported by several more recent studies from other laboratories. For example, Nagao *et al.*[189] performed a study using Chinese hamster ovary (CHO) cells in which they investigated the effect of SM depletion on apoA-I-mediated lipid efflux. They employed a CHO LY-A cell line that contained a missense mutation in the ceramide transfer protein CERT, which was therefore deficient in SM synthesis. In addition, they used an LY-A cell line that was stably transfected with human CERT cDNA (LY-A/CERT). As SM is a major lipid raft component, LY-A cells grown in SM-free medium were unable to form sufficient lipid rafts in the plasma membrane. Interestingly, apoA-I-dependent efflux from SM-deficient LY-A cells was increased 1.65-

fold compared to that from LY-A/CERT cells, while ABCA1 expression levels in both cell lines were identical. This indicated that non-raft expansion through non-ABCA1 mechanisms can also enhance cholesterol efflux. In addition, this study found that the amount of cholesterol available to cold MCD extraction from LY-A cell was increased by 40% when ABCA1 expression was induced, similar to our observations. Also, cholesterol in LY-A cells is more susceptible to cold MCD extraction than that in LY-A/CERT cells, verifying that the extent of cold MCD extraction indeed reflects membrane lateral organizations. Most importantly, another study by Koseki *et al.*[190] analyzed the lipid raft content of macrophages isolated from WT and *ABCA1*-null mice. This group employed two newly established fluorescent probes of lipid rafts. The first was a biotinylated and protease-nicked derivative of θ-toxin (BCθ) that selectively recognized membrane cholesterol in lipid rafts. The second was a polyethylene glycol cholesteryl ether that binds to cholesterol-rich membranes both in cells and in model membranes. They observed higher fluorescence on the membranes of macrophages isolated from *ABCA1*-null mice, compared to WT, indicating more lipid rafts when there is no ABCA1 expression. Significantly, identical results were obtained when they used macrophages from normal individuals and TD patients: there were more lipid rafts in TD macrophages compared to normal macrophages. Conversely, the reintroduction of functional ABCA1 into TD fibroblasts effectively decreased the degree of binding of BCθ, thus lipid raft microdomains. Collectively, these studies, along with our own, strongly support a causal relationship between ABCA1 expression and the expansion of non-raft microdomains.

While WT-ABCA1 seems to function intrinsically by generating non-raft microdomains, the precise nature of these domains remains to be elucidated. We have shown

that the plasma membrane of Mock cells also contains a significant proportion of Triton X-100-soluble domains. At the same time, apoA-I-mediated lipid efflux is absent in these cells. We could conclude that a protein-protein interaction between apoA-I and ABCA1 is required for efficient lipid acquisition from non-raft microdomains. This association between apoA-I and ABCA1 alone, however, is not sufficient to trigger lipid efflux as demonstrated by the W590S ABCA1 mutant[115]. Alternatively, it is possible that WT-ABCA1 actively generates non-raft microdomains that are compositionally and functionally distinct from those present in Mock cells. Since the lipid raft/non-raft partition in Mock cells is regulated through ABCA1-independent mechanisms, it is possible that the distinct packing and/or lipid composition of the non-raft microdomains found in Mock cells prevents them from interacting with apoA-I and taking part in active lipid efflux. Unfortunately, we are limited by currently available experimental protocols[7]. Future techniques will undoubtedly reveal more details about differences in the nature and composition of these membrane microdomains.

The concept that WT-ABCA1 alters the lipid packing conditions of the plasma membrane in the absence of apolipoproteins may significantly impact our understanding of apoA-I-mediated lipid efflux. There are multiple models that attempt to explain the cell association of apoA-I, as well as the mechanism by which ABCA1-dependent apoA-I efflux may occur. In this present study, our results strongly suggest that WT-ABCA1 increases the accessibility of FC to extraction by apoA-I, thereby actively participating in both phospholipid and FC efflux. This supports the hypothesis that ABC transport proteins play an active role in making the plasma membrane FC available for efflux. In addition to the cholesterol oxidase studies involving ABCA1, recent studies have shown that ABCG1 and

ABCG4 also expand the FC pool accessible to lipidated apolipoproteins[71]. A rapid mechanism by which ABCA1 is active in both phospholipid and FC efflux may explain why Smith *et al.*[191], among others, have reported difficulty in separating phospholipid and cholesterol efflux. In fact, by colocalizing apoA-I and FC to loosely packed non-raft microdomains that are also phospholipid-rich, ABCA1 may promote nearly simultaneous phospholipid and FC efflux, i.e. too rapid to be separately detected at a physiological temperature.

In addition to ABCA1-mediated lipid efflux, our results may also have more general implications. Membrane microdomains are thought to be functionally significant in living cells, by providing platforms to facilitate specific interactions among proteins[192]. In fact, caveolae microdomains have been considered by many to be universal signaling regulators[10]. Our results support the notion that microdomains in living cell membranes are actively maintained[193] and, most likely, held far from an equilibrated state[7]. Artificially created model membrane systems are mostly at equilibrium, while physiological membranes undergo constant disturbance. Such disturbances include endocytosis and exocytosis events, which consistently modulate the plasma membrane composition and shape. Consequently, most lipid components of physiological membranes have high rates of turn over. In addition, microdomain formation and clustering can be rapidly triggered upon oligomerization of membrane receptors in response to physiological ligands[194]. Most importantly, the plasma membrane of living cells has transbilayer asymmetry. This asymmetry is produced by translocation of lipid species, and is therefore actively maintained by various ATPases through the consumption of metabolic energy. The lateral organization of the plasma membrane is likely dynamically regulated through all the aforementioned mechanisms. It is

therefore not surprising that the properties of the physiological membranes often differ significantly from the model membrane systems. The constant disturbances experienced by physiological membranes may also explain why lipid rafts are highly dynamic and invisible (below optical resolution) as understood today[7].

We have provided multiple lines of evidence supporting the notion that the dynamics of lipid rafts regulate cellular functions. For instance, signaling cascades dependent on lipid rafts should be modified by the reorganization of the membrane through WT-ABCA1 activity. This was indeed observed by a reduction in EGF-mediated Akt phosphorylation in WT-ABCA1 cells. Akt activation is known to depend on the integrity of the lipid rafts, as cholesterol depletion by MCD can severely diminish this activation[183]. However, we are among the first to report that signaling events could also be significantly modulated through relatively minor changes in cholesterol content or even the mode of cholesterol packaging in the plasma membrane, as we have presented here. We were therefore interested in whether a similar disruption of caveolae/lipid rafts under physiological conditions could also lead to the interruption of signaling events. The adipocyte is a good model for such a study. Adipocytes are highly enriched in caveolae, and most interestingly, *CAV1*-null mice have little phenotype other than their failure to form enlarged adipocytes when fed a high-fat diet[195]. We therefore hypothesized that caveolae may regulate signaling events in adipocytes. In addition, many groups believe that caveolae may serve as a reservoir of plasma membrane, which can be flattened to accommodate the increasing cell size[10]. Therefore, we sought to disrupt plasma membrane caveolae by increasing cell size in a physiological manner. Adipocytes are designed to dynamically vary in size depending on the nutrient availability. During periods of positive energy balance in the body, the adipocytes

readily uptake excess lipids and glucose, and incorporate TG and FC into the lipid droplets. This leads to an enlargement of cell volume. Interestingly, adipocyte caveolae can fold together to form "bunches of grapes" of caveolae, a complex event that led some to consider these structures as cubic membrane infoldings capable of folding and flattening with little energy input[196].

We therefore turned to a preadipocyte cell line in order to investigate the potential disruption of caveolae due to increasing cell size. 3T3-L1 preadipocytes serve as an excellent *in vitro* model in that they can be injected into mice where they differentiate and form fat pads that are indistinguishable from normal adipose tissue[197]. Once differentiated in culture, 3T3-L1 adipocytes not only possess most of the ultrastructural characteristics of those found in animal tissue[198], but their lipid droplet formation mimics that of live adipose tissue[199]. Particularly, these *in vitro* differentiated adipocytes resemble natural adipocytes that are responsive to hormonal stimuli. However, under extensive positive energy balance, adipocytes *in vivo* continue to expand and frequently adopt a hypertrophic morphology. These hypertrophic adipocytes are commonly found in the adipose tissue of obese patients, especially those individuals that suffer from type II diabetes. As described, Dr. Sorisky's group was able to duplicate this phenomenon by differentiating 3T3-L1 preadipocytes, using supplemented RPMI medium, to produce hypertrophic adipocytes similar to what is observed *in vivo*. When we examined these hypertrophic adipocytes, we indeed observed a disruption of the caveolae rosette structures. We postulated that this might be a result of the increased demand for plasma membrane surface area. In other words, caveolae either flattened in order to supply extra surface area, or were disrupted due to a redistribution of FC from the plasma membrane to the lipid droplet. Further investigation is required to

distinguish between these possibilities. Regardless of the reason for caveolae disruption, such alterations in caveolae morphology seem to have functional consequences. First of all, insulin-stimulated glucose uptake, performed by Dr. Gagnon of Dr. Sorisky's group, was severely impaired in hypertrophic adipocytes, relative to normal cells. This led us to analyze the insulin signaling pathway in these cells. We found that hypertrophic adipocytes seemed to express elevated levels of IRS-1, and, following insulin stimulation, an elevated level of tyrosine phosphorylated IRS-1 (P-IRS-1). Interestingly, when we calculated the ratio of P-IRS-1 to total IRS-1, it seemed that the overall activation of IRS-1 through insulin stimulation was slightly decreased in hypertrophic adipocytes. This could be important, as various downstream processes might be differentially triggered by the degree of IRS-1 phosphorylation. In any case, as insulin signaling and glucose uptake are known to be dependent on the presence of caveolae/lipid rafts[38, 200, 201], it remains a possiblity that the disruption of caveolae rosettes in hypertrophic adipocytes resulted in this functional impairment. Interestingly, we found that a downstream component of insulin signaling, Akt, did not appear to be affected by hypertrophy. Akt was activated to a similar extent in both normal and hypertrophic adipocytes, although these results remain preliminary. This could imply that there was enough IR activation to activate Akt in the hypertrophic adipocytes. We can perhaps speculate that, while the amount of P-IRS-1 in hypertrophic adipocytes may be sufficient to activate Akt, the decreased IRS-1 activation could be insufficient to stimulate some other cellular processes that lead to glucose uptake. Alternatively, IRS-1 contains multiple tyrosine and serine/threonine phosphorylation sites that function to positively and negatively regulate IRS-1 activity. It is possible that specific phosphorylation sites are impaired in the hypertrophic adipocytes. Further detailed analysis of these sites is required

before we can examine these possibilities. As insulin activates Akt through IRS-1 and phosphoinositide 3-kinase (PI3K), it is possible that the disruption of caveolae in the hypertrophic adipocytes may abrogate PI3K-independent pathways that are involved in glucose uptake. For example, insulin stimulation also activates CAP/Cbl translocation, a process mediated by TC10, to stimulate glucose uptake. Interestingly, TC10-mediated glucose uptake is known to be independent of Akt activation. As TC10 has been shown to localize to caveolae rosettes, disruption of this pathway could be a bi-product of adipocyte hypertrophy. Again, these results are preliminary and further investigation is necessary. This includes characterization of PI3K-dependent and –independent insulin pathways, cellular cholesterol distribution as well as distributions of glucose transporters ie. GLUT4.

Conclusion

In summary, the present study demonstrates for the first time that WT-ABCA1 is capable of reorganizing plasma membrane microdomains, effectively expanding the proportion of non-raft microdomains. Importantly, this reorganization requires energy as it is dependent on a functional ABCA1 NBD/NBF. Because apoA-I primarily associates with non-raft membrane domains in WT-ABCA1-expressing cells, we speculate that this non-raft microdomain expansion plays a critical role in apoA-I-mediated FC efflux. WT-ABCA1 likely preconditions cells and generates a favorable membrane environment for apoA-I to acquire lipids, including FC. Further studies are needed to clarify the molecular requirements for ABCA1 to achieve this function. Such a capacity to manipulate membrane microdomains may represent a general mechanism for cells to dynamically maintain functional membrane micro-organizations.

References

1. Lange, Y. Disposition of intracellular cholesterol in human fibroblasts. *J. Lipid Res.* **32**, 329-339 (1991).
2. Attie, A.D. ABCA1: at the nexus of cholesterol, HDL and atherosclerosis. *Trends in Biochemical Sciences* **32**, 172-179 (2007).
3. Bloch, K. Speculations on the evolution of sterol structure and function. *CRC Crit Rev Biochem* **7**, 1-5 (1979).
4. Yeagle, P. Cholesterol and the cell membrane. *Biochimica et Biophysica Acta (BBA)* **822**, 267-87 (1985).
5. Tabas, I. Cholesterol in health and disease. **110**, 583-590 (2002).
6. Simons, K. & Ehehalt, R. 597-603 (2002).
7. Mayor, S. & Rao, M. Rafts: Scale-Dependent, Active Lipid Organization at the Cell Surface. *Traffic* **5**, 231-240 (2004).
8. Palade, G.E. 188-211 (1953).
9. Yamada, E. 445-458 (1955).
10. Parton, R.G. & Simons, K. The multiple faces of caveolae. *Nat Rev Mol Cell Biol* **8**, 185-194 (2007).
11. Stan, R.V. Structure of caveolae. *Biochimica et Biophysica Acta (BBA) - Molecular Cell Research* **1746**, 334-348 (2005).
12. Deurs, B.v., Roepstorff, K., Hommelgaard, A.M. & Sandvig, K. Caveolae: anchored, multifunctional platforms in the lipid ocean. *Trends in Cell Biology* **13**, 92-100 (2003).
13. Kurzchalia, T.V. & Parton, R.G. Membrane microdomains and caveolae. *Curr. Opin. Cell Biol.* **11**, 424-431 (1999).
14. Lisanti, M.P. et al. Caveolae, transmembrane signalling and cellular transformation. *Mol Membr Biol.* **12**, 121-124 (1995).
15. Williams, T.M. & Lisanti, M.P. C494-506 (2005).
16. Tang, Z. et al. 2255-2261 (1996).
17. Way, M. & Parton, R.G. M-caveolin, a muscle-specific caveolin-related protein. *FEBS Letters* **376**, 108-112 (1995).
18. Liu, P., Rudick, M. & Anderson, R.G.W. 41295-41298 (2002).
19. Nichols, B.J. A distinct class of endosome mediates clathrin-independent endocytosis to the Golgi complex. *Nat Cell Biol* **4**, 374-378 (2002).
20. Thomsen, P., Roepstorff, K., Stahlhut, M. & van Deurs, B. 238-250 (2002).
21. Murata, M. et al. 10339-10343 (1995).
22. Pelkmans, L. & Zerial, M. Kinase-regulated quantal assemblies and kiss-and-run recycling of caveolae. *Nature* **436**, 128-133 (2005).
23. Ortegren, U. et al. 2028-2036 (2004).
24. Rothberg, K.G. et al. Caveolin, a protein component of caveolae membrane coats. *Cell* **68**, 673-682 (1992).
25. Le, P.U., Guay, G., Altschuler, Y. & Nabi, I.R. 3371-3379 (2002).
26. Ito, J.-i., Nagayasu, Y., Kato, K., Sato, R. & Yokoyama, S. 7929-7935 (2002).
27. Li, W.P., Liu, P., Pilcher, B.K. & Anderson, R.G. 1397-1408 (2001).
28. Monier, S. et al. 911-927 (1995).

29. Monier, S., Dietzen, D.J., Hastings, W.R., Lublin, D.M. & Kurzchalia, T.V. Oligomerization of VIP21-caveolin in vitro is stabilized by long chain fatty acylation or cholesterol. *FEBS Letters* **388**, 143-149 (1996).
30. Pol, A. et al. 2091-2105 (2005).
31. Tagawa, A. et al. 769-779 (2005).
32. Pol, A. et al. Cholesterol and Fatty Acids Regulate Dynamic Caveolin Trafficking through the Golgi Complex and between the Cell Surface and Lipid Bodies 10.1091/mbc.E04-08-0737. *Mol. Biol. Cell* **16**, 2091-2105 (2005).
33. Cheng, Z.-J. et al. 3197-3210 (2006).
34. Choudhury, A., Marks, D.L., Proctor, K.M., Gould, G.W. & Pagano, R.E. Regulation of caveolar endocytosis by syntaxin 6-dependent delivery of membrane components to the cell surface. *Nat Cell Biol* **8**, 317-328 (2006).
35. Manninen, A. et al. 10087-10096 (2005).
36. Hernandez-Deviez, D.J. et al. 129-142 (2006).
37. Wyse, B.D. et al. 23738-23746 (2003).
38. Cohen, A.W. et al. C222-235 (2003).
39. Brazer, S.-c.W., Singh, B.B., Liu, X., Swaim, W. & Ambudkar, I.S. 27208-27215 (2003).
40. Maroto, R. et al. TRPC1 forms the stretch-activated cation channel in vertebrate cells. *Nat Cell Biol* **7**, 179-185 (2005).
41. Horton, J.D., Goldstein, J.L. & Brown, M.S. 1125-1131 (2002).
42. Goldstein, J.L., Rawson, R.B. & Brown, M.S. Mutant Mammalian Cells as Tools to Delineate the Sterol Regulatory Element-Binding Protein Pathway for Feedback Regulation of Lipid Synthesis. *Archives of Biochemistry and Biophysics* **397**, 139-148 (2002).
43. Gong, Y., Lee, J.N., Brown, M.S., Goldstein, J.L. & Ye, J. 6154-6159 (2006).
44. Gong, Y. et al. Sterol-regulated ubiquitination and degradation of Insig-1 creates a convergent mechanism for feedback control of cholesterol synthesis and uptake. *Cell Metabolism* **3**, 15-24 (2006).
45. Lee, J.N., Gong, Y., Zhang, X. & Ye, J. 4958-4963 (2006).
46. Bengoechea-Alonso, M.T. & Ericsson, J. SREBP in signal transduction: cholesterol metabolism and beyond. *Current Opinion in Cell Biology* **19**, 215-222 (2007).
47. Brown, M.S. & Goldstein, J.L. The SREBP Pathway: Regulation of Cholesterol Metabolism by Proteolysis of a Membrane-Bound Transcription Factor. *Cell* **89**, 331-340 (1997).
48. Edwards, P.A., Tabor, D., Kast, H.R. & Venkateswaran, A. Regulation of gene expression by SREBP and SCAP. *Biochimica et Biophysica Acta (BBA) - Molecular and Cell Biology of Lipids* **1529**, 103-113 (2000).
49. Horton, J.D. & Shimomura, I. Sterol regulatory element-binding proteins: activators of cholesterol and fatty acid biosynthesis. *Current Opinion in Lipidology* **10**, 143-150 (1999).
50. Sakakura, Y. et al. Sterol Regulatory Element-Binding Proteins Induce an Entire Pathway of Cholesterol Synthesis. *Biochemical and Biophysical Research Communications* **286**, 176-183 (2001).

51. Radhakrishnan, A., Sun, L.-P., Kwon, H.J., Brown, M.S. & Goldstein, J.L. Direct Binding of Cholesterol to the Purified Membrane Region of SCAP: Mechanism for a Sterol-Sensing Domain. *Molecular Cell* **15**, 259-268 (2004).
52. Brown, A.J., Sun, L., Feramisco, J.D., Brown, M.S. & Goldstein, J.L. Cholesterol Addition to ER Membranes Alters Conformation of SCAP, the SREBP Escort Protein that Regulates Cholesterol Metabolism. *Molecular Cell* **10**, 237-245 (2002).
53. Goldstein, J.L., DeBose-Boyd, R.A. & Brown, M.S. Protein Sensors for Membrane Sterols. *Cell* **124**, 35-46 (2006).
54. Olofsson, S.O. & Boren, J. 395-410 (2005).
55. Black, D.D. 00189.2007 (2007).
56. Cartwright, I.J. & Higgins, J.A. 48048-48057 (2001).
57. Siddiqi, S.A. et al. 20974-20982 (2006).
58. Kang, S. & Davis, R.A. Cholesterol and hepatic lipoprotein assembly and secretion. *Biochimica et Biophysica Acta (BBA) - Molecular and Cell Biology of Lipids* **1529**, 223-230 (2000).
59. Mahley, R.W. & Huang, Y. 94-98 (2007).
60. Brown, M.S. & Goldstein, J.L. A receptor-mediated pathway for cholesterol homeostasis. *Science* **232**, 34-47 (1986).
61. Tremblay, A.J. et al. Increased production of VLDL apoB-100 in subjects with familial hypercholesterolemia carrying the same null LDL receptor gene mutation. *Journal of Lipid Research* **45**, 866-872 (2004).
62. Plump, A.S. et al. Severe hypercholesterolemia and atherosclerosis in apolipoprotein E-deficient mice created by homologous recombination in ES cells. *Cell* **71**, 343-353 (1992).
63. Zhang, S.H., Reddick, R.L., Piedrahita, J.A. & Maeda, N. 468-471 (1992).
64. Kypreos, K. & Zannis, V. LDL receptor deficiency or apoE mutations prevent remnant clearance and induce hypertriglyceridemia in mice. *Journal of Lipid Research* **47**, 521-529 (2006`).
65. Mahley, R.W. et al. Intravenous infusion of apolipoprotein E accelerates clearance of plasma lipoproteins in rabbits. *Journal of Clinical Investigation* **83**, 2125-2130 (1989).
66. Chang, T.-Y. et al. Roles of acyl-coenzyme A: cholesterol acyltransferase-1 and -2. *Current Opinion in Lipidology* **12**, 289-296 (2001).
67. An, S. et al. A critical role for the histidine residues in the catalytic function of acyl-CoA:cholesterol acyltransferase catalysis: Evidence for catalytic difference between ACAT1 and ACAT2. *FEBS Letters* **580**, 2741-2749 (2006).
68. Zannis, V.I., Cole, F., Jackson, C., Kurnit, D. & Karathanasis, S. Distribution of apolipoprotein A-I, C-II, C-III, and E mRNA in fetal human tissues. Time-dependent induction of apolipoprotein E mRNA by cultures of human monocyte-macrophages. *Biochemistry* **24**, 4450-4455 (1985).
69. Yancey, P.G. et al. 712-719 (2003).
70. Wang, N., Ranalletta, M., Matsuura, F., Peng, F. & Tall, A.R. 1310-1316 (2006).
71. Vaughan, A.M. & Oram, J.F. 2433-2443 (2006).
72. Link, J.J., Rohatgi, A. & de Lemos, J.A. HDL Cholesterol: Physiology, Pathophysiology, and Management. *Current Problems in Cardiology* **32**, 268-314 (2007).

73. Sviridov, D. & Nestel, P.J. Genetic factors affecting HDL levels, structure, metabolism and function. *Current Opinion in Lipidology* **18**, 157-163 (2007).
74. Stein, O. & Stein, Y. Lipid transfer proteins (LTP) and atherosclerosis. *Atherosclerosis* **178**, 217-230 (2005).
75. Tamehiro, N. et al. 21090-21099 (2007).
76. Edwards, P.A., Kast, H.R. & Anisfeld, A.M. 2-12 (2002).
77. Plosch, T. et al. 33870-33877 (2002).
78. Hennekens, C.H. 1095-1102 (1998).
79. Kannel, W., Castelli, W., Gordon, T. & McNamara, P. Serum cholesterol, lipoproteins, and the risk of coronary heart disease. The Framingham study. *Ann. Int. Med.* **74**, 1-12 (1971).
80. Gordon, T., Castelli, W., Hjortland, M., Kannel, W. & Dawber, T. High density lipoprotein as a protective factor against coronary heart disease. The Framingham Study. *Am J Med* **62**, 707-714 (1977).
81. Matsuura, E., Kobayashi, K., Tabuchi, M. & Lopez, L.R. Oxidative modification of low-density lipoprotein and immune regulation of atherosclerosis. *Progress in Lipid Research* **45**, 466-486 (2006).
82. Arai, T., Wang, N., Bezouevski, M., Welch, C. & Tall, A.R. Decreased atherosclerosis in heterozygous low density lipoprotein receptor-deficient mice expressing the scavenger receptor BI transgene. *Journal of Biological Chemistry* **274**, 2366-2371 (1999).
83. Greaves, D.R. & Gordon, S. Recent insights into the biology of macrophage scavenger receptors. *Journal of Lipid Research* **46**, 11-20 (2005).
84. Sawamura, T. et al. An endothelial receptor for oxidized low-density lipoprotein. *Nature* **386**, 73-77 (1997).
85. Shimaoka, T. et al. Molecular cloning of a novel scavenger receptor for oxidized low density lipoprotein, SR-PSOX, on macrophages. *Journal of Biological Chemistry* **275**, 40663-40666 (2000).
86. Kunjathoor, V.V. et al. Scavenger receptors class A-I/II and CD36 are the principal receptors responsible for the uptake of modified low density lipoprotein leading to lipid loading in macrophages. *Journal of Biological Chemistry* **277**, 49982-49988 (2002).
87. Ross, R. 115-126 (1999).
88. Katz, S., Shipley, G. & Small, D. Physical chemistry of the lipids of human atherosclerotic lesions. Demonstration of a lesion intermediate between fatty streaks and advanced plaques. *Journal of Clinical Investigation* **58**, 200-211 (1976).
89. Nofer, J.-R. & Remaley, A. Tangier disease: still more questions than answers. *Cellular and Molecular Life Sciences (CMLS)* **62**, 2150-2160 (2005).
90. Fredrickson, D.S., Altrocchi, P.H., Avioli, L.V., Goodman, D.S. & Goodman, H.C. Tangier disease: combined clinical staff conference at the National Institute of Health. *Ann. Int. Med.* **55**, 1016-1030 (1961).
91. Schmitz, G., Assmann, G., Rall, S.C. & Mahley, R.W. 6081-6085 (1983).
92. Bojanovski, D., Gregg, R.E. & Brewer, H.B., Jr. 6049-6051 (1984).
93. Law, S.W. & Brewer, H.B., Jr. 12810-12814 (1985).

94. Francis, G.A., Knopp, R.H. & Oram, J.F. Defective removal of cellular cholesterol and phospholipids by apolipoprotein A-I in Tangier Disease. *J Clin Invest.* **96**, 78-87 (1995).
95. Remaley, A.T. et al. 1813-1821 (1997).
96. Rogler, G., Trumbach, B., Klima, B., Lackner, K.J. & Schmitz, G. 683-690 (1995).
97. Walter, M., Gerdes, U., Seedorf, U. & Assmann, G. The High Density Lipoprotein- and Apolipoprotein A-I-Induced Mobilization of Cellular Cholesterol Is Impaired in Fibroblasts from Tangier Disease Subjects. *Biochemical and Biophysical Research Communications* **205**, 850-856 (1994).
98. Hara, H. & Yokoyama, S. Interaction of free apolipoproteins with macrophages. Formation of high density lipoprotein-like lipoproteins and reduction of cellular cholesterol. *J. Biol. Chem.* **266**, 3080-3086 (1991).
99. Rust, S. et al. Assignment of Tangier disease to chromosome 9q31 by a graphical linkage exclusion strategy. **20**, 96-98 (1998).
100. Rust, S. et al. Tangier disease is caused by mutations in the gene encoding ATP-binding cassette transporter 1. **22**, 352-355 (1999).
101. Brooks-Wilson, A. et al. Mutations in ABC1 in Tangier disease and familial high-density lipoprotein deficiency. **22**, 336-345 (1999).
102. Bodzioch, M. et al. The gene encoding ATP-binding cassette transporter 1 is mutated in Tangier disease. **22**, 347-351 (1999).
103. Wenzel, J.J., Piehler, A. & Kaminski, W.E. ABC A-subclass proteins: Gatekeepers of cellular phospho- and sphingolipid transport. *Frontiers in Bioscience* **12**, 3177-3193 (2007).
104. Dean, M. & Annilo, T. Evolution of The ATP-Binding Cassette (ABC) Transporter Superfamily In Vertebrates. *Annu. Rev. Genomics Hum. Genet.* **6**, 123-142 (2005).
105. Kaminski, W.E., Piehler, A. & Wenzel, J.J. ABC A-subfamily transporters: Structure, function and disease. *Biochimica et Biophysica Acta (BBA) - Molecular Basis of Disease* **1762**, 510-524 (2006).
106. Dean, M. & Allikmets, R. Evolution of ATP-binding cassette transporter genes. *Curr. Opin. Genet. Dev.* **5**, 779-785 (1995).
107. Dean, M., Rzhetsky, A. & Allikmets, R. The Human ATP-Binding Cassette (ABC) Transporter Superfamily
10.1101/gr.GR-1649R. *Genome Res.* **11**, 1156-1166 (2001).
108. Hyde, S.C. et al. Structural model of ATP-binding proteing associated with cystic fibrosis, multidrug resistance and bacterial transport. **346**, 362-365 (1990).
109. Higgins, C. ABC transporters: from microorganisms to man. *Annu. Rev. Cell Biol.* **8**, 67-113 (1992).
110. Klein, I., Sarkadi, B. & Varadi, A. An inventory of the human ABC proteins. *Biochimica et Biophysica Acta (BBA) - Biomembranes* **1461**, 237-262 (1999).
111. Luciani, M.F., Denizot, F., Savary, S., Mattei, M.G. & Chimini, G. Cloning of Two Novel ABC Transporters Mapping on Human Chromosome 9. *Genomics* **21**, 150-159 (1994).
112. Langmann, T. et al. Molecular Cloning of the Human ATP-Binding Cassette Transporter 1 (hABC1): Evidence for Sterol-Dependent Regulation in Macrophages. *Biochemical and Biophysical Research Communications* **257**, 29-33 (1999).

113. Wang, N., Silver, D.L., Costet, P. & Tall, A.R. Specific binding of ApoA-I, enhanced cholesterol efflux, and altered plasma membrane morphology in cells expressing ABC1. *Journal of Biological Chemistry* **275**, 33053-33058 (2000).
114. Oram, J.F., Lawn, R.M., Garvin, M.R. & Wade, D.P. 34508-34511 (2000).
115. Fitzgerald, M.L. et al. 33178-33187 (2002).
116. Wang, N., Silver, D.L., Costet, P. & Tall, A.R. 33053-33058 (2000).
117. Bortnick, A.E. et al. 28634-28640 (2000).
118. Kypreos, K.E. & Zannis, V.I. 359-367 (2007).
119. Remaley, A.T. et al. 828-836 (2003).
120. Fitzgerald, M.L. et al. 287-294 (2004).
121. Chambenoit, O. et al. 9955-9960 (2001).
122. Lin, G. & Oram, J.F. Apolipoprotein binding to protruding membrane domains during removal of excess cellular cholesterol. *Atherosclerosis* **149**, 359-370 (2000).
123. Drobnik, W. et al. 268-278 (2002).
124. Panagotopulos, S.E. et al. 39477-39484 (2002).
125. Gillotte, K.L. et al. 2021-2028 (1999).
126. Rothblat, G.H., de la Llera-Moya, M., Favari, E., Yancey, P.G. & Kellner-Weibel, G. Cellular cholesterol flux studies: methodological considerations. *Atherosclerosis* **163**, 1-8 (2002).
127. Gillotte, K.L., Davidson, W.S., Lund-Katz, S., Rothblat, G.H. & Phillips, M.C. 1918-1928 (1998).
128. Neufeld, E.B. et al. 27584-27590 (2001).
129. Takahashi, Y. & Smith, J.D. 11358-11363 (1999).
130. Fielding, P.E., Nagao, K., Hakamata, H., Chimini, G. & Fielding, C.J. 14113-14120 (2000).
131. Wang, N., Silver, D.L., Thiele, C. & Tall, A.R. 23742-23747 (2001).
132. Costet, P., Luo, Y., Wang, N. & Tall, A.R. 28240-28245 (2000).
133. Fu, X. et al. 38378-38387 (2001).
134. Schwartz, K., Lawn, R.M. & Wade, D.P. ABC1 Gene Expression and ApoA-I-Mediated Cholesterol Efflux Are Regulated by LXR. *Biochemical and Biophysical Research Communications* **274**, 794-802 (2000).
135. Chinetti, G. et al. PPAR-[alpha] and PPAR-[gamma] activators induce cholesterol removal from human macrophage foam cells through stimulation of the ABCA1 pathway. *Nat Med* **7**, 53-58 (2001).
136. Murthy, S., Born, E., Mathur, S.N. & Field, F.J. 1054-1064 (2002).
137. Yokoyama, S. 20-27 (2006).
138. Suzuki, S. et al. 519-525 (2004).
139. Sparrow, C.P. et al. 10021-10027 (2002).
140. Orso, E. et al. Transport of lipids from Golgi to plasma membrane is defective in Tangier disease patients and Abc1-deficient mice. *Nat Genet* **24**, 192-196 (2000).
141. Tanaka, A.R. et al. 8815-8819 (2003).
142. Arakawa, R. & Yokoyama, S. Helical Apolipoproteins Stabilize ATP-binding Cassette Transporter A1 by Protecting It from Thiol Protease-mediated Degradation. **277**, 22426-22429 (2002).
143. Wang, N. et al. 99-107 (2003).
144. Yamauchi, Y., Hayashi, M., Abe-Dohmae, S. & Yokoyama, S. 47890-47897 (2003).

145. Arakawa, R. et al. Phosphorylation and Stabilization of ATP Binding Cassette Transporter A1 by Synthetic Amphiphilic Helical Peptides. **279**, 6217-6220 (2004).
146. Buechler, C., Boettcher, A., Maa Bared, S., Probst, M.C.O. & Schmitz, G. The carboxyterminus of the ATP-binding cassette transporter A1 interacts with a [beta]2-syntrophin/utrophin complex. *Biochemical and Biophysical Research Communications* **293**, 759-765 (2002).
147. Munehira, Y. et al. 15091-15095 (2004).
148. Okuhira, K.-i. et al. 39653-39664 (2005).
149. Singaraja, R.R. et al. 33969-33979 (2001).
150. Vaisman, B.L. et al. 303-309 (2001).
151. Brunham, L.R. et al. 1052-1062 (2006).
152. Timmins, J.M. et al. 1333-1342 (2005).
153. Hamon, Y. et al. ABC1 promotes engulfment of apoptotic cells and transbilayer redistribution of phosphatidylserine. *Nature Cell Biology* **2**, 399-406 (2000).
154. Marguet, D., Luciani, M.-F., Moynault, A., Williamson, P. & Chimini, G. Engulfment of apoptotic cells involves the redistribution of membrane phosphatidylserine on phagocyte and prey. *Nature Cell Biology* **1**, 454-456 (1999).
155. Smith, J.D., Waelde, C., Horwitz, A. & Zheng, P. Evaluation of the role of phosphatidylserine translocase activity in ABCA1-mediated lipid efflux. *Journal of Biological Chemistry* **277**, 17797-17803 (2002).
156. Rosenberg, M.F., Callaghan, R., Ford, R.C. & Higgins, C.F. Structure of the multidrug P-glycoprotein to 2.5 nm resolution determined by electron microscopy and image analysis. *Journal of Biological Chemistry* **272**, 10685-10694 (1997).
157. Williamson, P. et al. Transbilayer Phospholipid Movements in ABCA1-Deficient Cells. *PLoS ONE* **2** (2007).
158. Remaley, A.T. et al. Human ATP-binding cassette transporter 1 (ABC1): genomic organization and identification of the genetic defect in the original Tangier disease kindred. *Proceedings of the National Academy of Sciences* **96**, 12685-12690 (1999).
159. Lin, G. Theory of cation-phospholipid-induced shape changes in a lipid bilayer couple. *Bull Math Biol.* **42**, 601-625 (1980).
160. Sheetz, M.P. & Singer, S.J. Biological membranes as bilayer couples. A molecular mechanism of drug-erythrocyte interactions. *PNAS* **71**, 4457-4461 (1974).
161. Bared, S.M. et al. Association of ABCA1 with syntaxin 13 and flotillin-1 and enhanced phagocytosis in tangier cells. *Molecular Biology of the Cell* **15**, 5399-5407 (2004).
162. Zha, X., Genest, J.J. & McPherson, M. Endocytosis is enhanced in Tangier fibroblasts: possible role of ATP-binding cassette protein A1 in endosomal vesicular transport. *Journal of Biological Chemistry* **276**, 39476-39483 (2001).
163. Vedhachalam, C. et al. 25123-25130 (2007).
164. Alder-Baerens, N. et al. Headgroup-specific Exposure of Phospholipids in ABCA1-expressing Cells. **280**, 26321-26329 (2005).
165. Hamon, Y. et al. ABC1 promotes engulfment of apoptotic cells and transbilayer redistribution of phosphatidylserine. *Nat Cell Biol* **2**, 399-406 (2000).
166. Luciani, M.F. & Chimini, G. The ATP binding cassette transporter ABC1, is required for the engulfment of corpses generated by apoptotic cell death. *EMBO J.* **15**, 226-235 (1996).

167. Zha, X., Genest, J., Jr. & McPherson, R. 39476-39483 (2001).
168. Vaughan, A.M. & Oram, J.F. ABCA1 redistributes membrane cholesterol independent of apolipoprotein interactions
10.1194/jlr.M300078-JLR200. *J. Lipid Res.* **44**, 1373-1380 (2003).
169. Lange, Y., Ye, J. & Steck, T.L. 11664-11667 (2004).
170. Wang, M.M., Olsher, M., Sugar, I.P. & Chong, P.L.G. 2159-2166 (2004).
171. Wang, Y., O'Malley, B., Jr, Tsai, S. & O'Malley, B. A Regulatory System for Use in Gene Transfer
10.1073/pnas.91.17.8180. *PNAS* **91**, 8180-8184 (1994).
172. Mukherjee, S., Zha, X., Tabas, I. & Maxfield, F.R. Cholesterol Distribution in Living Cells: Fluorescence Imaging Using Dehydroergosterol as a Fluorescent Cholesterol Analog. *Biophys. J.* **75**, 1915-1925 (1998).
173. Hao, M., Mukherjee, S. & Maxfield, F.R. Cholesterol depletion induces large scale domain segregation in living cell membranes
10.1073/pnas.231377398. *PNAS* **98**, 13072-13077 (2001).
174. Mukherjee, S., Soe, T.T. & Maxfield, F.R. Endocytic Sorting of Lipid Analogues Differing Solely in the Chemistry of Their Hydrophobic Tails
10.1083/jcb.144.6.1271. *J. Cell Biol.* **144**, 1271-1284 (1999).
175. Smart, E., Ying, Y., Mineo, C. & Anderson, R. A Detergent-Free Method for Purifying Caveolae Membrane from Tissue Culture Cells
10.1073/pnas.92.22.10104. *PNAS* **92**, 10104-10108 (1995).
176. Pike, L.J. & Casey, L. Cholesterol Levels Modulate EGF Receptor-Mediated Signaling by Altering Receptor Function and Trafficking. *Biochemistry* **41**, 10315-10322 (2002).
177. Sun, Y. et al. 5813-5820 (2003).
178. Chang, W.J., Rothberg, K.G., Kamen, B.A. & Anderson, R.G. 63-69 (1992).
179. Schnitzer, J.E., Oh, P., Pinney, E. & Allard, J. 1217-1232 (1994).
180. Fu, Y. et al. 14140-14146 (2004).
181. Mundy, D.I., Machleidt, T., Ying, Y.-s., Anderson, R.G.W. & Bloom, G.S. 4327-4339 (2002).
182. Thorn, H. et al. 3967-3976 (2003).
183. Zhuang, L., Lin, J., Lu, M.L., Solomon, K.R. & Freeman, M.R. 2227-2231 (2002).
184. Haidar, B., Denis, M., Krimbou, L., Marcil, M. & Genest, J., Jr. 2087-2094 (2002).
185. Mendez, A.J., Lin, G., Wade, D.P., Lawn, R.M. & Oram, J.F. 3158-3166 (2001).
186. Ntambi, J.M. & Young-Cheul, K. 3122S-3126 (2000).
187. Simons, K. & Ikonen, E. 1721-1726 (2000).
188. Brown, D.A. & Rose, J.K. Sorting of GPI-anchored proteins to glycolipid-enriched membrane subdomains during transport to the apical cell surface. *Cell* **68**, 533-544 (1992).
189. Nagao, K. et al. 14868-14874 (2007).
190. Koseki, M. et al. 299-306 (2007).
191. Smith, J.D. et al. 635-644 (2004).
192. Simons, K. & Toomre, D. Lipid rafts and signal transduction. *Nat Rev Mol Cell Biol* **1**, 31-39 (2000).
193. Sharma, P. et al. Nanoscale Organization of Multiple GPI-Anchored Proteins in Living Cell Membranes. *Cell* **116**, 577-589 (2004).

194. Harder, T., Scheiffele, P., Verkade, P. & Simons, K. 929-942 (1998).
195. Razani, B. et al. 8635-8647 (2002).
196. Landh, T. From entangled membranes to eclectic morphologies: cubic membranes as subcellular space organizers. *FEBS Letters* **369**, 13-17 (1995).
197. Green, H. & Kehinde, O. Formation of normally differentiated subcutaneous fat pads by an established preadipose cell line. *J Cell Physiol.* **101**, 169-171 (1979).
198. Novikoff, A.B., Novikoff, P.M., Rosen, O.M. & Rubin, C.S. 180-196 (1980).
199. Green, H. & Meuth, M. An established pre-adipose cell line and its differentiation in culture. *Cell* **3**, 127-133 (1974).
200. Cohen, A.W., Combs, T.P., Scherer, P.E. & Lisanti, M.P. Role of caveolin and caveolae in insulin signaling and diabetes. *Am J Physiol Endocrinol Metab* **285**, E1151-E1160 (2003).
201. Fruhbeck, G., Lopez, M. & Dieguez, C. Role of caveolins in body weight and insulin resistance regulation. *Trends in Endocrinology & Metabolism* **18**, 177-182 (2007).

Contributions of Collaborators

All experiments and results presented in this thesis are the work of the thesis author, Yves Landry, except for the following:

- Sub-cloning of A937V mutant was performed by Ying Feng.
- Triton X-100 extraction of FC, SM, and PC were performed by Dr. Maxime Denis
- MCD cholesterol efflux assays were performed by Dr. Maxime Denis
- ApoA-I association experiment was performed by Dr. Maxime Denis
- Insulin stimulation of 3T3-L1 adipocytes was performed by Dr. Anne Marie Gagnon

Curriculum Vitae

LANGUAGES

- Bilingual, fluent spoken and written, in French and English.

EDUCATION

Master of Science, Biochemistry **Sept. 2005-Sept. 2007**
University of Ottawa, Ottawa, ON
- Supervisor: Dr. Xiaohui Zha

Honours Bachelor of Science, Biochemistry **Sept. 2001-Apr. 2005**
University of Ottawa, Ottawa, ON
- Thesis: The distribution of caveolin-1 is influenced by the expression of ABCA1

AWARDS, DISTINCTIONS AND FELLOWSHIPS

- University of Ottawa Faculty of Medicine Award of Excellence : $500
  - December, 2007
- Ontario Graduate Scholarship: $15,000 / year (offered 2 years)
  - April, 2006-August, 2007
- University of Ottawa Excellence Scholarship: Tuition Payment
  - April, 2006-August, 2007
- OHRI Graduate Research Presentation Award: $100
  - November, 2005
- Dean's Honour List, Honours Year
  - September, 2004-April, 2005
- University of Ottawa Admission Scholarship: $2,500
  - September,2001-December, 2001
- Greyhound Canada Award: $1000 (Approximate Value)
  - June, 2001

CONFERENCE ABSTRACTS/PRESENTATIONS

1. M. Denis, **Y. D. Landry**, X. Zha; "The ATP-binding Cassette A1 (ABCA1)-mediated Apolipoprotein A-I Lipidation Occurs at the Plasma Membrane and not in the Endocytic Compartments".American Heart Association. (June, 2007)

2. **Y. D. Landry**, M. Denis, S. Nandi, S. Bell, A.M.Vaughan and X. Zha; "ABCA1 Expression Disrupts Raft Membrane Microdomains Through its ATPase-Fueled Functions". American Society for Cell Biology annual meeting (December, 2005). San Francisco, CA, USA

3. **Y. D. Landry**, M. Denis, S. Nandi, S. Bell, A.M.Vaughan and X. Zha; "Membrane microdomain re-organization by ABCA1 and its implications in apoA-I-mediated cholesterol efflux". Canadian Lipoprotein Conference (October 2005). Montebello, PQ

4. **Y. D. Landry**, S. Bell, A. Vaughan, X. Zha; "The distribution of caveolin-1 is dependent on the expression of ABCA1". American Society for Cell Biology annual meeting (December, 2004). Washington, DC, USA.

PUBLICATIONS

1. M. Denis, **Y. D. Landry**, X. Zha; The ATP-binding Cassette A1-mediated Lipidation of Apolipoprotein A-I Occurs at the Plasma Membrane and Not in the Endocytic Compartments". Manuscript accepted by JBC (pending review), December, 2007.

2. **Y. D. Landry**, M. Denis, S. Nandi, S. Bell, A.M.Vaughan and X. Zha; "ABCA1 Expression Disrupts Raft Membrane Microdomains through its ATPase-Related Functions". J. Biol. Chem, November 24; 281(47), 36091-36101. (2006)

WORK EXPERIENCE

- **Research Assistant, OHRI, Ottawa, ON** **2007**
  - Continued research on 3T3-L1 hypertrophic adipocytes
  - Microscopy analysis of retroendocytic ABCA1-mediated HDL formation
  - General assistance with confocal microscopy system and spectral imager
- **Summer Research Student, OHRI, Ottawa, ON** **2004-2005**
  - Continued research on ABCA1 and Caveolae formation
- **Store / Computer Technician, Best Buy, Ottawa, ON** **2003**
  - Performed upgrades, repairs and performance improvements on computer systems.
  - Maintained functionality of store networks and displays.
  - Screened all customer returns for fraudulent activity.
- **Safe Water Sampler / West Nile Virus Surveillance, Algoma Health Unit, Sault Ste. Marie, ON (summer position)** **2001-2002**
  - Collected drinking water and recreational water samples for analysis.
  - Advised the public health inspectors and medical officer of health of any adverse results.
  - Updated records and prepared specified reports.
  - Provided valuable surveillance information to the agency regarding the spread of West Nile Virus in the region.
- **CAP (Community Access Program) Site Manager, Algoma District School Board, Sault Ste. Marie, ON** **2001**
  - Computer set-up, maintenance and troubleshooting.
  - Monitoring of site access and provision of user support.

- **Computer Assistant / Technician, Great Lakes Forestry Centre, Sault Ste. Marie, ON** **1999-2000**
    - Troubleshooting of various computer hardware and software problems.
    - Network maintenance and employee support.

TEACHING EXPERIENCE

- **BCH2733 Introduction a la biochimie, Dept. de biochimie** **Oct.2006-May 2007**
  University of Ottawa, Ottawa, ON.
- **BIO1110 Introduction to Biology Laboratory, Dept. Biology.** **Jan.06-Apr.06**
  University of Ottawa, Ottawa, ON.